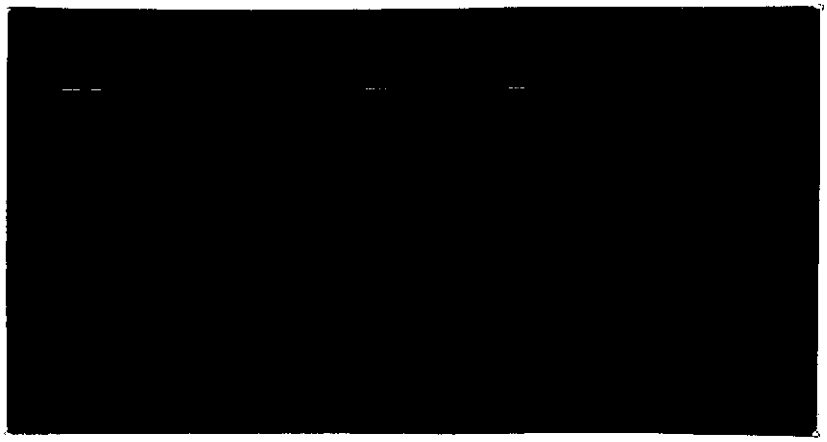

(NASA-CR-143710) DESIGN, DEVELOPMENT AND TESTING OF A CRYOGENIC TEMPERATURE HEAT PIPE FOR THE ICICLE SYSTEM Final Technical Report (Dymatherm Corp., Cockeysville, Md.) 138 p HC $5.75 CSCL 13A G3/34

N75-21559

Unclas 18770

dymatherm CORPORATION

DTM-73-15

FINAL TECHNICAL REPORT

for

DESIGN, DEVELOPMENT AND TESTING OF A CRYOGENIC TEMPERATURE HEAT PIPE FOR THE ICICLE SYSTEM

May 31, 1974

Prepared under Contract NAS5-21563

by

Dynatherm Corporation
One Industry Lane
Cockeysville, Maryland

for

National Aeronautics and Space Administration
Goddard Space Flight Center

FOREWORD

This report was prepared under NASA Contract NAS5-21563, "Design, Development and Testing of a Cryogenic Temperature Heat Pipe for the ICICLE System." The work was administered by the Goddard Space Flight Center, Greenbelt, Maryland; and Mr. Thomas A. Cygnarowicz was the NASA Technical Officer.

The program was conducted by the Dynatherm Corporation, Cockeysville, Maryland, with Dr. Walter B. Bienert serving as Program Manager and Mr. Donald S. Trimmer as Principal Investigator.

Several people contributed to the technical work described in this report. Messrs. Harold Fox and Noel Lee formulated the analytical models and generated most of the analytical curves. Special thanks are accorded to Mr. Thomas Cygnarowicz for his participation in many discussions and for his overall support during the program.

ABSTRACT

The objectives of this program were to develop the analytical tools necessary to design heat pipes to meet the requirements of the ICICLE system and to design, fabricate, and test two prototype heat pipes satisfying these requirements. An analytical model was formulated for a cryogenic heat pipe. Thermal and transport analyses were developed to predict the performance characteristics of various heat pipe designs. These analyses also permitted optimization of various design parameters.

A series of four breadboard heat pipes were fabricated and tested to provide inputs such as internal film coefficients, minimum capillary radii, and wick permeabilities which are required for the analyses. In addition, during the breadboard tests, a great deal was learned concerning instrumentation, charging, and testing of cryogenic heat pipes; and this knowledge was applied to the prototype heat pipes.

After a thorough design analysis of three potential heat pipe wicks (slab, artery, and axial groove), the first two were chosen for application to two prototype heat pipes. Detailed designs were made of the two heat pipes and the units were fabricated.

Tests were conducted which verified the integrity and safety margin of the design to withstand the internal pressure at ambient temperature and fatigue of thermal cycling.

During the acceptance testing in the vacuum chamber, no difficulty was experienced in priming the slab-wick heat pipe and it met the performance design requirements. Cool-down tests indicate two limitations for the rate of cool-down -- transport within the heat pipe and heat sink capability. Since the heat sinking method used during testing could not reproduce the heat removal characteristics of the VM engine, no direct correlation could be made with the test results.

The artery-wick heat pipe would not prime with nitrogen working fluid for any test conditions. It would not prime even after repairs were made to assure that the artery was positioned near the bottom of the tube. It is predicted that the artery can prime at an elevation of 0.06 cm, assuming a parasitic heat load of 1.6 watts. However, if the heat load is doubled, the heat pipe will no longer prime. To assure that

the failure to prime was not caused by damage to the wick, tests were conducted with ammonia. The artery was primed successfully many times. Experimentally, a static wicking height of 3/4 of that theoretically obtainable with 325-mesh screen was indicated.

TABLE OF CONTENTS

LIST OF FIGURES

LIST OF FIGURES (Cont'd)

LIST OF FIGURES (Cont'd)

LIST OF TABLES

I. INTRODUCTION AND SUMMARY

Meteorological and communication spacecraft are experiencing requirements for more sophisticated IR scanning radiometers, IR laser systems, and microwave systems. These devices benefit, in sensitivity and performance, by being cooled to cryogenic temperatures.

An Integrated Cryogenic Isotope Cooling Engine (ICICLE) system appears to be an attractive concept for providing long life (two years or more) cryogenic cooling in space. A miniature Vuilleumier (VM) cycle cryogenic engine is the central cooling unit. A radioisotope heat source provides the thermal power to operate the VM engine. Because safety considerations will dictate the location of the isotope and experiment requirements will dictate the location of detectors which must be cooled, the components of the ICICLE System will probably be distributed throughout the spacecraft. Consequently, heat pipes will be used to couple the centrally located VM engine to other components of the system. Cryogenic heat pipes (operating at about $77^{o}K$ and transferring 1 to 5 watts) will distribute the cryogenic cooling to one or more remotely located sensors.

The purpose of this program was to develop a cryogenic temperature heat pipe to interface with the VM engine being developed by GSFC for the ICICLE System to be used in cooling an infrared sensor. In addition to developing a heat pipe demonstrating adequate thermal performance, it was an essential requirement of the program that the heat pipe be designed to meet the environmental requirements of the ICICLE System. To develop a flight qualified heat pipe, ambient temperature storage, thermal cycling, launch vibration, cryogenic insulation, and spacecraft structure interfacing were investigated during the program.

The program was divided into three main tasks:

- Task I - Technical Evaluation: Analytical tools were developed and design data generated.
- Task II - Design: Several designs were selected and analyzed; the best two were carried to the point where detailed engineering drawings were generated.

- Task III - Prototype Fabrication and Testing: The two heat pipes were qualified to meet the program requirements including acceptance testing in a vacuum chamber.

In Task I, a thermal analysis was conducted on a model of the cryogenic heat pipe. A computer code (CRYOTHERM) was developed to predict the temperature profile along the heat pipe and perform design optimizations. In addition, another computer code (HPAD) was used to evaluate heat transport capability of various wicks (assuming uniform heat input) and to perform a design study for vapor storage. However, cryogenic heat pipes for the ICICLE application will, in general, dictate that the heat input be nonuniform as predicted by the thermal model. A code, CRYOTA, was developed to verify the transport capability of the design for nonuniform heat input. Also, in Task I, four breadboard heat pipes (one with axial grooves and the remaining three with slab wicks) were tested to verify the application of the computer codes and to provide design data. The axial-grooved heat pipe demonstrated good performance; however, the agreement with theory was poor. In all probability, the cause of this poor agreement was the sensitivity of this design to elevation and susceptibility of this design to "puddle" formation. The agreement with the slab-wick heat pipes was fairly good. An insulation design study was made which permits an insulation design selection to be made for a specific application.

In Task II, three preliminary wick designs (axial grooves, slab wick, and artery) were selected. An optimization and design analyses were conducted on each design with the result that the slab wick and the artery were selected for final detailed designs. A Test Plan was generated which specified qualification and acceptance test programs.

Two heat pipes were fabricated under Task III. All stages of assembly were conducted under flight hardware conditions. Qualification tests were conducted to verify the ability of the heat pipes to contain the cryogen under various environmental conditions. The slab-wick heat pipe was acceptance tested; the results of which agreed fairly well with predictions. The artery heat pipe could not be primed with nitrogen as the working fluid; however, it was tested andprimed quite successfully with ammonia.

The inability of the artery to prime with nitrogen was probably caused by the magnitude of the heat load that the unprimed artery was required to carry and by small inconsistencies in the artery shape and/or position. The poor fluid properties of nitrogen lead to unreliable and inconsistent artery wick performance.

The remaining sections of this report elaborate the results obtained in this program. Section 2 describes the analytical tools developed. In Section 3 the breadboard heat pipe tests are described and compared with analytical results. The development of the two prototype heat pipes is discussed in Section 4.

2. CRYOGENIC HEAT PIPE ANALYSIS

The analysis of cryogenic heat pipes which is presented in this section can be separated into three individual parts:

- Heat transfer through the walls and liquid film into and out of the vapor space
- Hydrodynamics of the liquid and vapor flow
- Radiative heat transfer through the insulation surrounding the heat pipe

2.1 Heat Transfer Analysis

A thermal model of a heat pipe was developed. This model considers the radial heat transfer at the evaporator and condenser and accounts for the axial conduction within the heat pipe envelope. A typical application would be in a heat pipe which is used to cool an infrared sensor. The sensor will be firmly mounted to a platform which, in turn, is butted against the end of the heat pipe. Thus, the heat generated by the sensor will, at first, be conducted along the wall of the evaporator and then gradually be transferred to the vapor of the heat pipe. Because of the interface requirements at the condenser end, the heat removal will take place in a similar manner; i.e., at first, radially from the vapor to the condenser wall and then axially along the wall to the condenser interface. The analytical model assumes that all heat into and out of the vapor is transferred through the cylindrical part of the heat pipe. (The end surfaces will be neglected for heat transfer.) Figure 2.1 identifies the analytic model for heat transfer. The model assumes cylindrical symmetry. The heat pipe is divided into "n" regions of constant thermal and physical properties. Each region will be characterized by external (h_o) and internal (h_i) film coefficients, outside diameter (D_o), perimeter (P_o), wall thickness (t), and the wall thermal conductivity (k). In addition, each region is specified by a length (l). The surrounding environmental temperature (T_o) is also specified. Boundary conditions are the temperature (T_s) at the evaporator end of the heat pipe and the input heat flux (Q_o) at the same location. This model results in a closed form solution for the temperature profile.

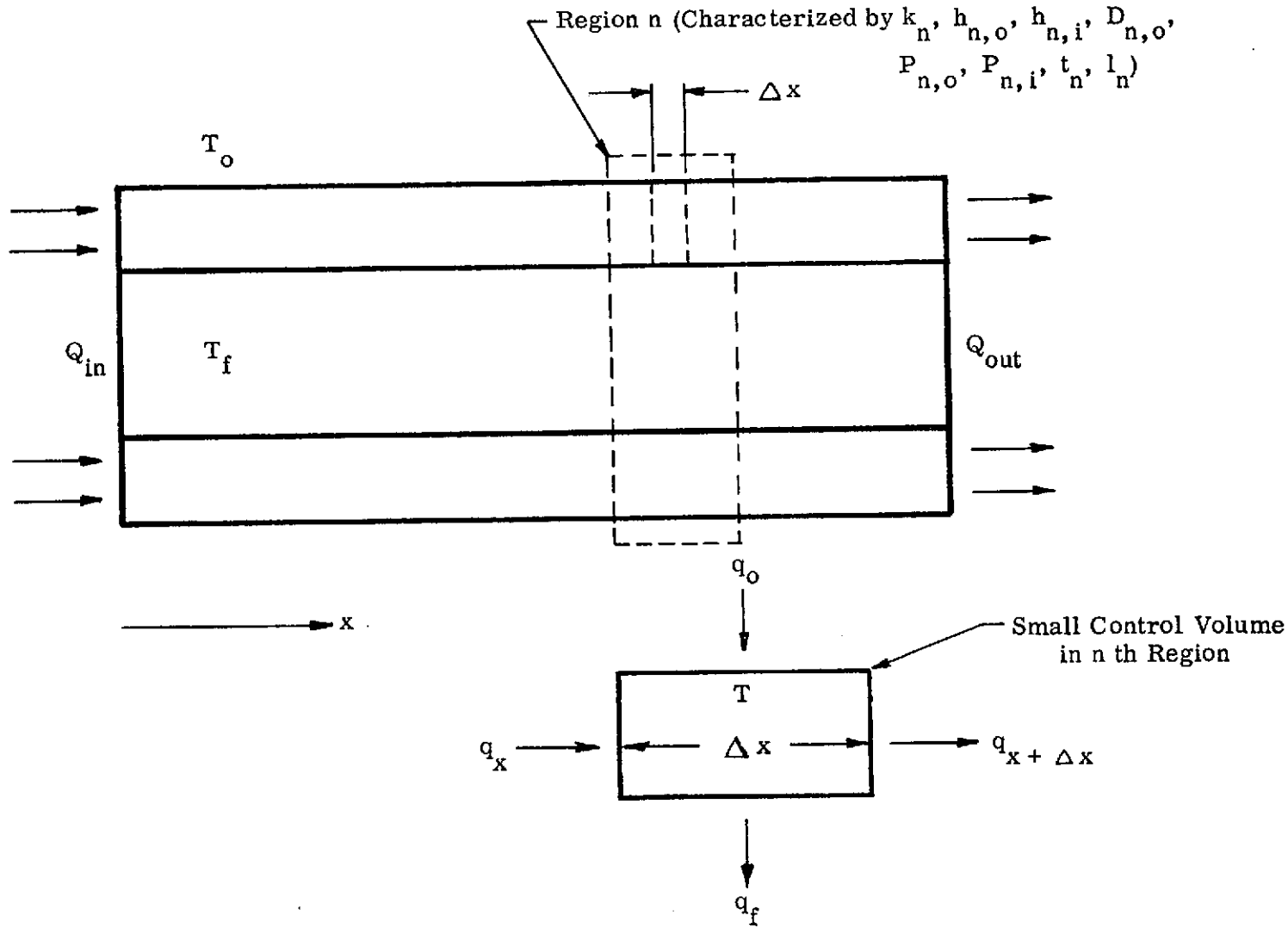

FIGURE 2.1

HEAT TRANSFER MODEL OF CYLINDRICAL HEAT PIPE

The heat balance for the control volume shown in Figure 2.1 requires that:

$$q_x - q_{x+\Delta x} + q_o = q_f \qquad 2\text{-}1$$

The first two terms represent the incremental change in heat conduction along the wall, the next term is the heat input from the surrounding environment, and the term on the right is the heat input to the vapor.

Replacing each term with its proper expression for heat transfer:

$$\frac{d}{dx}\left(kA\ \frac{dT}{dx}\right)\Delta x + h_o\ P_o\ \Delta x\ (T_o - T) = h_i\ P_i\ \Delta x\ (T - T_f) \qquad 2\text{-}2$$

where A is the cross-sectional area of the heat pipe wall, P_i is the inner perimeter, and T_f is the vapor temperature of the working fluid (assumed constant throughout the heat pipe). Equation 2-2 can be rewritten as:

$$\frac{d^2T}{dx^2} - \left(\frac{h_o\ P_o + h_i\ P_i}{kA}\right) T = -\left(\frac{h_o\ P_o\ T_o + h_i\ P_i\ T_f}{kA}\right) \qquad 2\text{-}3$$

The solution of this equation has the form:

$$T = \alpha + \beta T_f + C\ e^{mx} + K\ e^{-mx} \qquad 2\text{-}4$$

where α, β, and m are constants involving h_o, P_o, h_i, P_i, k, and A. An analogous solution holds for each region along the heat pipe. Continuity between regions is maintained using the following boundary conditions:

- The axial heat flux within the wall across each boundary must be continuous.
- The temperature must be continuous across the boundary.
- The total net heat input by all sections to the vapor must be zero.

For a heat pipe with "n" regions, each of the first two boundary conditions result in "n" equations (after including the external boundary condition at the end of the heat pipe).

The remaining boundary condition results in one more equation which is sufficient to solve for the $2n + 1$ unknowns; i.e., the $2n$ integration constants C_n and K_n and the fluid temperature T_f.

A computer program (CRYOTHERM) was developed which calculates the temperature profile along the wall, heat transfer to and from the working fluid and pipe wall, the axial heat transport requirement by the fluid $\int_o^x Q_f \, dx$, and the heat transfer per unit length to the fluid. The thermal model can handle up to 25 regions in which each of the geometric parameters (i.e., wall conductivity, and film coefficients) can vary from region to region. Appendix A describes in more detail the computer code CRYOTHERM. Input information and a listing of the program are also presented.

The simplest case which was analyzed involves one single region. Figure 2.2 shows the predicted temperature profile calculated by the program. The internal film coefficient used in the calculation corresponds to a single layer of 200-mesh stainless steel screen in contact with the inner wall of the tube. The working fluid is liquid nitrogen. The external film coefficient is representative of twenty-five layers of aluminized mylar wrapped around the pipe in a vacuum environment. Significant thermal gradients occur only at the evaporator and condenser regions. The transport section, by far the largest section of the heat pipe, is essentially isothermal, although it is in this region that the major heat leak into the pipe occurs. Note that the temperature drop in the condenser is significantly greater than that in the evaporator. This results from the fact that the heat rejected at the condenser is the sum of the heat input at the evaporator and the heat leak into the pipe from the environment.

Using this single region analysis, the effects of variation in heat pipe length and tube diameter can be investigated. Figure 2.3 indicates the variation of overall temperature drop and heat removed with heat pipe length. The heat input, at the evaporator end in all cases, was one watt. Notice that the heat output at the condenser increases linearly with length due to a corresponding increase in the surface area of the pipe. The linear increase in temperature difference is a direct result of the increasing heat leak. The temperature difference across the condenser increases correspondingly as the heat leak increases. The temperature difference at the evaporator, on the other hand, remains constant as long as the heat input from the sensor does not change.

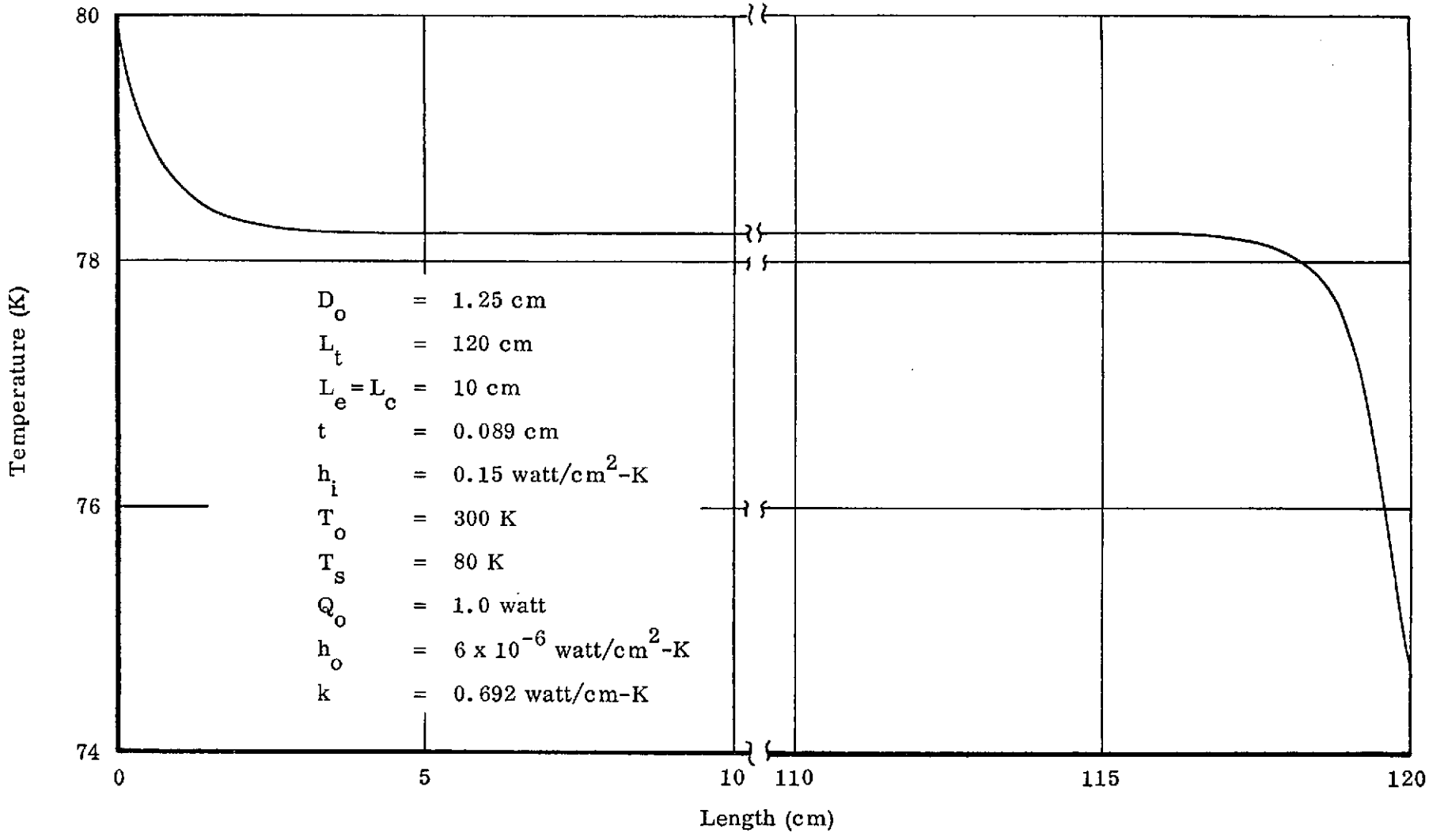

FIGURE 2.2

TEMPERATURE PROFILE OF CRYOGENIC HEAT PIPE

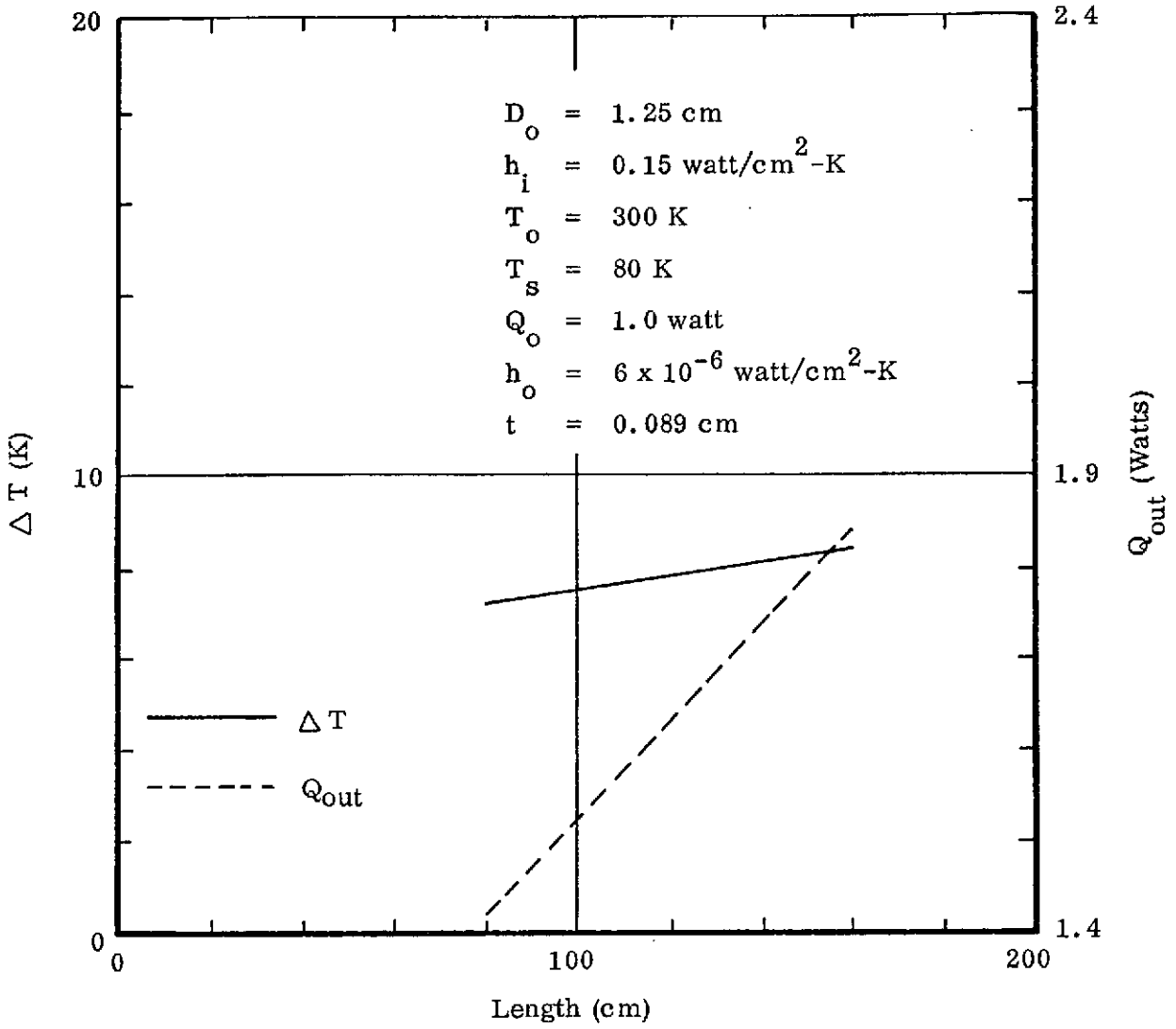

FIGURE 2.3

TEMPERATURE DIFFERENCE AND HEAT
TO VM ENGINE Vs. LENGTH

The effect of the variation in heat pipe outside diameter is shown in Figure 2.4. As with increasing length, the heat removed from the condenser increases linearly with diameter due to the increased surface area. However, the overall temperature difference decreases with diameter because of the increase in cross-sectional area of the tube. Thus, the evaporator and condenser temperature differences are smallest when the diameter is large. But the heat delivered to the condenser, which is affected mostly by the length of the transport region, is smallest when the diameter of the heat pipe is small. These observations lead to the following conclusions. A heavy walled region is desirable in the evaporator and condenser regions, and a small diameter thin-walled tube is optimum for the transport region. A model which represents an optimized geometry is shown in Figure 2.5. The inside diameter of the heat pipe remains constant throughout the entire length. The wall thickness varies however, being greater in the evaporator and condenser regions and small in the transport region. These regions of thicker wall resemble collars around the heat pipe. A typical profile curve is also shown in Figure 2.5. The basic shape of the curve does not appear different from that shown in Figure 2.2. However, the differences lie in the lengths of the effective evaporator and condenser regions (regions where the temperature is varying noticeably) and the magnitude of the overall temperature drop. In the profile curve of Figure 2.5, the long flat region corresponds approximately to the vapor temperature of the fluid in the heat pipe; hence this is essentially adiabatic. Note that the true evaporator (region where the input heat flux enters the vapor and where a large gradient occurs) is much shorter than the length of the arbitrarily selected evaporator collar. The same is true of the condenser end of the pipe. This mismatch between actual and physical evaporator and condenser lengths occurs because the collar lengths chosen for this example were longer than necessary for the heat flux and other parameters of the system. By adjusting the lengths of the collars it is possible to arrive at an optimum length without appreciably increasing the overall temperature drop across the pipe and, at the same time, decreasing slightly the parasitic heat losses of the system. The weight of the collars for this example would then be minimized.

Both the thickness and the length of the collars affect the temperature profile along the heat pipe. Figure 2.6 shows the effects of various collar thicknesses (evaporator and condenser collars of equal thickness), all of which were chosen to be ten

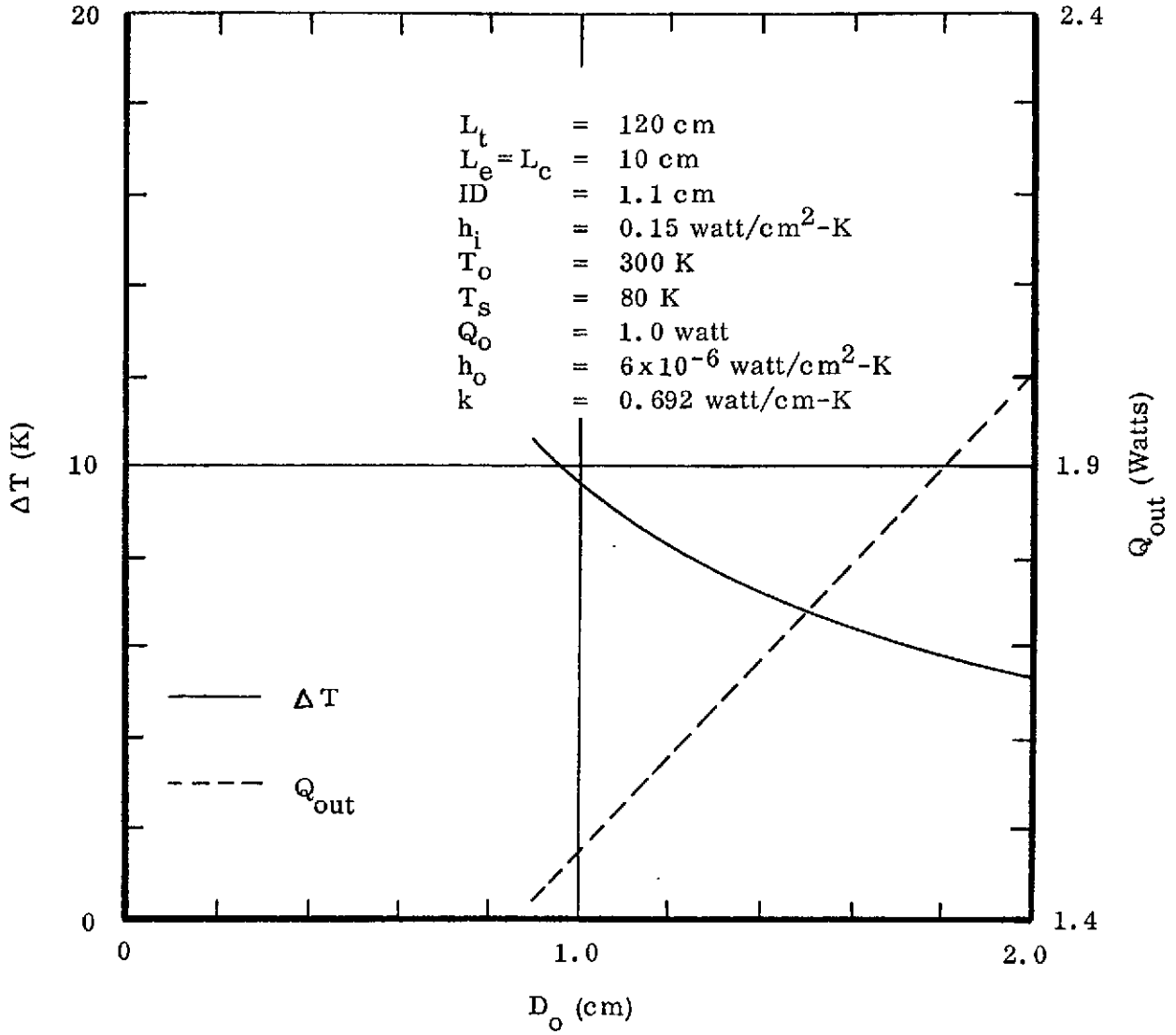

FIGURE 2.4

TEMPERATURE DIFFERENCE AND HEAT
TO VM ENGINE Vs. DIAMETER

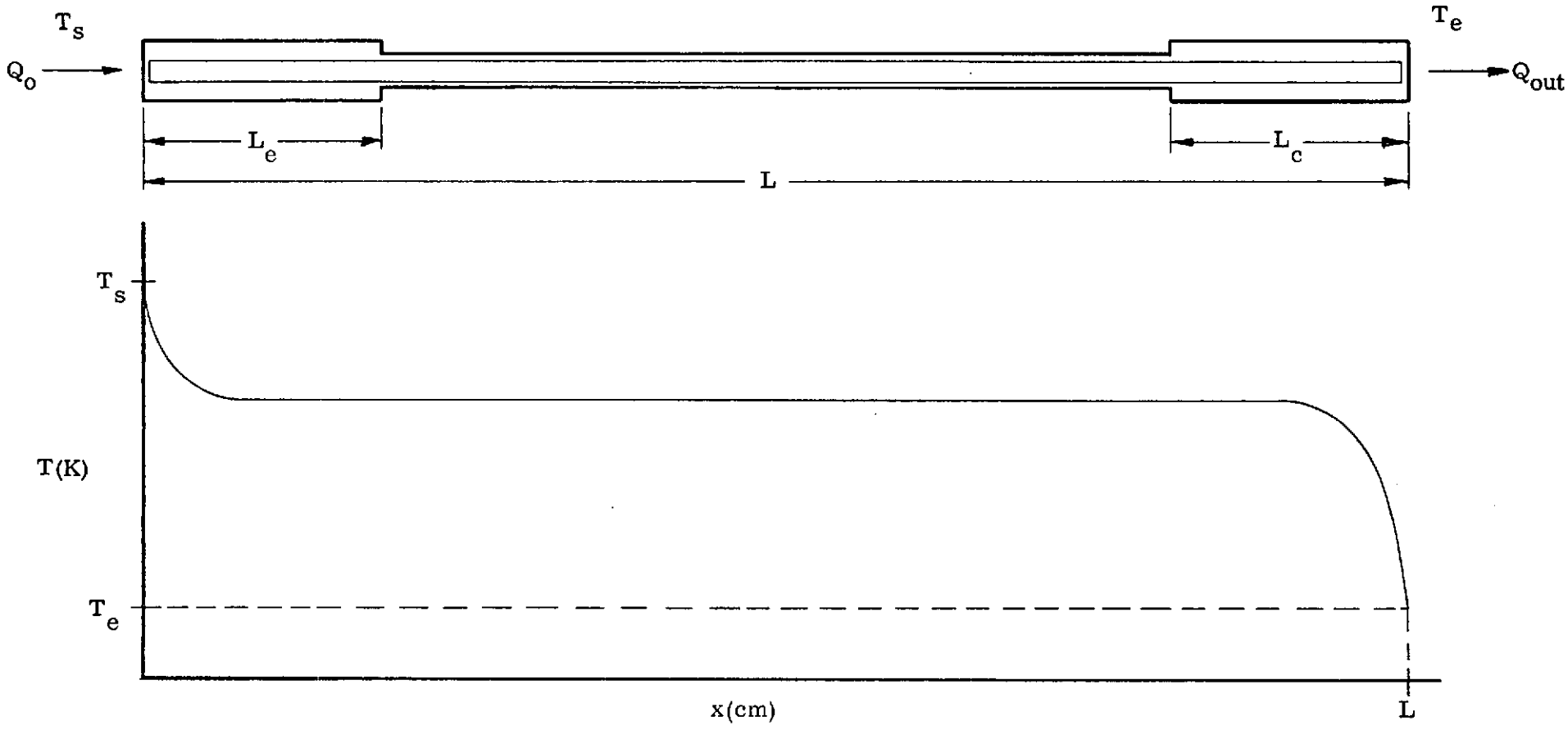

FIGURE 2.5

THREE REGION ANALYTICAL MODEL

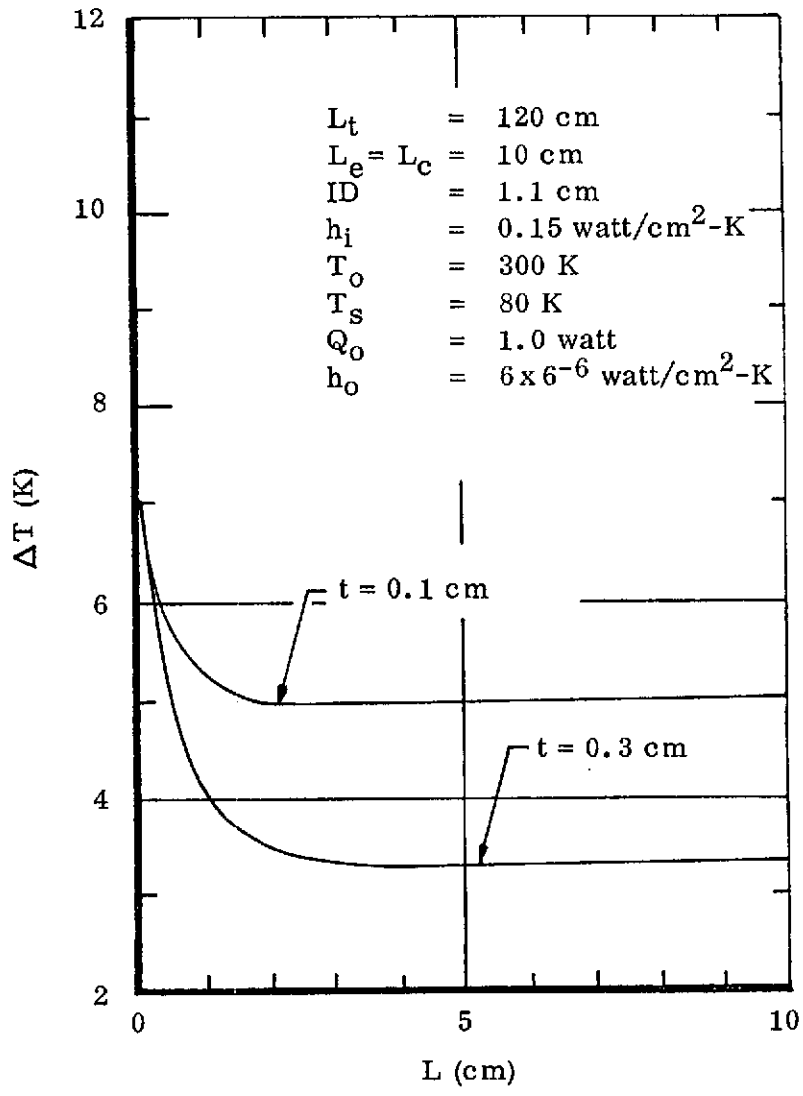

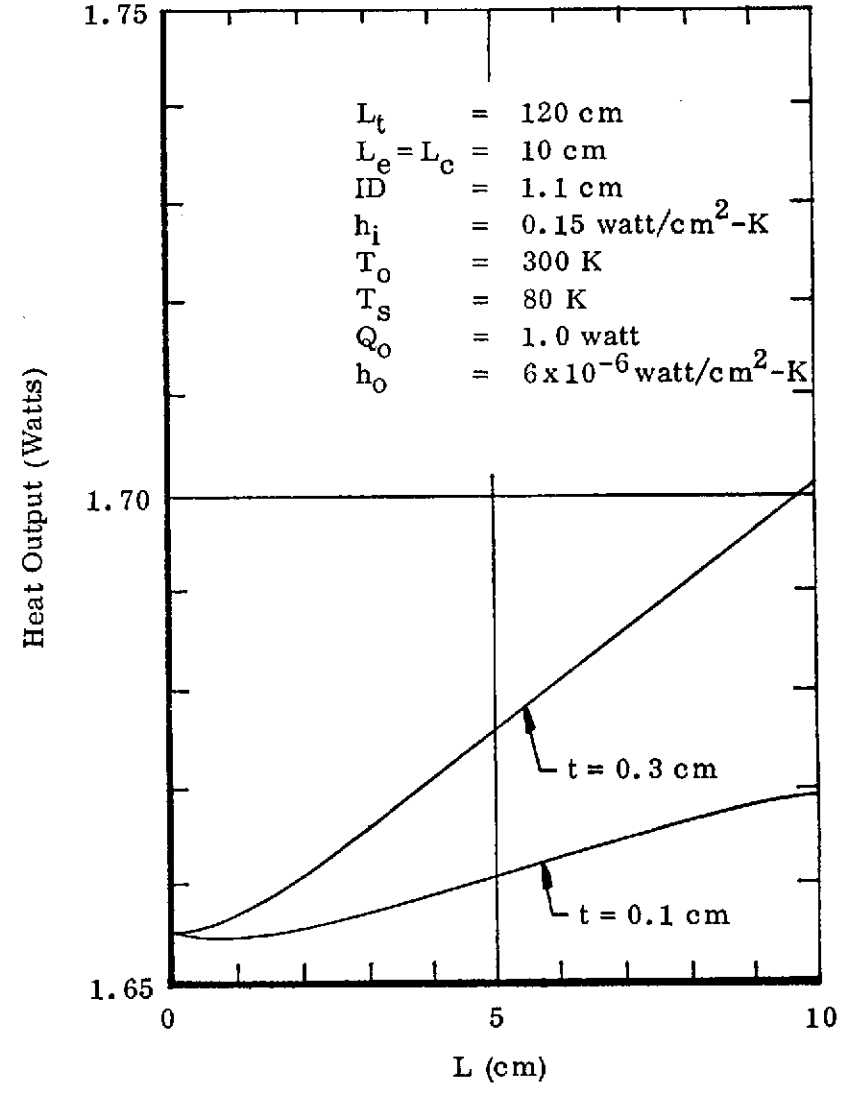

FIGURE 2.6

OPTIMIZATION OF COLLAR LENGTH

centimeters long. As the collars become thicker, the temperature drop across the condenser and evaporator decreases due to the larger cross-sectional area of heat conduction in the collar. At the same time, the effective evaporator and condenser lengths (defined by the rapidly changing temperature regions) become longer as the thickness of the collars increases. For a fixed heat input, the vapor temperature increases as a direct result of the smaller temperature drop at the evaporator, and the overall ΔT across the heat pipe decreases. The heat output at the condenser end, as determined by the temperature gradient at that end of the heat pipe, increases with greater collar thickness due to the increased outer surface area exposed to the ambient environment.

The gross effect of varying the length of evaporator and condenser collars on the overall ΔT and the heat output (both collars of equal length and thickness) is illustrated in Figure 2.6. Starting with a long collar the temperature drop remains essentially constant until the collar length equals the actual length over which heat is entering the vapor. Beyond this point, the temperature drop increases rapidly. The heat output for the two cases decreases as the collar is shortened because of a decrease in surface area for transfer of parasitic heat into the system. The optimum length of collar is a trade-off between weight, heat output, and overall temperature drop. The particular application for a cryogenic heat pipe will determine the criteria for choosing the optimum length collar. In Section 4, where a design of a cryogenic heat pipe is developed, specifications are presented which allow such an optimization to be made.

2.2 Heat Transport Analysis

The heat transport analysis considered the hydrodynamic aspects of the heat pipe using two separate digital computer codes. First, the "Heat Pipe Analysis and Design" (HPAD) code was used to make a preliminary selection of a wick based on uniform heat load. The selected design was then further evaluated for the nonuniform heat load conditions consistent with the results obtained in the heat transfer portion (Section 2.1). This was accomplished using the Cryogenic Heat Pipe Transport Analysis (CRYOTA) computer code. Basically, this latter program solves two first order ordinary differential equations which describe the vapor and liquid pressure drops in

the heat pipe. Since the radial heat inputs vary along the pipe, the pressure balance must be satisfied by numerical integration. To perform this task, a fourth order Runge-Kutta method has been incorporated into the program. A pressure balance on a control volume requires that:

$$\begin{bmatrix}\text{net}\\ \text{capillary}\\ \text{head}\end{bmatrix} = \begin{bmatrix}\text{liquid}\\ \text{pressure}\\ \text{drop}\end{bmatrix} + \begin{bmatrix}\text{vapor}\\ \text{pressure}\\ \text{drop}\end{bmatrix} + \begin{bmatrix}\text{body force}\\ \text{head}\\ \text{(if any)}\end{bmatrix}$$

$$\Delta P_c = \Delta P_l + \Delta P_v + B.F.$$

The above equation can be written in differential form:

$$\frac{dP_c}{dx} = \frac{dP_l}{dx} + \frac{dP_v}{dx} + \rho_l \, g \, \text{Sin}\, \phi \qquad 2\text{-}5$$

The liquid pressure drop is:

$$\frac{dP_l}{dx} = \frac{\mu_l \, \dot{m}_l (x)}{k \, A_l \, \rho_l} \qquad 2\text{-}6$$

The vapor pressure drop is given by:

$$\frac{dP_v}{dx} = \begin{cases} \dfrac{0.0655 \, \mu_v^{\,2}}{\rho_v \, R_v^{\,3}} \, (Re)^{7/4} & , \quad Re \geq 2200 \qquad 2\text{-}7 \\ \dfrac{8 \, \mu_v \, \dot{m}_v (x)}{\rho_v \, A_v \, R_v^{\,2}} & , \quad Re < 2200 \qquad 2\text{-}8 \end{cases}$$

where:
$$\frac{d\dot{m}_v (x)}{dx} = \frac{d\dot{m}_l (x)}{dx} = \frac{Q_{rad} (x)}{\lambda} \quad , \quad Re = \frac{\dot{m}_v (x)}{\pi \, \mu_v \, R_v} \qquad 2\text{-}9$$

and
ρ_l = liquid density

g = gravitational force

ϕ = tilted angle

μ_l = dynamic viscosity of liquid

k = permeability

A_l = liquid area

μ_v = dynamic viscosity of vapor

ρ_v = vapor density

R_v = hydraulic radius of vapor

Q_{rad} = radial heat flux

A flow chart, input/output information, and a listing of "Cryogenic Heat Pipe Transport Analysis" are presented in Appendix B.

The computer program "CRYOTA", which handles nonuniform heat inputs, is used to determine the cross-sectional area of the wick needed for the particular heat pipe and specified thermal load distribution. The thermal input conditions for CRYOTA are obtained as part of the output of the heat transfer analysis. First, the program checks if the vapor flow has exceeded the sonic limit. The output of the computer analysis is either "yes" or "no"; i.e., the heat pipe with the specified wick geometry either can or cannot handle the heat load applied. If the answer is yes, the program will determine the required fluid charge and, for comparison, an equivalent heat transport capability based on a uniform heat input. If the vapor flow is laminar, it will also determine an effective Heat Transport Capability Factor QL_{eff}.

As stated before, the HPAD computer code was used to analyze various wick geometries using uniform heat load. This program also determines the wall thickness necessary to contain the working fluid at a specified storage temperature and the weight of the heat pipe including fluid and wick. If a weight analysis is performed, the computer program does not take into account variations in wall thickness along the heat pipe. Thus, the weight of collars at the evaporator or condenser must be added to the weight of the heat pipe calculated using the program.

Figures 2.7 and 2.8 are examples of performance curves obtained using the HPAD computer code for one specific composite slab wick containing alternate layers of 50 and 200-mesh screen. Figure 2.7 presents the maximum heat transport capability of this design as a function of nitrogen vapor temperature for two heat pipe diameters. Figure 2.8 shows the corresponding weights of the heat pipes having maximum transport capability. The weight determination assumes stainless steel screen mesh and an aluminum heat pipe wall of uniform thickness sufficient to contain the working fluid at ambient temperature with a safety factor of 2 greater than its yield strength. Notice that in Figure 2.7 the maximum transport capability occurs near the normal boiling point of the fluid (77 K for nitrogen). Also, the minimum heat pipe weight as shown in Figure 2.8 occurs near this same temperature. If similar curves are computed for other mesh sizes (the same large mesh which provides fluid flow and various fine screens which provide capillary pumping), a summary curve can be plotted which illustrates the effect of screen size. Figures 2.9 and 2.10 are two such curves for a nitrogen vapor temperature of 80 K. Figure 2.10 presents the weight of heat pipes designed for maximum heat transport. Note that Figure 2.10 shows very little weight reduction advantage for screen sizes greater than 300 mesh. This is due to the increased wall thickness needed to contain the fluid at ambient temperature.

Typical performance curves for an arterial wick are shown in Figures 2.11, 2.12, and 2.13. The artery sits on the bottom of the heat pipe wall. The first curve gives the maximum transport capability of the open artery versus heat pipe elevation. The curve has been optimized for artery diameter. This curve would be used to predict the maximum elevation of the heat pipe for which the artery would prime if the heat load is known (for a cryogenic heat pipe this load is, at a minimum, the parasitic heat leak into the system). Figure 2.12 can then be used to determine the diameter of the artery which provides the required transport capability for priming at the selected elevation. The maximum heat transport of the closed artery versus artery diameter is presented in Figure 2.13. Curves are given for two screen mesh sizes. The performance of the open artery does not depend on the screen mesh but only on the diameter of the artery.

Figure 2.14 shows performance curves for an axially-grooved heat pipe. The maximum transport capability versus aspect ratio (groove depth to width ratio) is shown

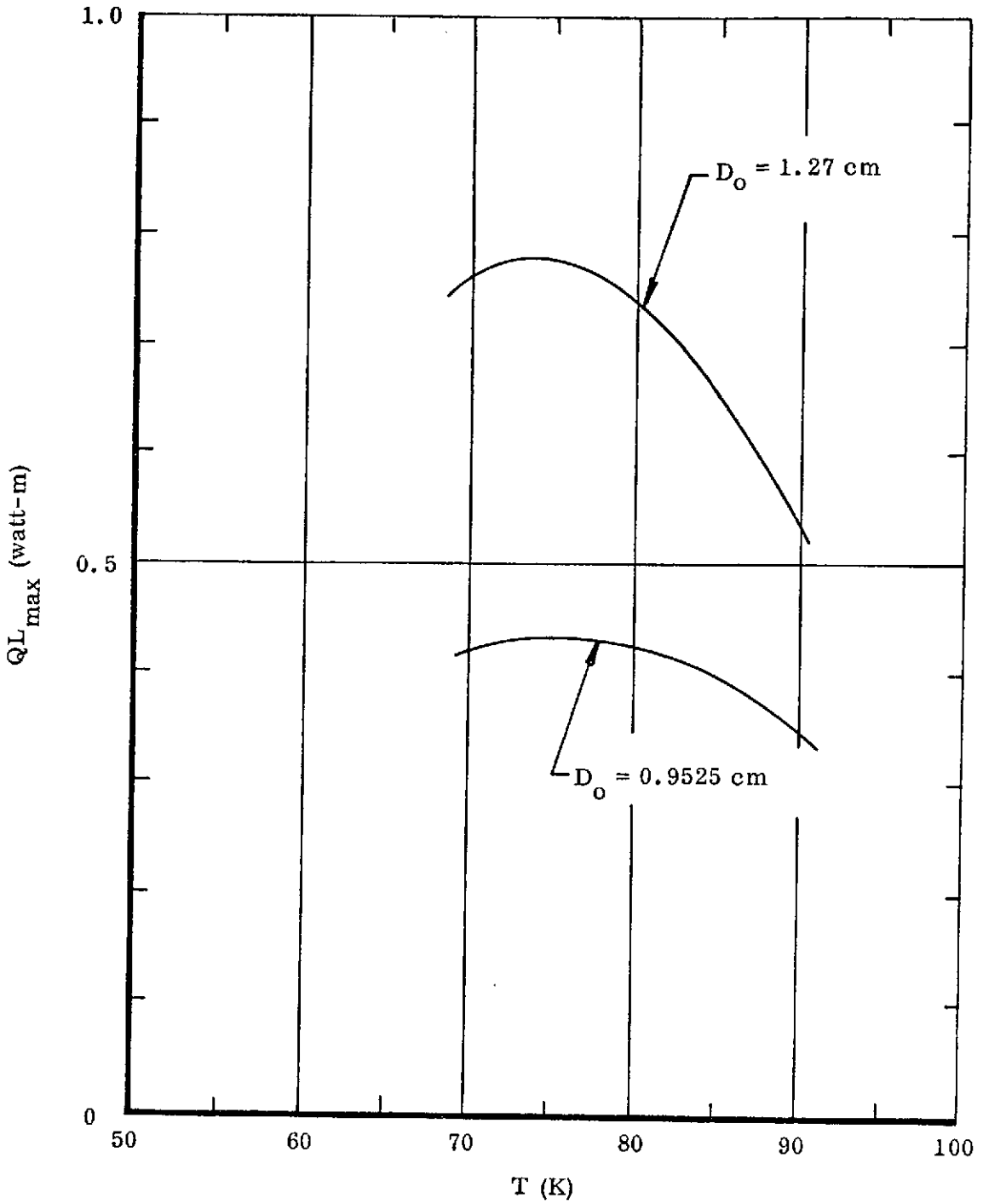

FIGURE 2.7

MAXIMUM HEAT TRANSPORT VS. N_2 VAPOR TEMPERATURE
FOR A 50/200-MESH SLAB-WICK HEAT PIPE

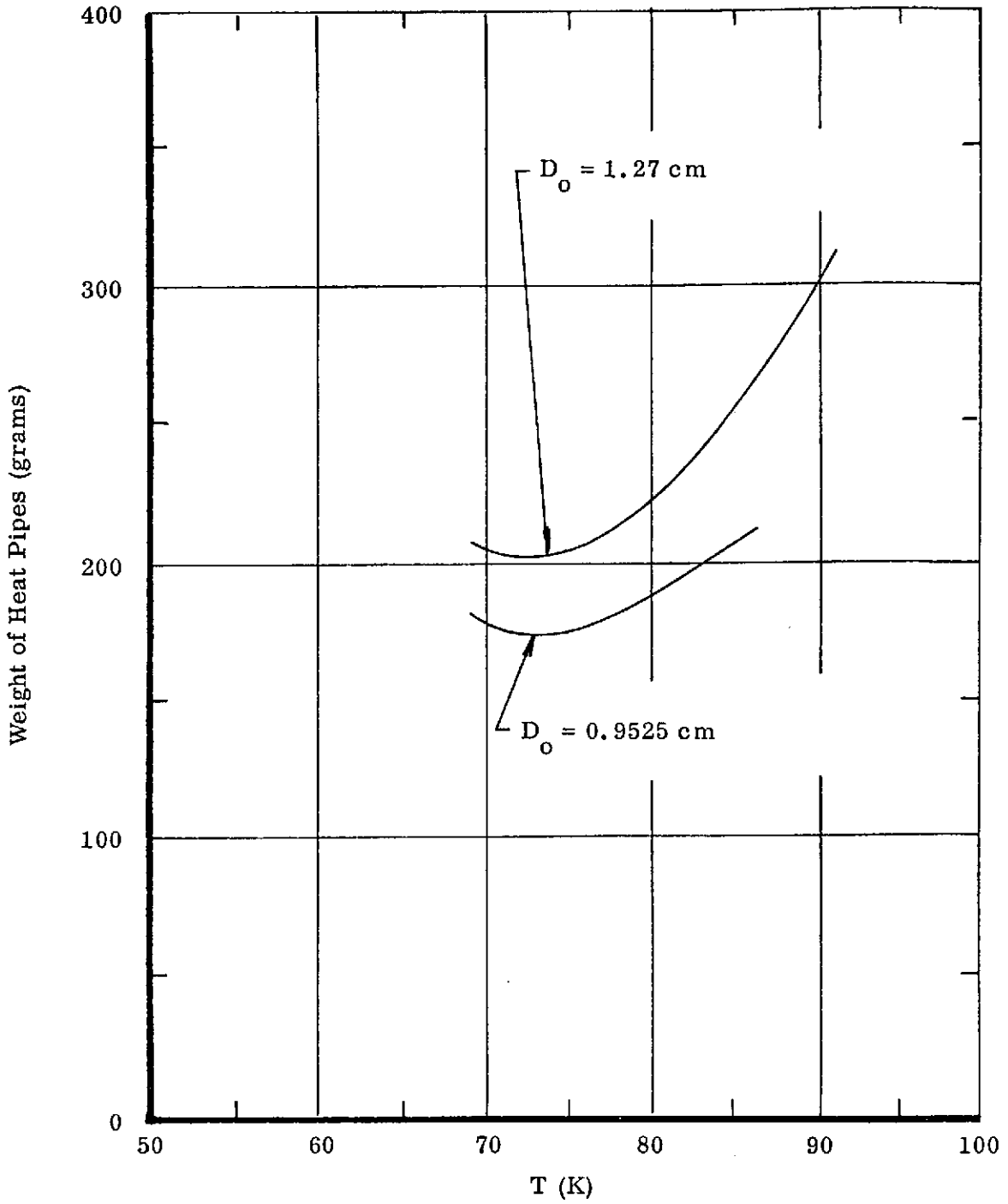

FIGURE 2.8

WEIGHT OF 50/200-MESH SLAB-WICK HEAT PIPE
WITH MAXIMUM TRANSPORT CAPABILITY

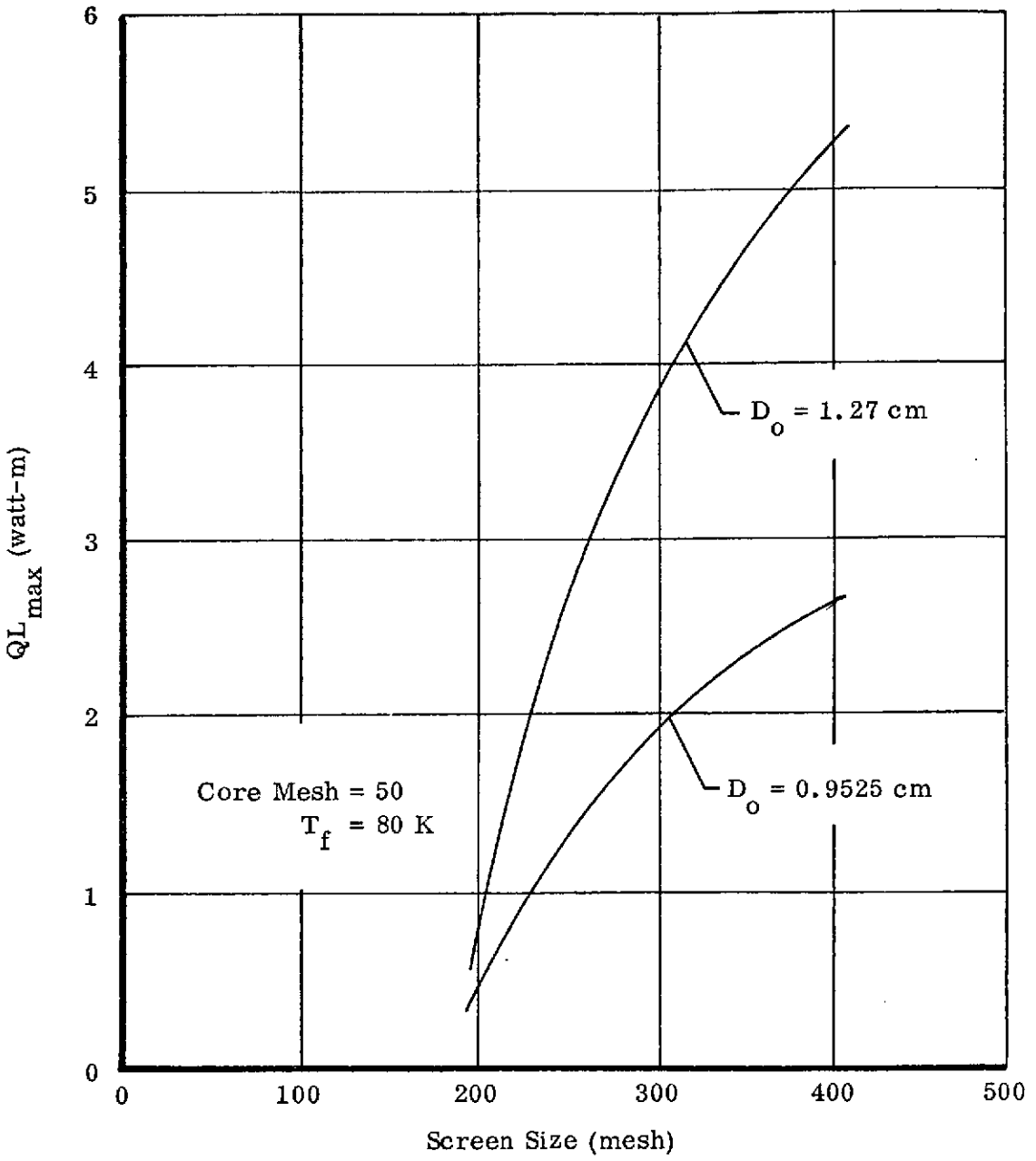

FIGURE 2.9

MAXIMUM HEAT TRANSPORT FOR N_2 COMPOSITE SLAB-WICK HEAT PIPES VS. MESH SIZE OF FINE SCREEN

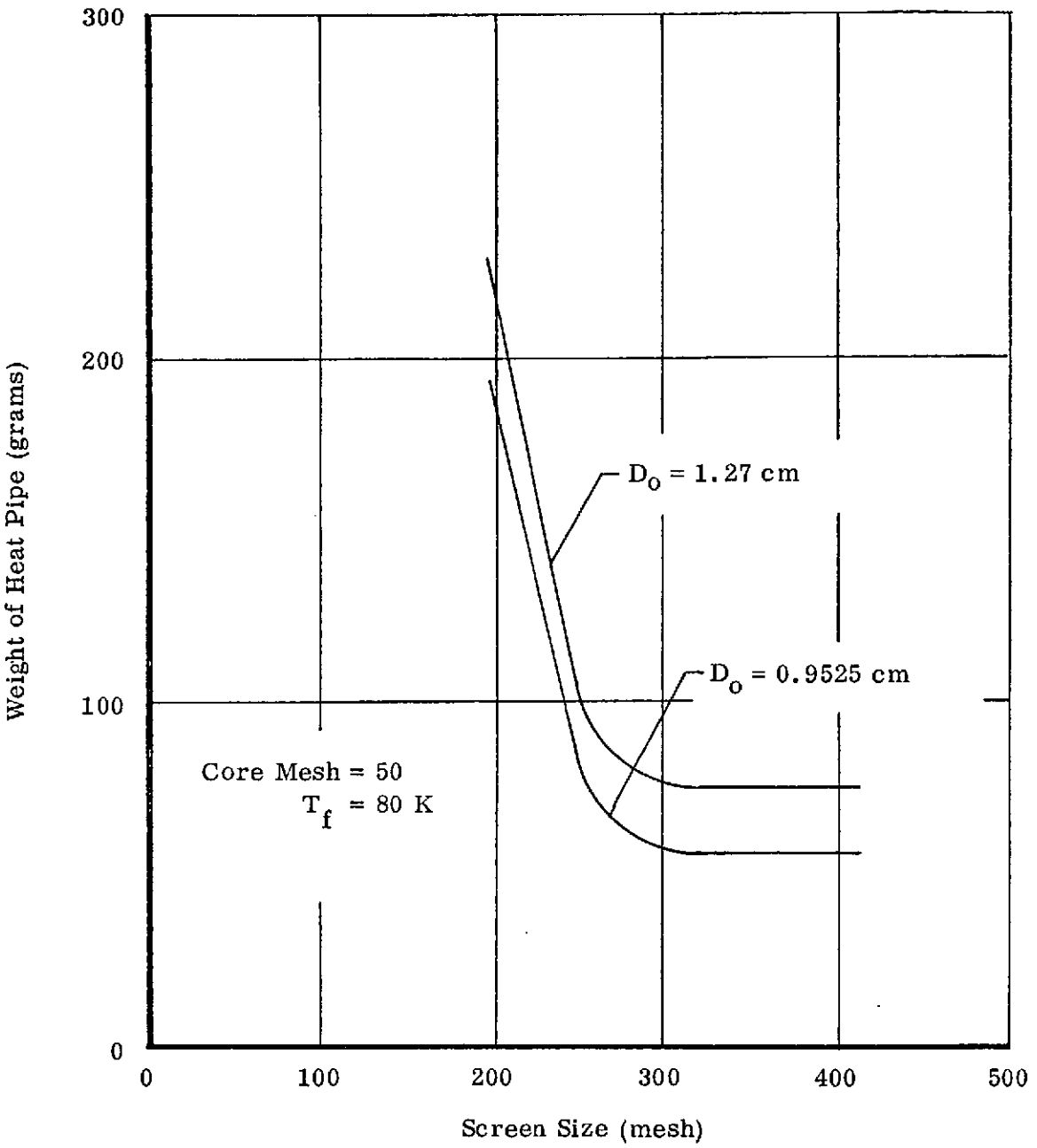

FIGURE 2.10

WEIGHT OF OPTIMIZED N_2 COMPOSITE-WICK HEAT PIPE VS. MESH SIZE OF FINE SCREEN

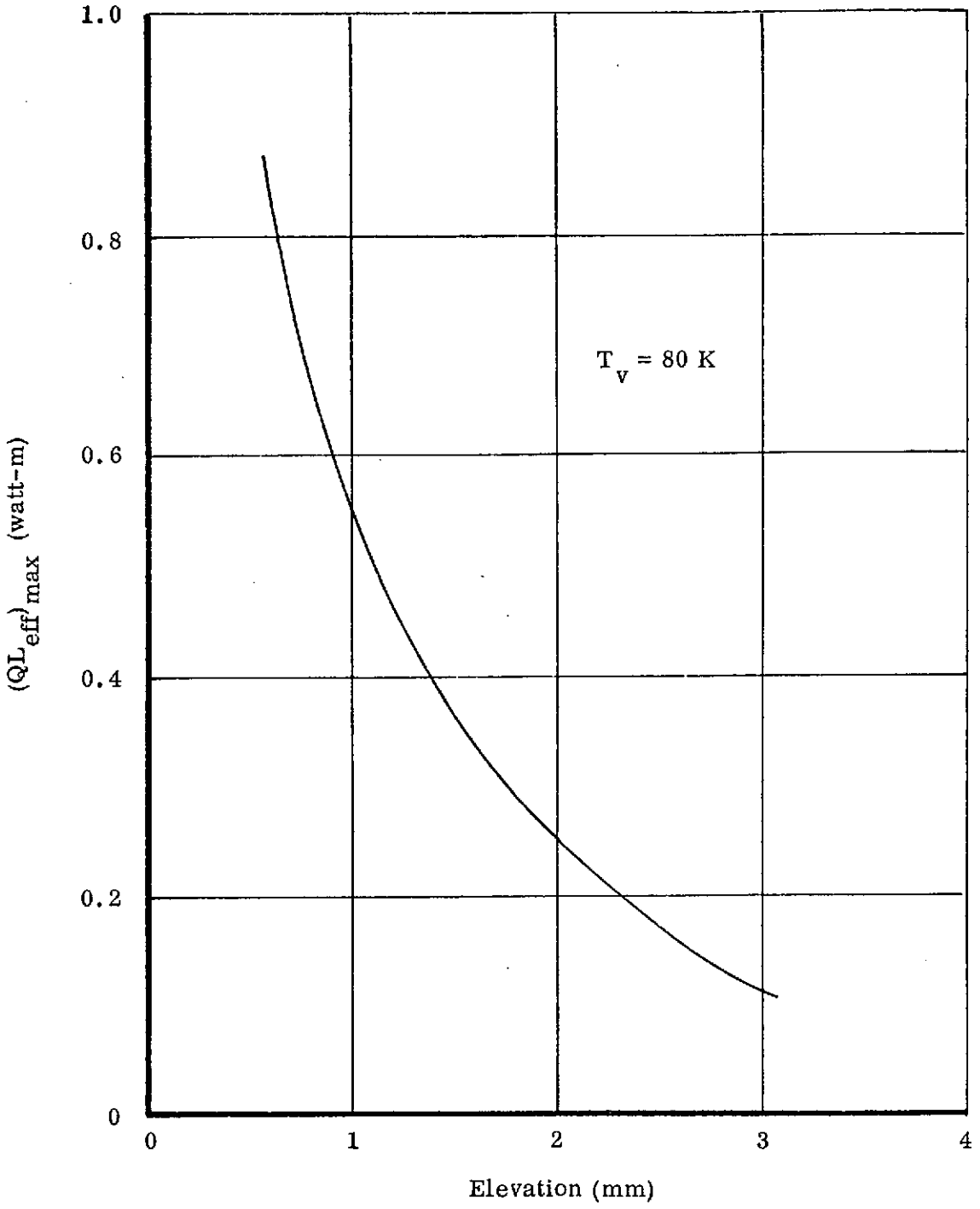

FIGURE 2.11

OPTIMIZED PERFORMANCE CURVE FOR AN N_2 OPEN-ARTERY HEAT PIPE

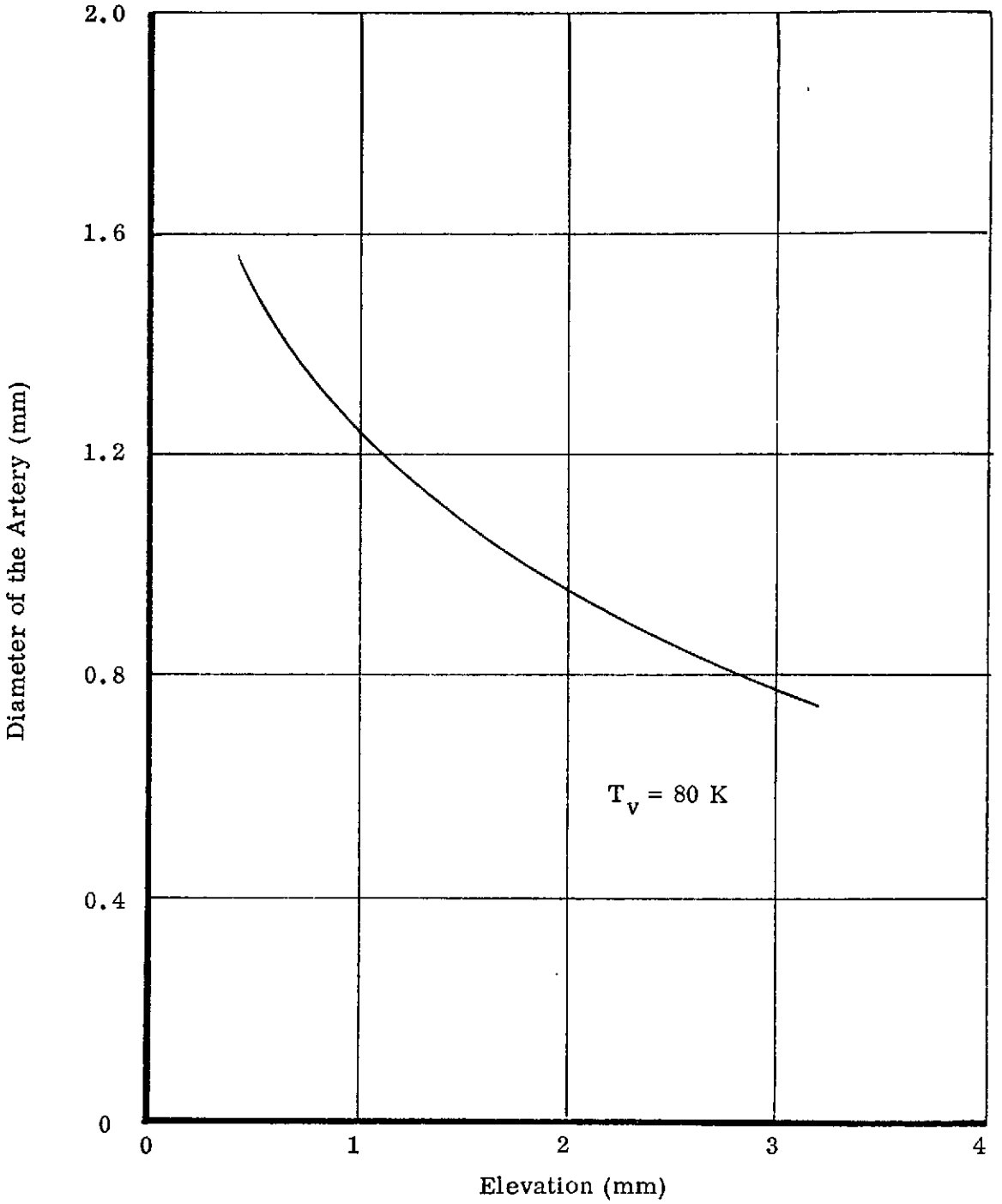

FIGURE 2.12

DIAMETER OF OPTIMIZED N_2
OPEN-ARTERY HEAT PIPE VS. ELEVATION

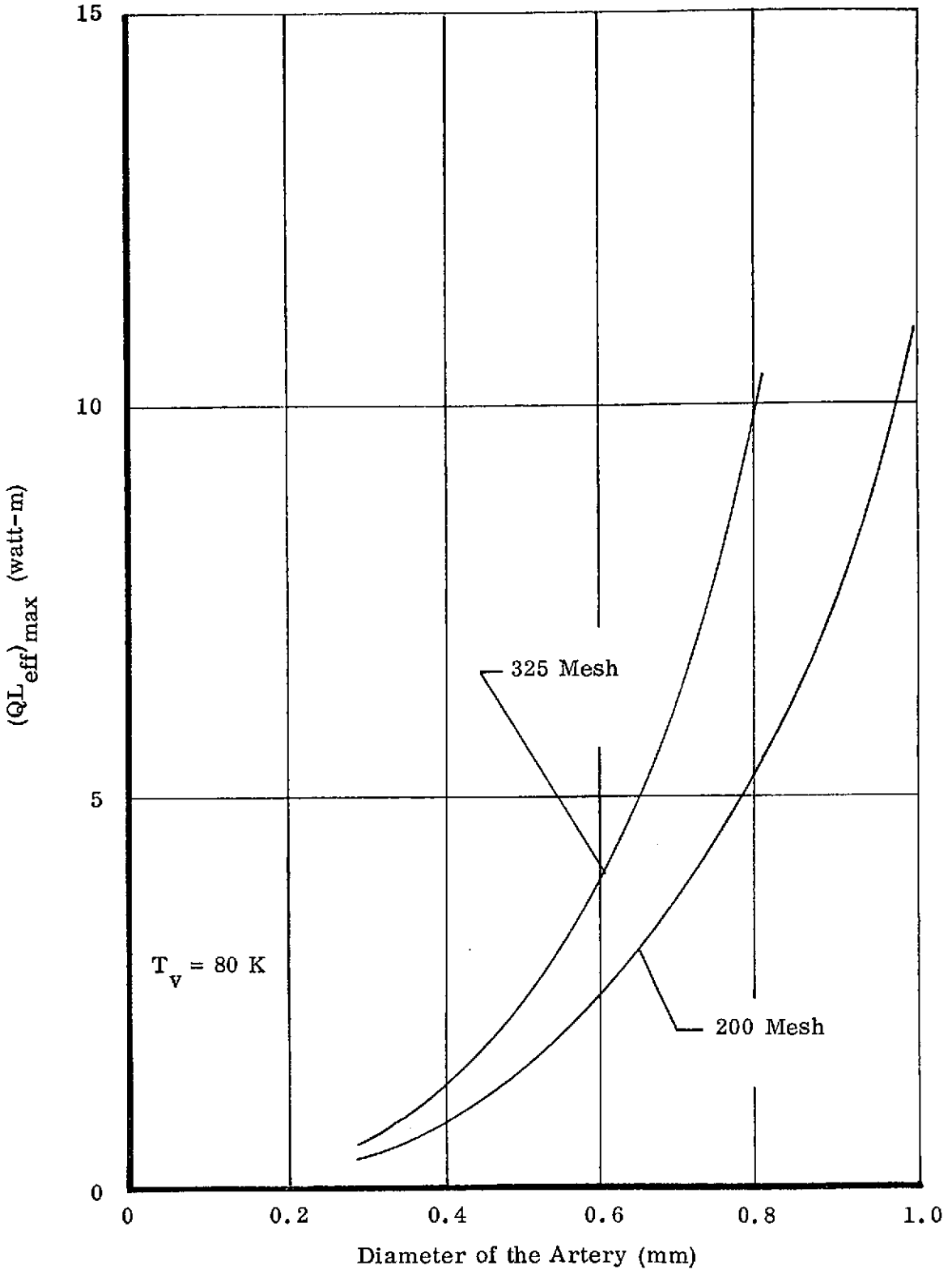

FIGURE 2.13

PERFORMANCE CURVE FOR AN N_2
CLOSED-ARTERY HEAT PIPE

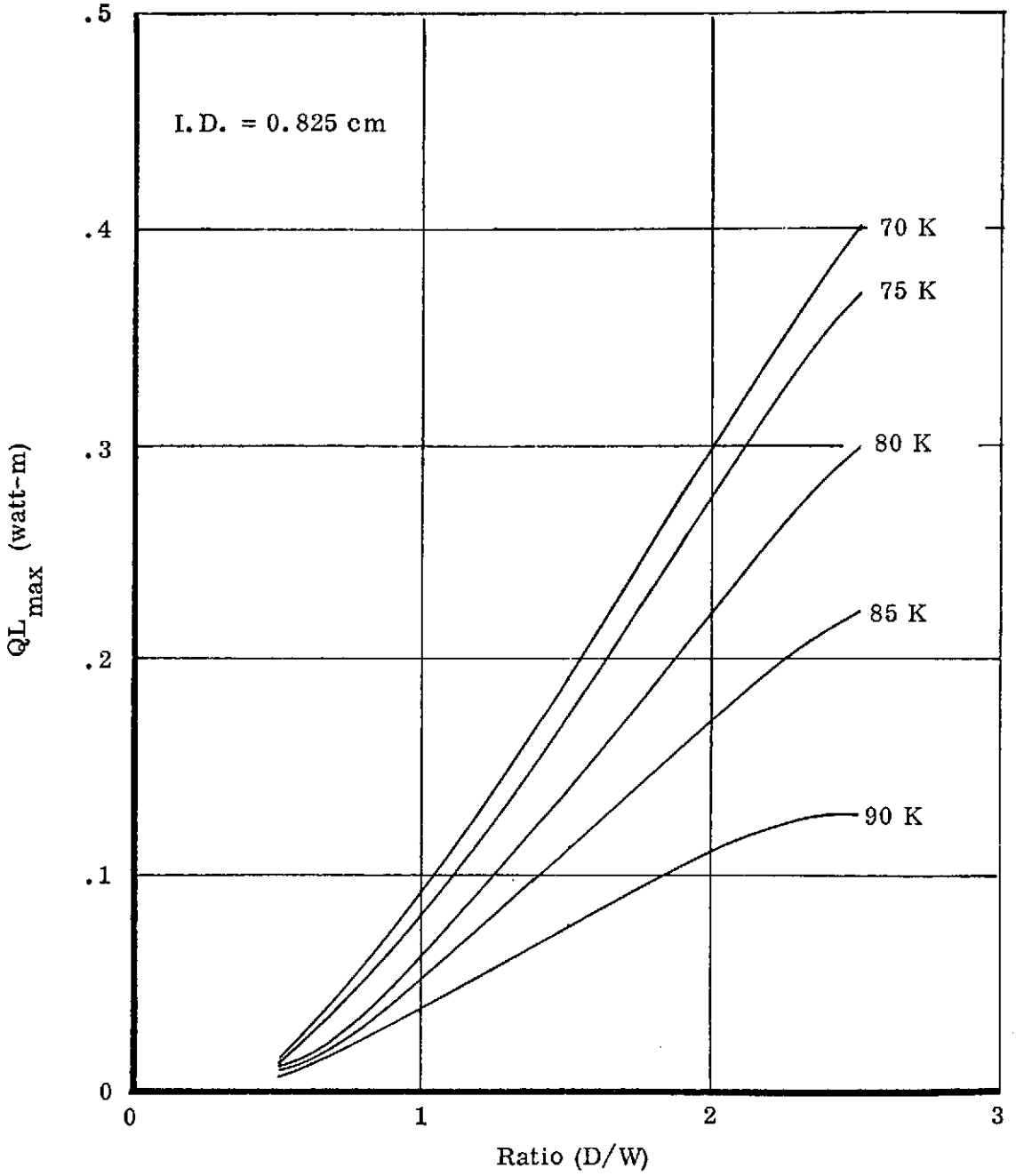

FIGURE 2.14

OPTIMIZED HEAT TRANSPORT VS. ASPECT RATIO
FOR AN AXIALLY-GROOVED HEAT PIPE

for several vapor temperatures. As expected, the greater this ratio the greater is the transport capability. The computer code also determines the optimum number of grooves and the land width for each aspect ratio.

Similar performance curves are required in a later section of this report to design cryogenic heat pipes for specific requirements.

2.3 Thermal Insulation

Adequate thermal insulation of a cryogenic heat pipe is critical because of its extremely low transport capabilities. In most cases, the parasitic heat leaks into the system are as great or greater than the heat transport requirements of the intended application. Every attempt must be made to keep these losses to a minimum by adequately insulating the heat pipe.

The effectiveness of NRC-2 multilayer superinsulation was studied for use with these heat pipes.[1] This type of insulation is frequently used for cryogenic applications. The heat leak was determined for various thicknesses of insulation. A gold-plated radiation barrier was assumed to minimize the heat leaks at the edges of the insulation.

Figure 2.15 illustrates the configuration of the NRC-2 insulation and radiation barrier around the cryogenic heat pipe. The heat leaks associated with this insulation system are the thermal losses radially through the insulation and the end losses associated with the radiation barrier. Ambient temperature is taken to be 300 K, and the heat pipe and thermal barrier are assumed to be at 80 K. For NRC-2 insulation, a minimum conductivity of 4.15×10^{-7} watt/cm-K can be achieved at a packing density of 60 layers per cm. The governing equation for radial heat conduction from a cylindrical tube through the insulation is:

$$\frac{Q}{L} = \phi\left(\frac{T_f}{T_i}\right) \frac{2\pi k_{min} (T_i - T_f)}{\ln\left(\frac{r_o}{r_i}\right)} \qquad 2\text{-}10$$

[1] NRC-2 Superinsulation Data Sheet; Metallized Products Division of King-Seeley Thermos Company

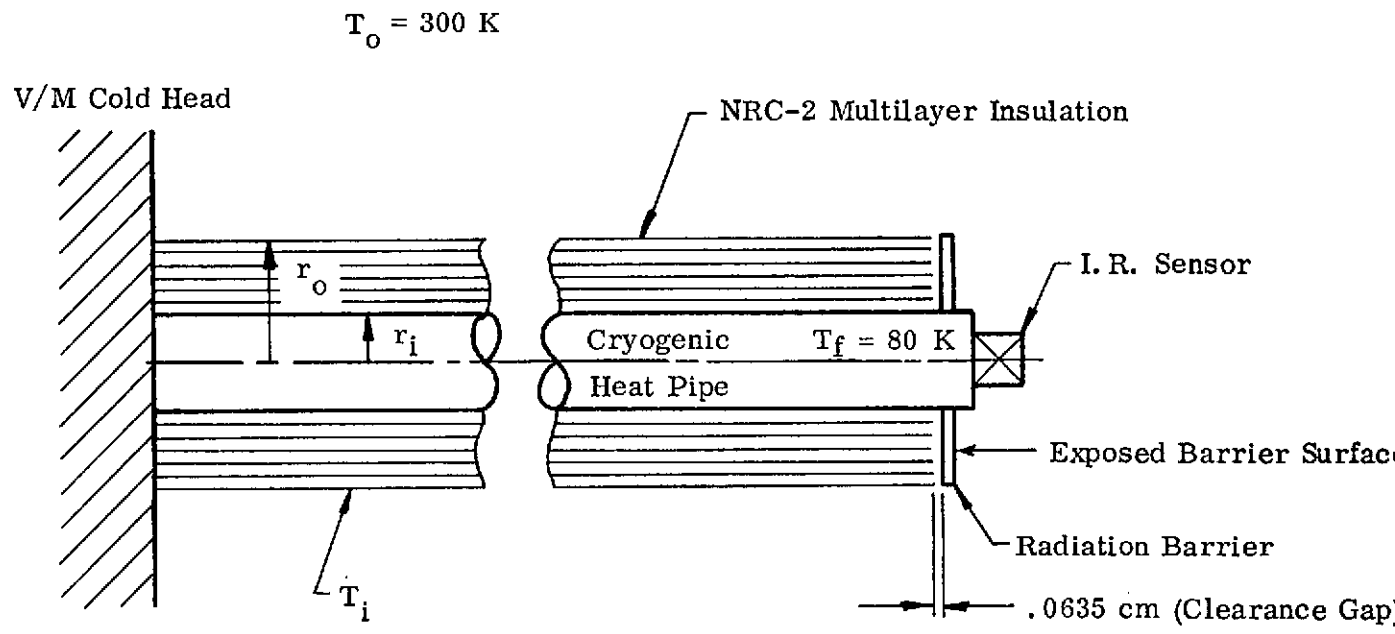

FIGURE 2.15

INSULATION SYSTEM FOR CRYOGENIC HEAT PIPE

where $\phi\,(T_f/T_i)$ is a correction factor for NRC-2 insulation, T_f is the heat pipe temperature, and T_i is the temperature of the outer wrap of insulation. The heat loss, due to radiation from the outer layer of the insulation, must equal the conduction term above. An iteration shows that $T_i \approx T_o$ where T_o is the ambient temperature of the surroundings. With this approximation, the above equation can be solved for various values of r_o/r_i. Figure 2.16 summarizes the results. The heat leak through the insulation decreases with increasing ratios of r_o/r_i.

The radiation heat leak associated with the barrier shown in Figure 2.15 is the sum of the radiation into the clearance gap ($\epsilon = 1.0$) and the radiation to the exposed surface of the barrier ($\epsilon = 0.05$). Figure 2.17 summarizes the total heat leak for various heat pipe diameters and ratios r_o/r_i. The barrier has been assumed to be isothermal and at the heat pipe temperature. The results shown in Figures 2.16 and 2.17 indicate that the lowest total heat leak exists for the smallest heat pipe diameter. Obviously, minimum practical heat pipe diameter is determined by the heat transport requirements and by fabricability.

2.4 Method of Design Selection

In order to arrive at a cryogenic heat pipe design, several initial specifications are necessary. Because of the characteristics of the VM engine, it is desirable to specify both the temperature at the condenser and the maximum amount of heat to be rejected. The total length of the heat pipe may also be a specified requirement. The thermal performance specification should include a description of the operation of the heat pipe, the heat input, orientation, and the maximum permissible temperature drop.

Parameters which are to be determined by the analyses are the wick configuration and size, the inside pipe diameter, minimum pipe wall thickness, and the length and thickness of the evaporator and condenser collars. Several wick structures should be investigated; and the final design will depend on factors such as cost, reliability, fabricability, and ability to meet thermal performance specifications.

The following is the design approach to be used. First, a heat transport analysis using HPAD will give performance curves (similar to those shown in Section 2.2)

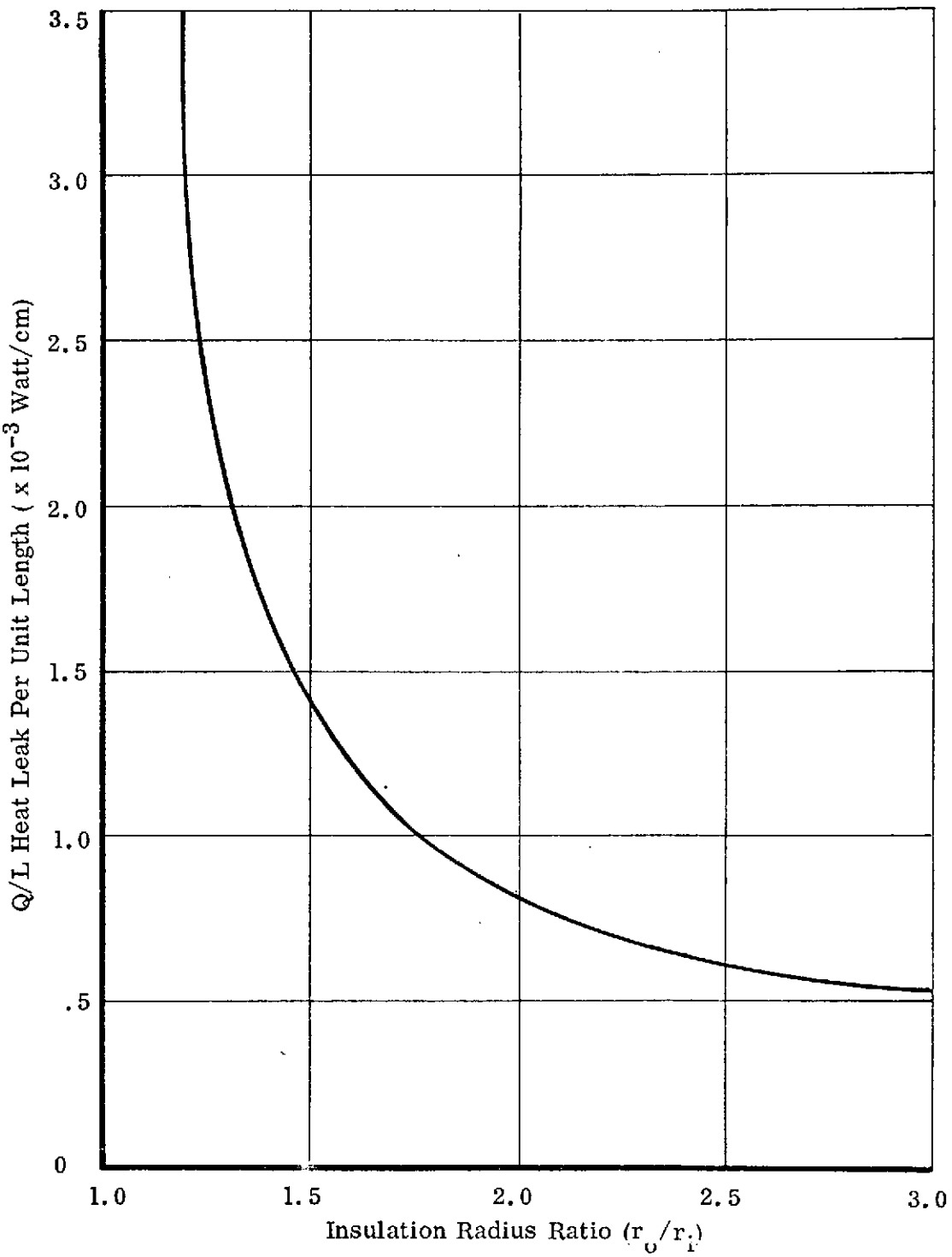

FIGURE 2.16

RADIATION HEAT LEAK VS. INSULATION RADIUS RATIO

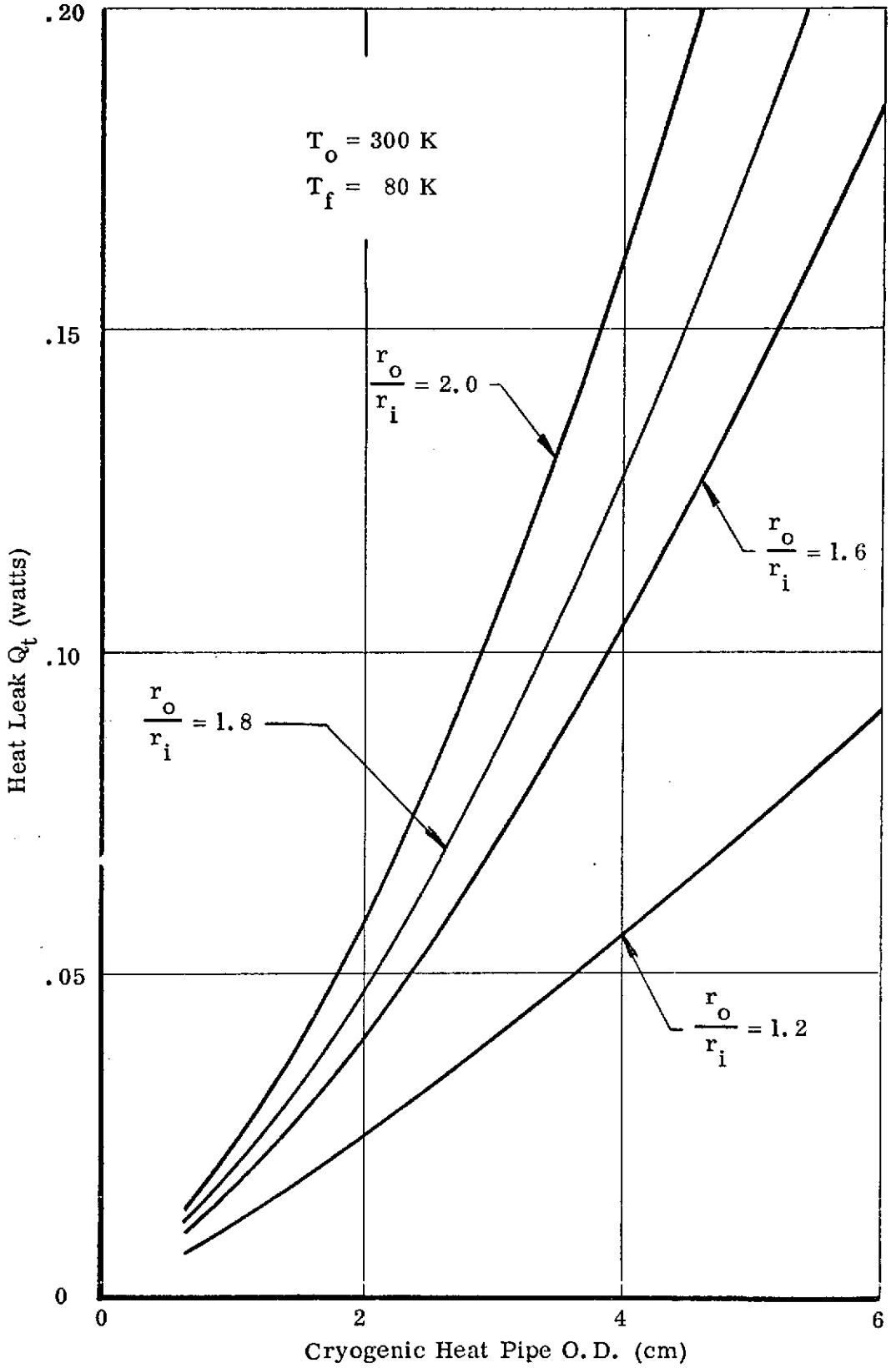

FIGURE 2.17

INSULATION EDGE HEAT LEAK Vs. HEAT PIPE O.D.

for each wick structure under investigation. After a wick structure which best meets the specifications has been selected, the inside diameter of the heat pipe is chosen and the minimum wall thickness is determined by the pressure containment requirements.

CRYOTHERM is utilized to determine the remaining design parameters. Film coefficients, necessary to perform the analysis, must be supplied by independent measurement or by separate analysis. The parasitic heat leaks through the insulation and the supports are represented by external film coefficients. The thermal analysis yields thermal profile curves similar to those shown in Section 2.1. The minimum evaporator and condenser lengths are not sensitive to collar thickness; therefore, each can be optimized independently. The collar thickness must be selected based on the specific requirements. Larger collar thicknesses lower the total temperature drop at the expense of increased weight and amount of heat rejected. As a final step, CRYOTA is employed to verify that the heat pipe with the selected wick design operates with the nonuniform heat input determined by the heat transfer analysis.

3. BREADBOARD EXPERIMENTS

Four cryogenic heat pipes were fabricated and tested in this phase of the program. One heat pipe had an axial-grooved wick and the remaining three contained various forms of slab wicks.

There were several reasons for conducting these breadboard tests. Comparisons of experimental and analytical results were necessary to verify the analytical models. In some cases, certain parameters, which could only be arrived at experimentally, were also needed to make correct analytical predictions. For the cryogenic heat pipes, the evaporator and condenser film coefficients had to be experimentally determined. To a lesser extent, this technique was also needed to determine wick properties, such as minimum pumping radius and permeability. Because of the varied techniques in producing or forming various wick structures, the standard analytical approach for determining these parameters may not be valid in all cases.

An additional advantage of the breadboard experiments was that they provided valuable experience in testing cryogenic heat pipes. Methods of thermocouple attachment, installation of insulation, condenser heat sinking, and cryogen charging were investigated. The techniques developed were incorporated in the testing of the prototype heat pipes.

Each heat pipe was cleaned and assembled in accordance with accepted practices. None of the heat pipes were designed to contain the internal pressure at ambient temperature. Each heat pipe was tested at several cryogen fills and therefore could not be hermetically sealed. The cryogen charge was introduced while the instrumented heat pipe was in the vacuum chamber and ready for thermal testing.

3.1 Axial-Grooved Heat Pipe

This heat pipe was 141 cm long with an outside diameter of 1.27 cm and contained 30 axial grooves along the inside surface. Each groove was 0.06 cm wide and 0.09 cm deep. The grooves were not rectangular in cross-section but were wider at the bottom than at the top, and each had an average area of 6.3×10^{-3} cm^2. Figure

3.1 shows a cross-section of the heat pipe. The evaporator and condenser lengths were 10 cm each. The pipe was constructed of 6061-T6 aluminum, and the outside surface was plated with nickel so that thermocouples and a condenser collar could be firmly attached by soldering. At each end of the heat pipe the grooves were sealed with a weld. This was done in order to isolate each groove from the others. Experimental evidence indicates that with open grooves the liquid will drain from the upper grooves when the pipe is operated in a gravity field. This drainage occurs because the liquid communicates, between all grooves, at the end of the heat pipes. Consequently, the liquid in the upper grooves must sustain a gravity head approximately equal to the tube diameter. If, on the other hand, the grooves are isolated, the characteristic height in a gravity field is of the order of the width or depth of the groove depending on its angular position on the circumference.

Figure 3.2 illustrates schematically the heat pipe and its instrumentation for testing within the vacuum chamber. The heat pipe was mounted on a support frame and leveled after inserting the frame into the vacuum chamber. The orientation of the pipe was changed by adjusting the leveling pads supporting the entire vacuum chamber. The elevation was measured using a surveyor's transit to sight on two machinists' scales positioned at opposite ends of the chamber. A blanket, consisting of sixteen wraps of super insulation, was wrapped around the pipe along its entire length and around the liquid nitrogen reservoir. Tests were conducted with and without this insulation to determine its effectiveness.

The procedure for charging the pipe consisted of first filling the liquid nitrogen reservoir in order to cool the condenser end of the heat pipe. A relatively large and precisely metered storage volume was then pressurized to a predetermined nitrogen pressure. A known mass of gas was, therefore, contained within the storage tank. The gas was then released into the heat pipe where it condensed on the cold condenser walls and slowly filled the grooves. The change in pressure within the storage reservoir was proportional to the mass of nitrogen entering the heat pipe. In addition to the mass of nitrogen required to fill the grooves, the heat pipe charge must provide for the mass of the vapor needed to fill the vapor volume of the heat pipe. The mass of vapor needed to fill the volume of all the connecting tubing, valves, and gauges back to the valve between the pipe and storage

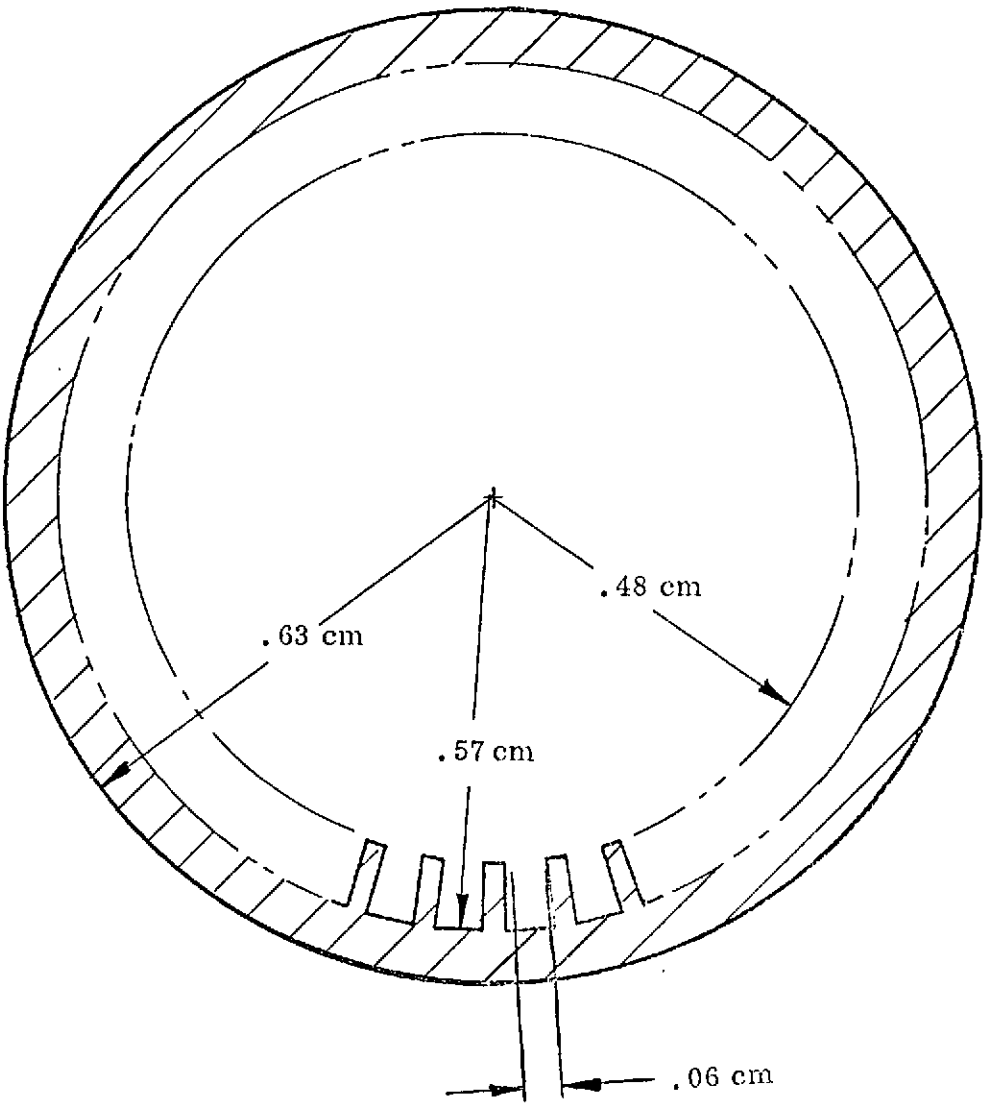

FIGURE 3.1

CROSS-SECTION OF AXIAL-GROOVED HEAT PIPE

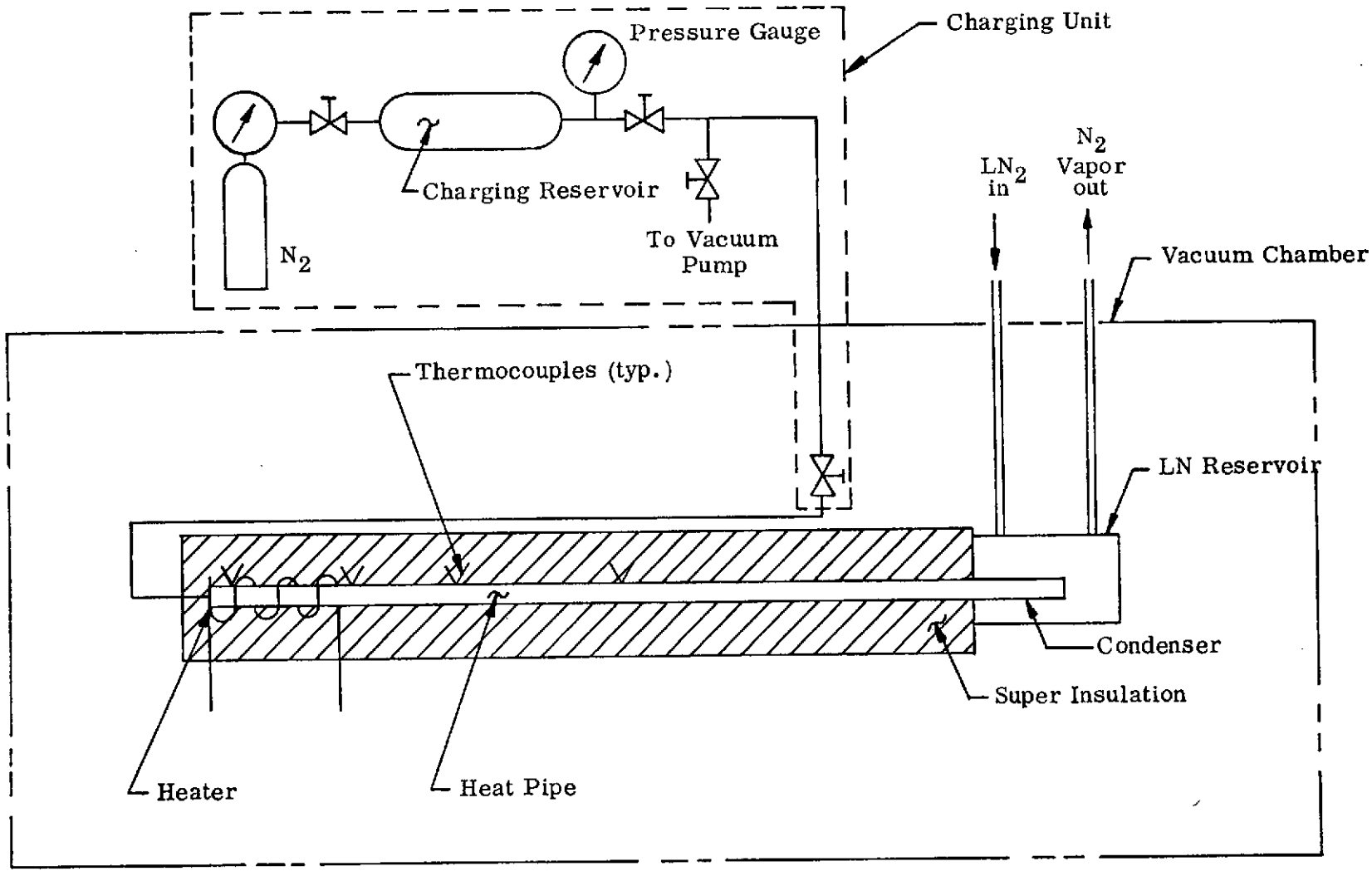

FIGURE 3.2

CHARGING AND TEST SETUP FOR CRYOGENIC BREADBOARD HEAT PIPE

volume must be accounted for. However, this correction is small, amounting to only about 3% of the total charge. A charge of 21.5 grams of nitrogen corresponds to a 100% fill of the grooves.

Observations of start-up of the pipe during the charging procedure indicate the heat pipe becomes isothermal over a progressively longer portion of its total length as the grooves slowly fill with fluid. The rate of cooldown depends, to a great extent, on the rate at which the cold reservoir can remove heat from the condenser and on the thermal mass of the heat pipe system. For the geometry of this experiment where the condenser is surrounded by a bath of liquid nitrogen, this heat removal is much greater than that which could be achieved in a VM engine.

The heat pipe was tested in a horizontal orientation and at several negative (evaporator above condenser) elevations up to 0.56 cm. Tests were conducted with fluid charges corresponding to 95%, 110%, and 120% of the theoretical fill.

The maximum measured heat transport capability versus elevation is shown in Figure 3.3. Also included in the figure is the theoretical curve calculated using the HPAD computer code. The theoretical model predicts a much lower static height and a lower transport capability for the horizontal orientation. The experimental curve implies a minimum pumping radius of 1.5×10^{-2} cm while the analysis is based on one-half the groove width (3.0×10^{-2} cm) for this radius. The permeability given by the experimental curve for 110% fill is 8.0×10^{-4} cm^2, and the analysis computes a value of 1.1×10^{-3} cm^2. The difference in permeability may be partly caused by irregular variations in the groove shape along the length of the pipe. The discrepancy between the two curves could also be caused by the "puddle" effect which, if present, enhances the performance. This effect is elevation dependent, being more predominant at low elevations since at this orientation the puddle extends further towards the evaporator. The theoretical curve indicates that the grooved heat pipe is not capable of supporting a high elevation. This implies that the heat pipe performance will be extremely sensitive to even a small puddle in the condenser. The results shown in Figure 3.3 for the other fills support this argument. The underfilled data (95%) results in less puddle; hence the performance is less for the same elevation. The 120% fill data indicates higher performance and suggests a large puddle.

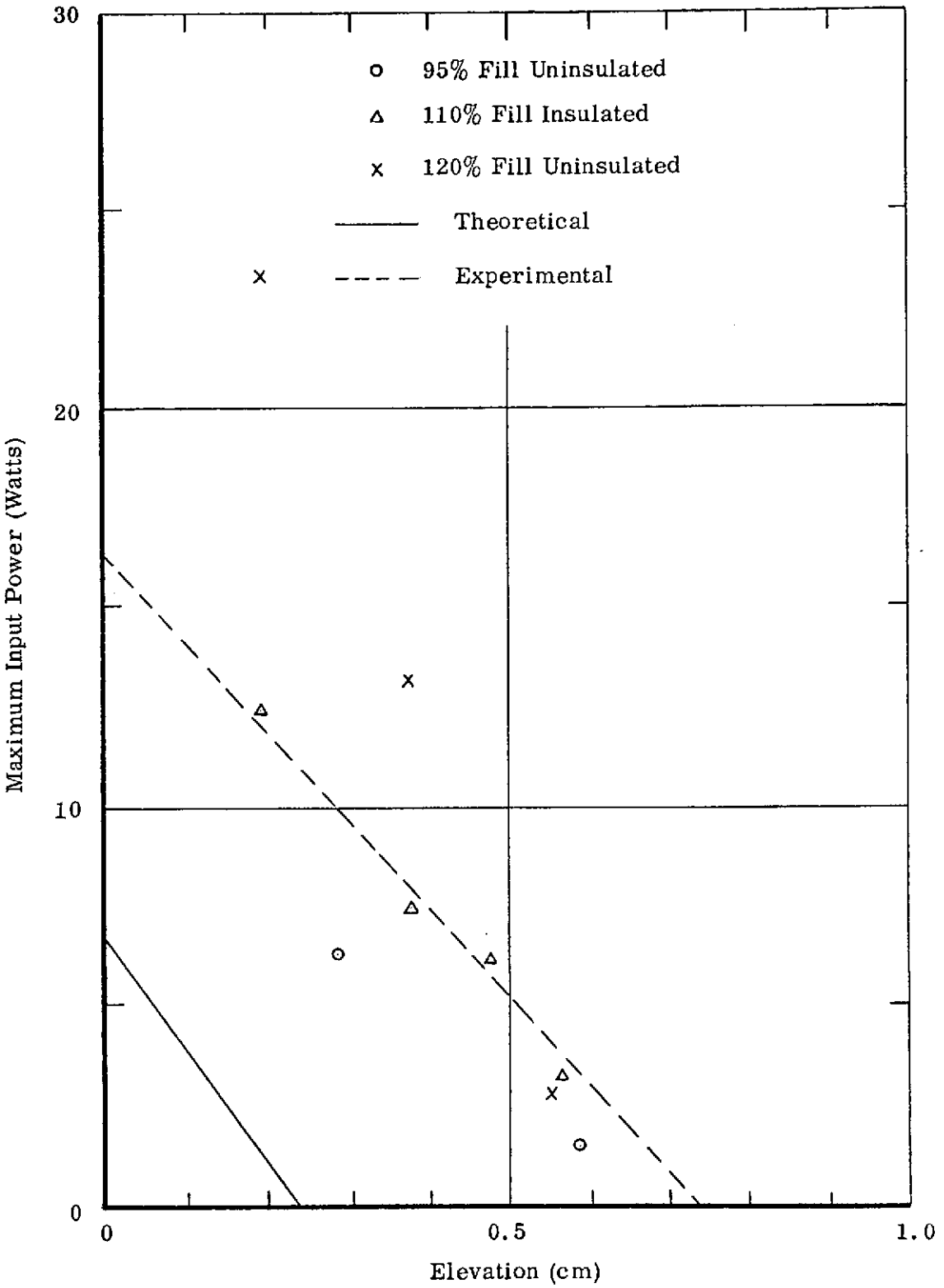

FIGURE 3.3

MAXIMUM HEAT TRANSPORT (80K) VS. TILT FOR CRYOGENIC GROOVED HEAT PIPE

In Figure 3.4 the evaporator and condenser temperature drops are plotted as a function of input heat for the insulated heat pipe. The tilt of the pipe does not have a significant effect on the trend as shown by the data points. A straight line drawn through the data can be related to a film coefficient for the respective regions of the pipe. The measured film coefficient was .0235 watt/cm^2-^{o}C for the evaporator and .206 watt/cm^2-^{o}C for the condenser.

3.2 Slab-Wick Heat Pipe #1

This heat pipe was made from 6061-T6 aluminum tubing with an outside diameter of 1.27 cm, a wall thickness of 0.089 cm, and an overall length of 91.5 cm. The inside of the tube was threaded along its entire length (19 grooves/cm, 0.01 cm deep) to provide for circumferential fluid distribution. The main wick was a centrally located porous slab wick consisting of a core of Regimesh[2] (0.159 cm thick by 0.636 cm wide) surrounded by several layers of 200-mesh screen to give a final thickness of 0.318 cm. The Regimesh core was composed of alternate layers of 100 and 200-mesh screen. Figure 3.5 illustrates the cross-section of the wick and the heat pipe instrumentation used for testing. Heat was applied by means of resistance heaters located along 10 cm of the pipe at one end. The other end was inserted 10 cm into the liquid nitrogen reservoir to provide cooling for the condenser. Thermocouples were peened into small weld beads of aluminum located on the outside of the pipe. The heat pipe was installed on the fixture and placed in the vacuum chamber for testing.

The pipe was charged with nitrogen in a manner identical to that described previously. Tests were conducted with various fluid charges and at several elevations from horizontal to -1.85 cm (evaporator above condenser). The slab wick was oriented in the vertical plane.

The heat pipe was capable of transporting 5.2 watts in the horizontal orientation and the maximum wicking height was 2.54 cm. The maximum transport capability is shown in Figure 3.6 for several elevations and fluid charges. The analytical curve shown in the figure is for a slab wick of 100 and 200-mesh screen which is similar but not quite the same configuration as the wick which was actually used.

---

[2]Trade name for sintered screen material fabricated by Aircraft Porous Media, Inc., Glen Cove, New York

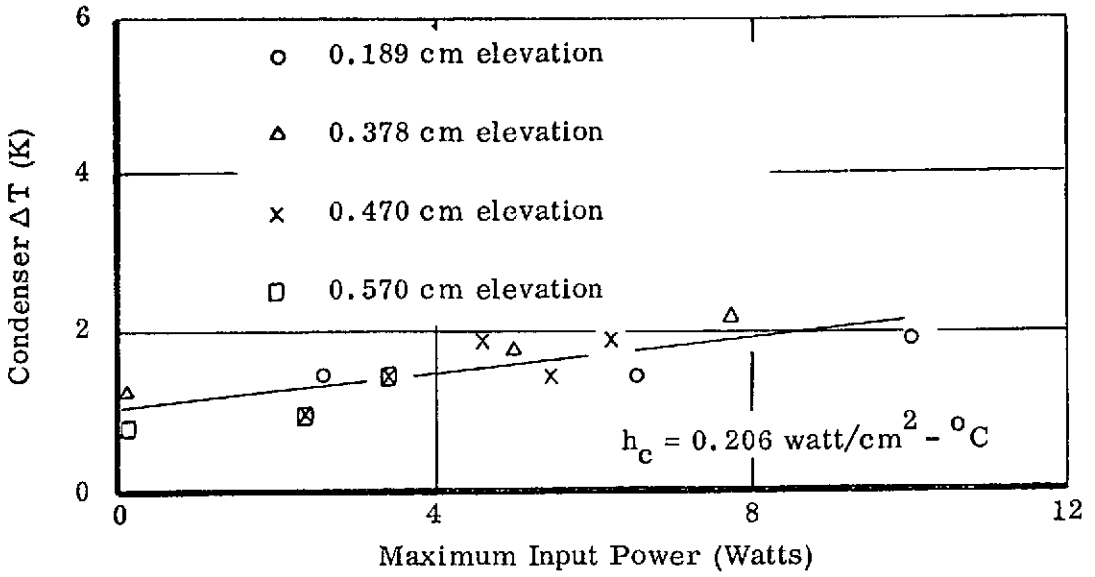

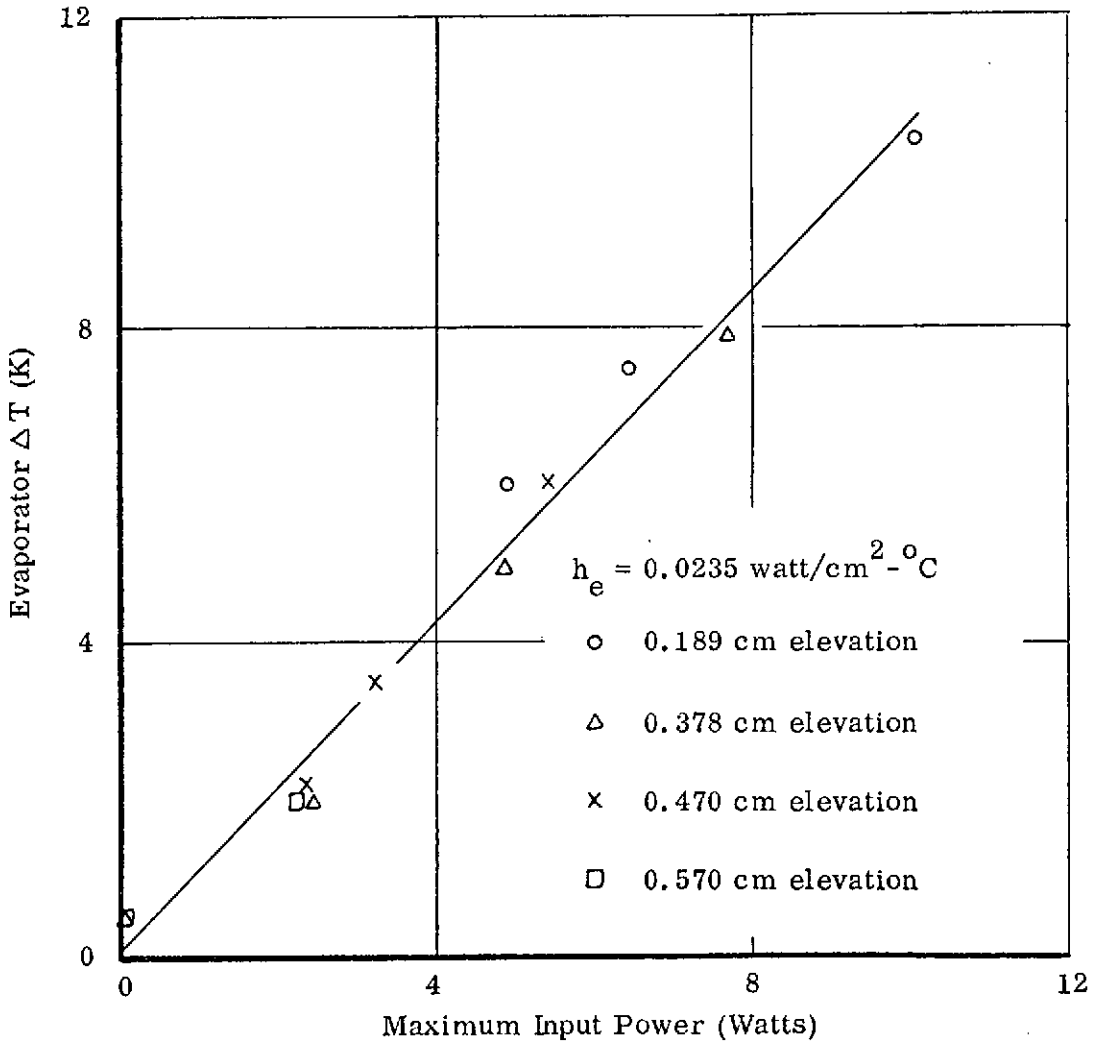

FIGURE 3.4

EVAPORATOR & CONDENSER TEMPERATURE DROPS VS. INPUT POWER

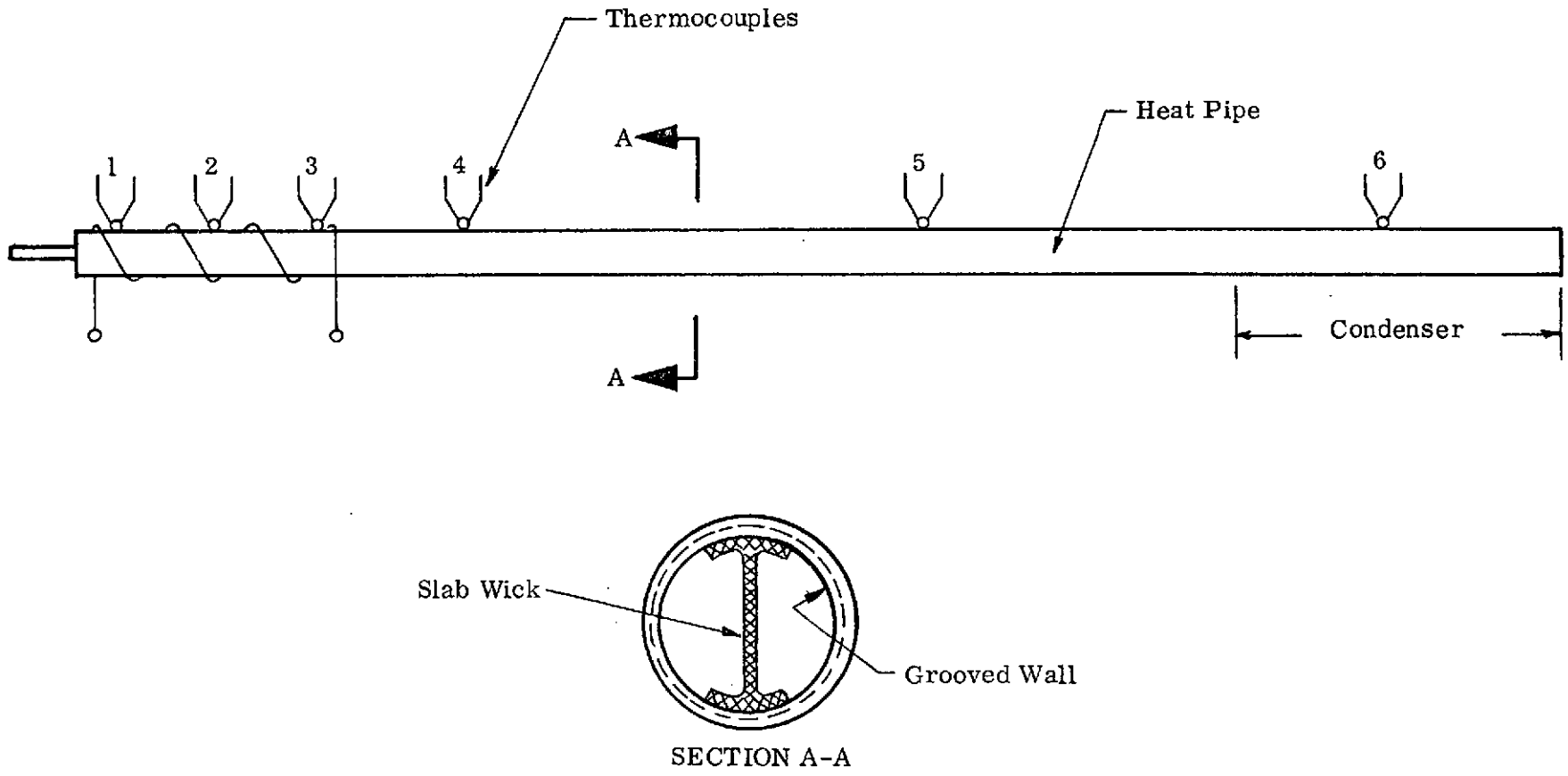

FIGURE 3.5

CRYOGENIC SLAB-WICK HEAT PIPE

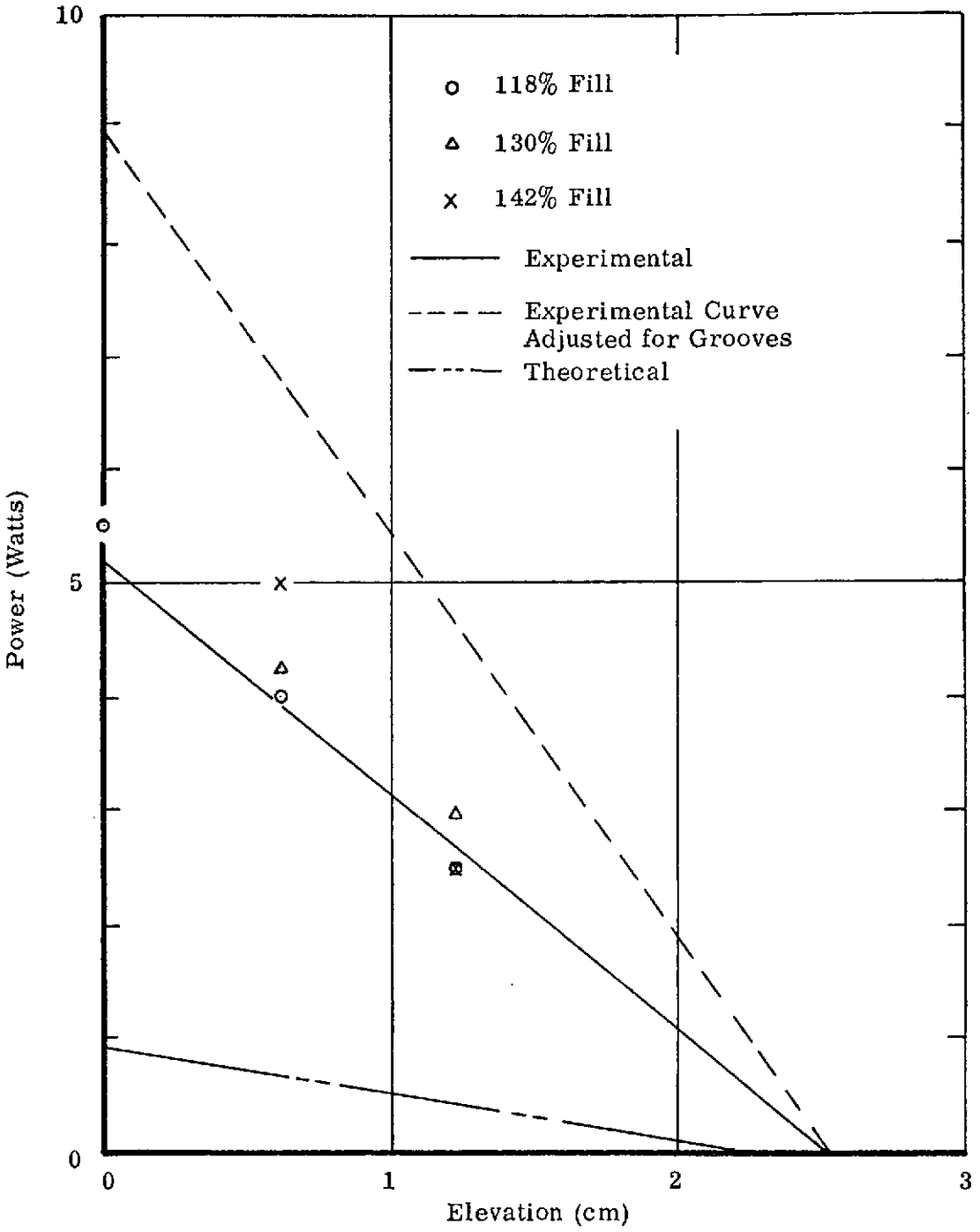

FIGURE 3.6

TRANSPORT CAPABILITY OF SLAB-WICK HEAT PIPE #1

The effect on heat transport capability of the flow resistance of the circumferential grooves was investigated in another program[3]. The transport capability can be adjusted for this effect to show the true performance of the slab wick, and this adjustment is shown in Figure 3.6. The permeability and minimum capillary radius determined from the adjusted experimental curve are 1.0×10^{-5} cm^2 and 6.2×10^{-3} cm respectively. The radius is approximately that of 200-mesh screen (6.85×10^{-3} cm) but the permeability is much greater than the theoretical value for 100-mesh screen (1.9×10^{-6} cm^2). However, the actual permeability should be greater because the 200-mesh screen also contributes significantly to the fluid flow. The two screens are relatively close in mesh size and much more 200-mesh was used in its fabrication. The measured film coefficients were 0.08 watt/cm^2-^oC for the evaporator and 0.13 watt/cm^2-^oC for the condenser.

Tests were conducted with this heat pipe to evaluate different orientations of the slab wick. Theoretically, a horizontal orientation should result in a slightly larger transport capability in a one "g" environment. The underlying assumption is that the effective static height which the wick has to support is less when the wick is oriented horizontally. However, in this orientation the fluid must be transported by the secondary circumferential threads from the puddle into the screen wick. This added liquid pressure drop in the condenser overrides the advantage of the wick orientation. Test results showed that a vertical orientation of the slab actually yielded slightly higher transport capability.

3.3 Slab-Wick Heat Pipe #2

An aluminum tube 62.0 cm long, having an outside diameter of 1.27 cm and a wall thickness of 0.089 cm, was used to fabricate this heat pipe. The same circumferential grooves were employed as in the previous slab wick heat pipe. The wick was made of alternate layers of 30 and 200-mesh stainless steel screen which was spotwelded together. The entire wick was finally completely wrapped with another layer of 200-mesh screen. Ten layers of 30-mesh and nine layers of 200-mesh screen, having a total cross-section of 0.597 cm by 1.04 cm, were used. The evaporator and condenser lengths were 10 cm each. The heat pipe was tested first with ammonia and then in the vacuum chamber with Freon-13 and nitrogen. The transport capability versus elevation is shown in Figure 3.7 for the three fluids. Table 3.1 summarizes the experimental parameters and, for

[3] DTM-73-7, "Technical Summary Report for Heat Pipe Development", July 1973

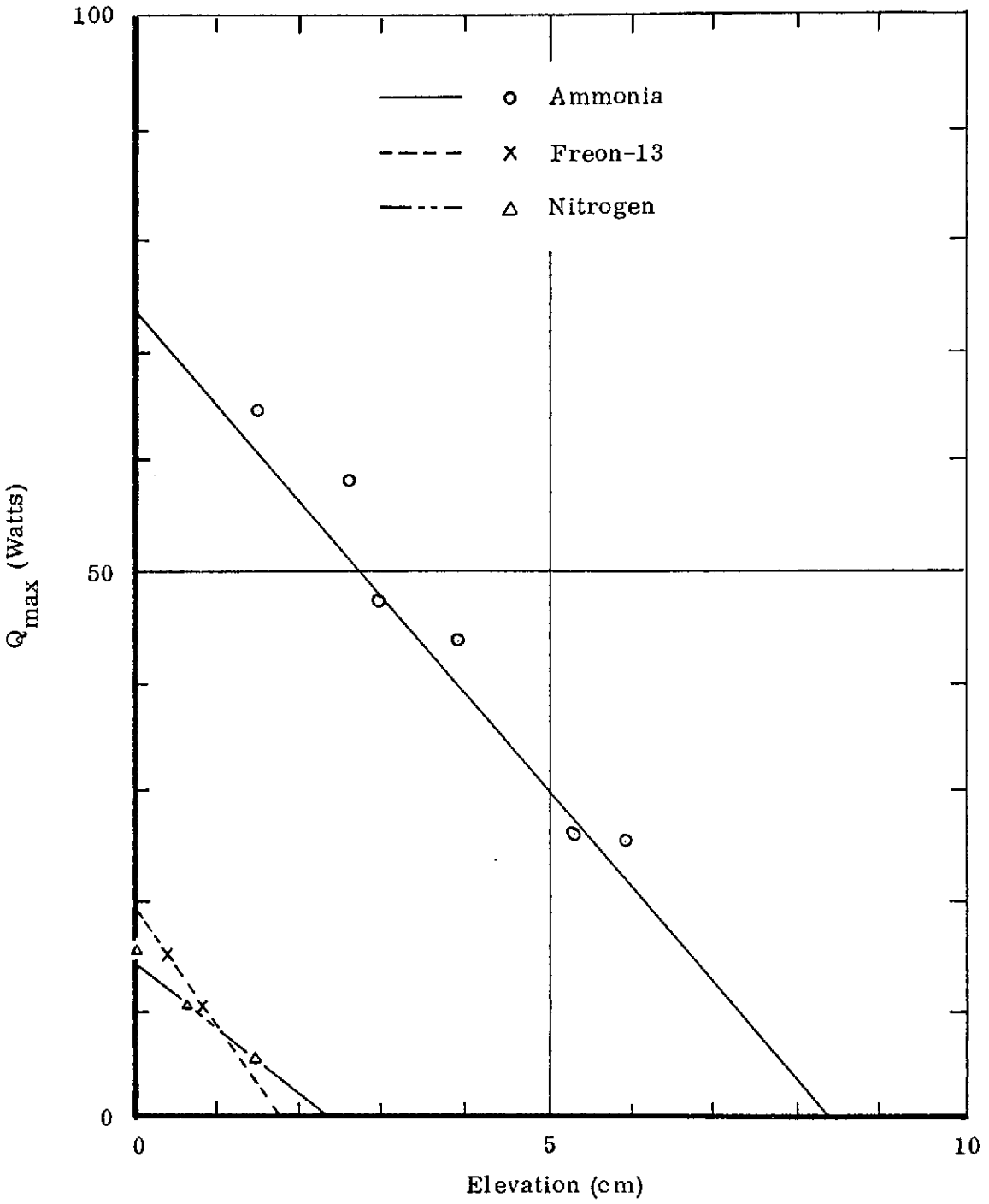

FIGURE 3.7

TRANSPORT CAPABILITY FOR SLAB-WICK HEAT PIPE #2
FOR THREE FLUIDS

Fluid	Experimental		Analytical	
	K (cm^2)*	r_p (cm)	K (cm^2)	r_p (cm)
Ammonia	1.64×10^{-5}	6.75×10^{-3}	1.79×10^{-5}	6.85×10^{-3}
Freon-13	7.0×10^{-5}	5.65×10^{-3}		
Nitrogen	3.62×10^{-5}	6.85×10^{-3}		

*Adjusted for Groove Effect

TABLE 3.1

COMPARISON OF EXPERIMENTAL AND ANALYTICAL RESULTS FOR SLAB-WICK HEAT PIPE #2

comparison, analytical values are also included. The experimental values are in fair agreement with the analytical values for ammonia and nitrogen. For Freon-13, the properties are not well known and the experimental results were based on only two data points which may explain the larger variations. The experimental film coefficients for nitrogen are 0.18 watt/cm^2-^{o}C for the evaporator and 0.12 watt/cm^2-^{o}C for the condenser.

3.4 Slab-Wick Heat Pipe #3

This heat pipe was fabricated from an aluminum tube which was 91.5 cm long and had an outside diameter of 1.27 cm and a wall thickness of 0.089 cm. As with the other two slab wick heat pipes, the tube was circumferentially grooved internally. On the outside of the tube, small beads of aluminum were welded so that thermocouples could be peened into holes drilled into the beads. The wick was composed of six layers of 50-mesh and seven layers of 200-mesh stainless steel screen which were spotwelded together. A final layer of 200-mesh screen was wrapped around the entire wick. Heat was applied with an electric heater over 10 cm at one end, and the 11.4 cm long condenser was placed in the liquid nitrogen reservoir. The test setup and charging techniques are the same as described in Section 3.1.

Measurements were made of the maximum heat transport capability for various elevations and charges (19.1 grams of nitrogen corresponded to 100% fill). The results are summarized in Figure 3.8 and, for comparison, the theoretical curve is also shown. The data obtained near horizontal orientation exhibits the characteristic "puddle" effect, thus the measured performance is greater than predicted.

The experimentally determined capillary pumping radius is 8.1×10^{-3} cm compared to a theoretical value of 6.85×10^{-3} cm for 200-mesh screen. The measured permeability of 8.0×10^{-6} cm^2 agrees well with the theoretical value of 7.8×10^{-6} cm^2 for 50-mesh screen. The evaporator film coefficient was 0.014 watt/cm^2-^{o}C. This is much smaller than coefficients measured on the other three slab-wick heat pipes. It is possible that, because of poor contact between wick and threaded tube in the evaporator, the wick cannot feed sufficient fluid to the inner walls. This increased flow resistance would cause the grooves to dry out and result in an increased ΔT in the evaporator.

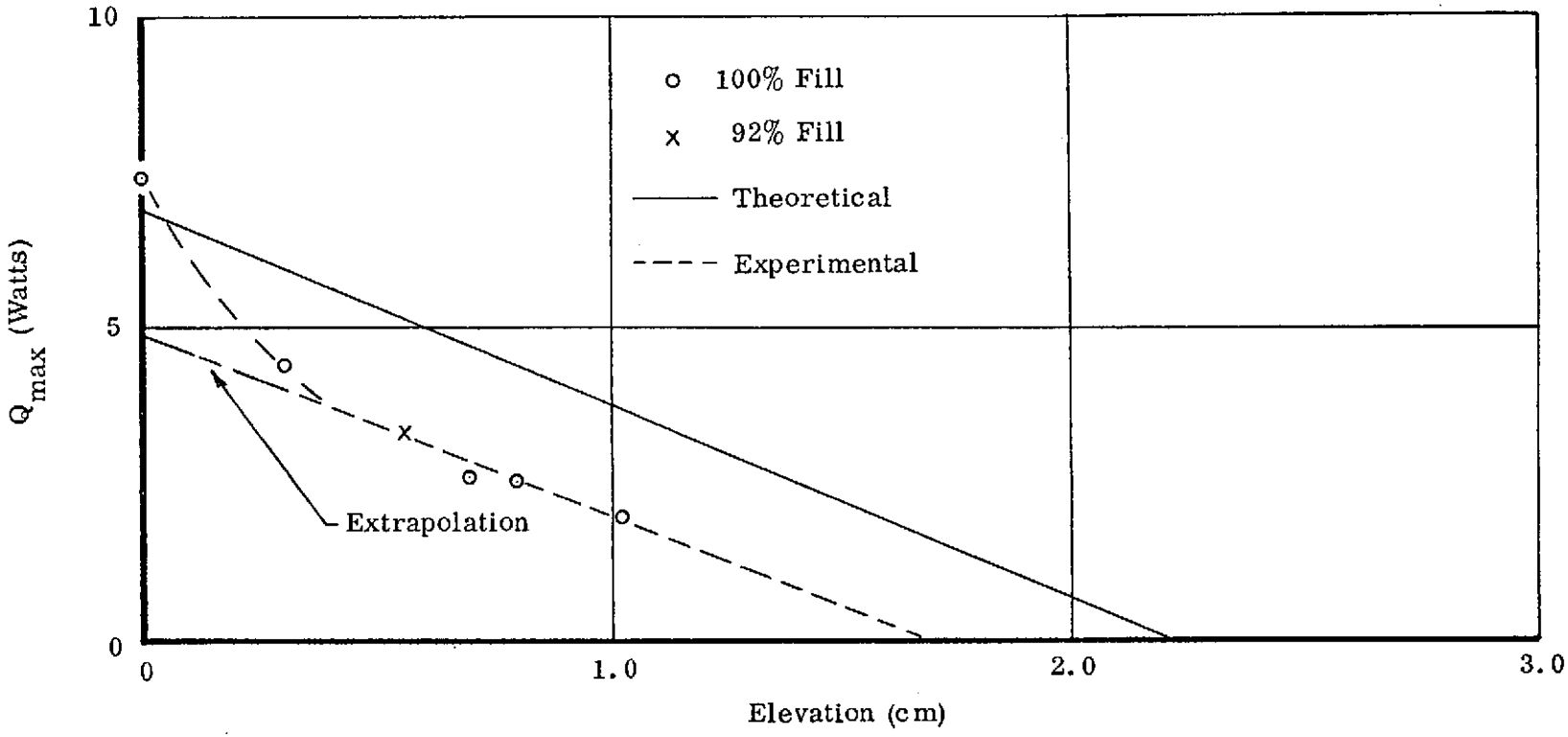

FIGURE 3.8

COMPARISON OF EXPERIMENTAL AND THEORETICAL RESULTS FOR SLAB-WICK HEAT PIPE #3

4. PROTOTYPE HEAT PIPE DEVELOPMENT

This section describes the design, development, fabrication, and testing for two prototype heat pipes. In the design phase, several wick configurations were investigated and two were chosen for fabrication of heat pipes. Development tests were conducted to verify the integrity of the design from the standpoint of safety and reliability of cryogen retention. The purpose of the test program was to verify the analytical models, to measure the operating characteristics and limitations of such heat pipes, and to provide engineering data for future designs. Also, the tests were used to uncover any design weaknesses and evaluate possible design improvements to correct these weaknesses.

4.1 Design

The objective of this task was to arrive at the final design of two cryogenic heat pipes which could best meet the thermal and mechanical requirements of the ICICLE system. In order to select two final designs, three preliminary designs were initially investigated (composite-screen wick, axial grooves, and closed artery). The preliminary designs were based on conclusions reached during Task I of the program. Design considerations were ground and flight safety at ambient temperature, sensor interface requirements, heat pipe to spacecraft attachment, and insulation techniques.

Several basic parameters were selected during an interface meeting between GSFC and Dynatherm. The overall length of the heat pipe was established as 100 cm, and 2.54 cm was the largest diameter permitted for the outline of the heat pipe (excluding support rings and condenser interface). The condenser interface design was specified in the Cryogenic Heat Pipe Interface Specification #69-5869(21) submitted by Airesearch Manufacturing Company after concurrence by Dynatherm Corporation. This design will be discussed in more detail in the following section. The maximum heat rejected at the condenser was specified as 4.0 watts. The nominal power input at the evaporator was specified as 0.5 watt with the evaporator elevated 0.254 cm above the condenser. The condenser temperature was selected to be 80 K. In order to meet the above requirements, the heat pipes were designed to handle an evaporator input of 2-3 watts.

Detailed thermal and mechanical designs were generated for all three configurations (slab wick, arterial wick, and axial grooves). Later, the axially-grooved heat pipe was eliminated because of its sensitivity to elevation. The following sections describe the design approaches for all three configurations.

4.1.1 Slab-Wick Heat Pipe

An analysis as described in Section 2 was based on the specified requirements. Table 4.1 summarizes the mechanical design parameters and Figure 4.1 shows a schematic of the heat pipe.

In the analysis, evaporator and condenser film coefficients of 0.18 watt/cm^2-^{o}C and 0.12 watt/cm^2-^{o}C, respectively, were used (experimental results obtained with the breadboard slab-wick heat pipe #2). In the transport region, where there are no circumferential grooves on the wall, the internal film coefficient was assumed to be 0.0005 watt/cm^2-^{o}C which corresponds to a forced convection film coefficient. This value was used since only vapor should be in contact with the tube wall in this region. The heat loss through the insulation was determined using Figure 2.16 in Section 2.3 and $r_o/r_i = 2$. The film coefficient, based on this heat loss, is 9.1×10^{-7} watt/cm^2-^{o}C. The supports consisted of 0.0735 cm diameter stainless steel stringer wires. They are described more fully in a following section. A conduction and radiation heat leak was determined for these wires. For the purposes of the analysis, it was assumed that the heat entered the walls uniformly over 1 cm length of the heat pipe. The external film coefficients associated with the supports were 1.23×10^{-4} watt/cm^2-^{o}C in the evaporator region and 2.36×10^{-4} watt/cm^2-^{o}C in the transport and condenser regions. The considerations in selecting the 325-mesh screen were availability, heat pipe weight, and pressure containment. The largest pore size screen, which can prime with nitrogen in a one "g" gravity field at the required elevation, is 60 mesh.

Including the heat leaks through the insulation and the support structure, the total temperature drop across the heat pipe was predicted to be 6.3^{o}C for an evaporator heat input of 3.0 watts. The heat rejected at the condenser is 4.7 watts. Figure 4.2 shows the predicted temperature profile. The supports and evaporator/condenser boundaries are also indicated on the curve. The uniform heat input analysis predicts that the

TABLE 4.1

OPTIMUM DESIGN OF SLAB WICK

Composite Wick

- 60/325-mesh stainless steel screen
- 0.227 cm thick
- 5 layers of each mesh size (a final wrap of 325 mesh)

Working Fluid

- Mass: 14.26 grams of nitrogen
- Pressure at ambient (300 K): 1.34×10^7 N/m^2
- Wall thickness to contain fluid: 0.089 cm
- Safety factor for containment of fluid at ambient temperature: 2.9

Evaporator

- Length: 6 cm
- O.D.: 2.54 cm; I.D.: 1.09 cm
- Circumferential fluid distribution by 31.5 full threads/cm
- Heated surface: 2.54 cm diameter flat end

Condenser

- Length: 6 cm
- O.D.: 2.54 cm; I.D.: 1.09 cm
- Circumferential fluid distribution by 31.5 full threads/cm
- End of condenser will have interface configuration (see Fig. 4.5)

Transport Section

- O.D.: 1.27 cm; I.D.: 1.09 cm
- Length: 88 cm

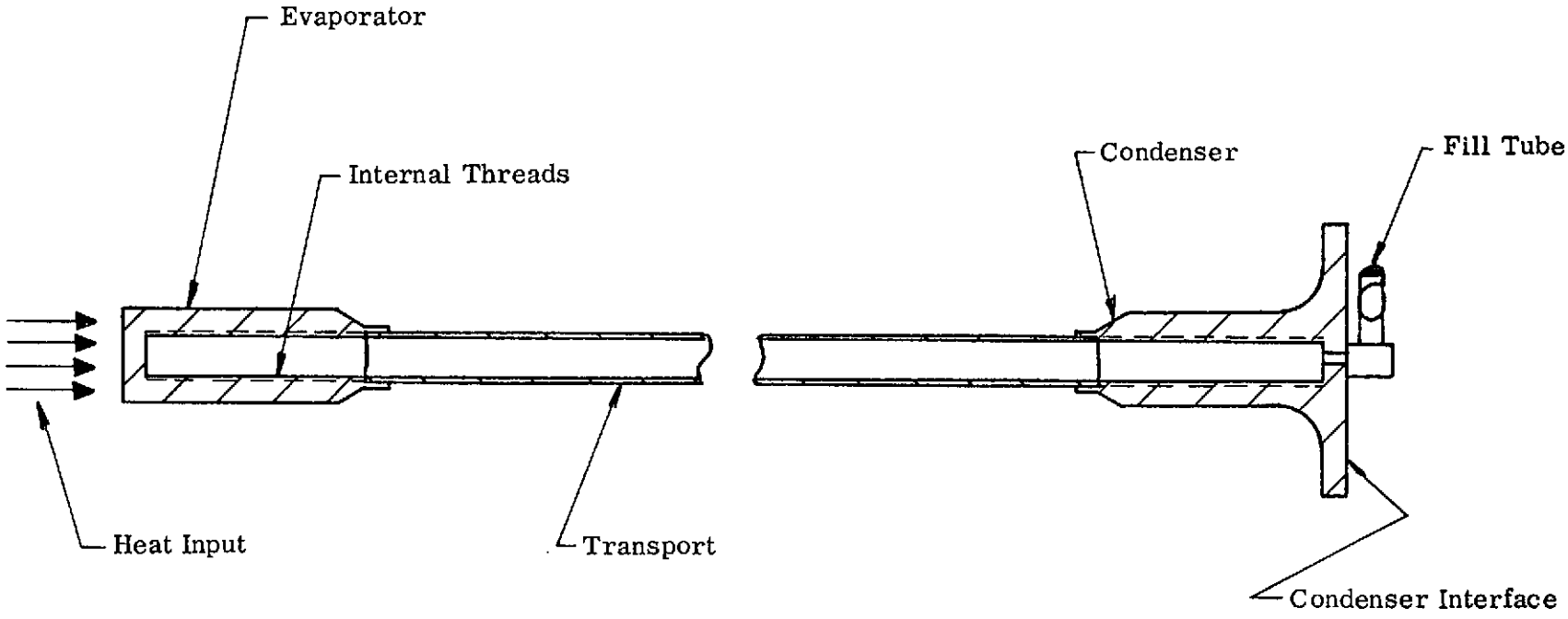

FIGURE 4.1

SCHEMATIC OF HEAT PIPE DESIGN

FIGURE 4.2

ANALYTICAL TEMPERATURE PROFILE FOR 1.27 Cm HEAT PIPE WITH SLAB WICK INCLUDING INSULATION & SUPPORT HEAT LEAK

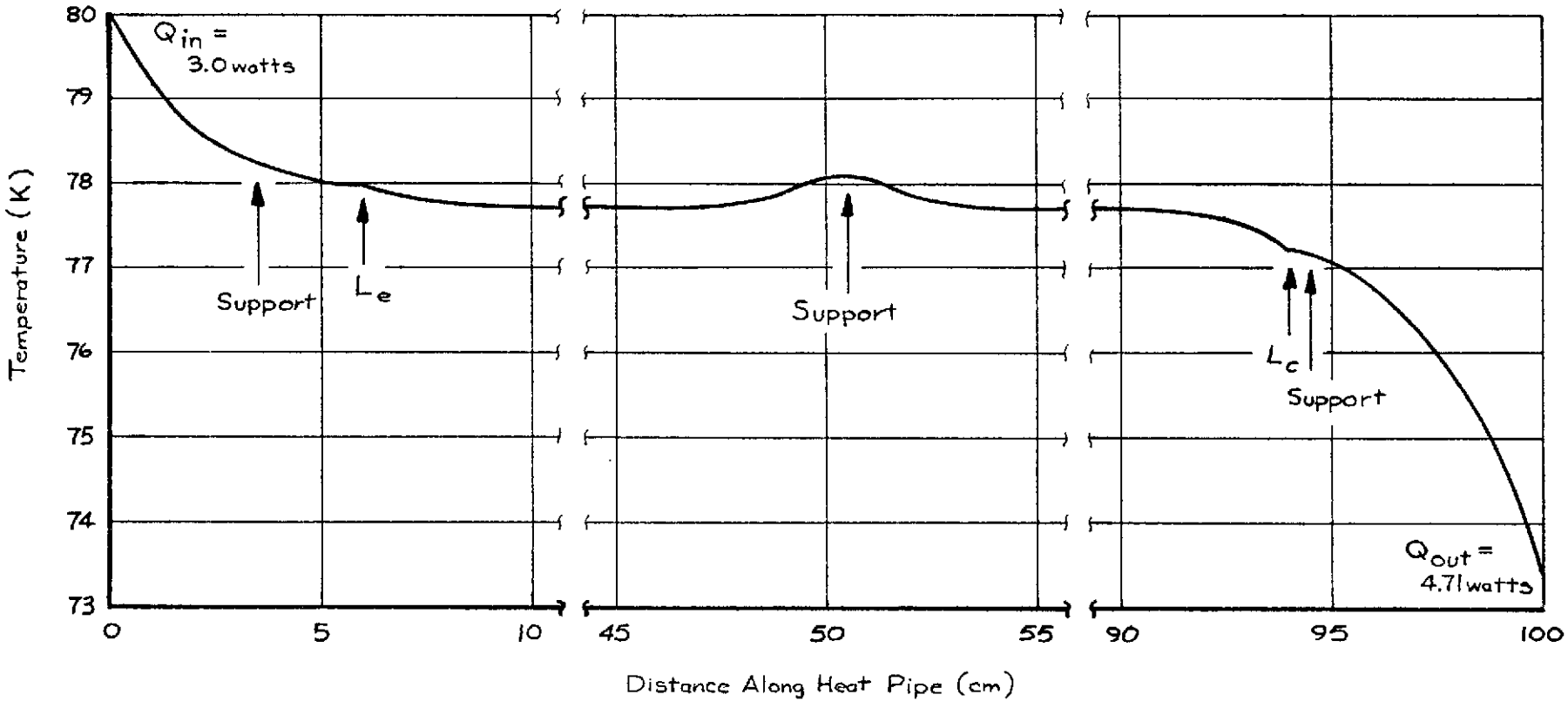

heat pipe will carry 4.06 watts at 0.254 cm elevation. In a zero "g" environment, the maximum heat transport capability is 5.44 watts.

The heat pipe material selected was 6061-T6 aluminum. The fill tube location (shown in Figure 4.1) was chosen to minimize interference with other design considerations. In the selected location, the fill tube is protected from accidental damage by the interface hardware. As shown in the figure, the increased wall thicknesses in the evaporator and condenser regions result in a collar-like appearance.

4.1.2 Artery Heat Pipe

The analysis presented in Section 2, when applied to an artery wick configuration, results in a mechanical design which is identical to the slab wick design for the evaporator, condenser, and transport regions. This result obtains because the film coefficients are the same for both cases. The predicted temperature profiles, therefore, are also identical. The minimum wall thickness, required for pressure containment, is also the same for the artery and the slab wick because this is the minimum wall thickness that it is practical to fabricate. The artery is constructed of 325-mesh stainless steel screen and has a diameter of 0.135 cm. The artery lies against the wall of the tube as shown in Figure 4.3. The bridge in the figure is used to hold the artery against the wall and is formed from the same screen. The unprimed artery can, theoretically, fill itself at an elevation of 0.06 cm, assuming the heat load during this time is only that of the parasitic heat leak. The calculated nitrogen charge is 2.6 grams which results in an internal pressure of 2.82×10^6 N/m^2 and a safety factor of 13. The predicted transport capability of the unprimed artery is 0.8 watt-meter at 0.06 cm elevation. When the artery is primed it is capable of transporting about 38 watts at which point the vapor flow is turbulent. The heat flux limit in the threads will limit the transport to inputs in the range of 10-20 watts.

4.1.3 Axial-Grooved Wick Heat Pipe

The design analysis of the axial-grooved heat pipe was optimized for minimum fluid inventory rather than for maximum transport capability because of the pressure containment requirement. Table 4.2 summarizes the mechanical design. The envelope material is 6061-T6 aluminum and, except for the relative lengths of each region, has

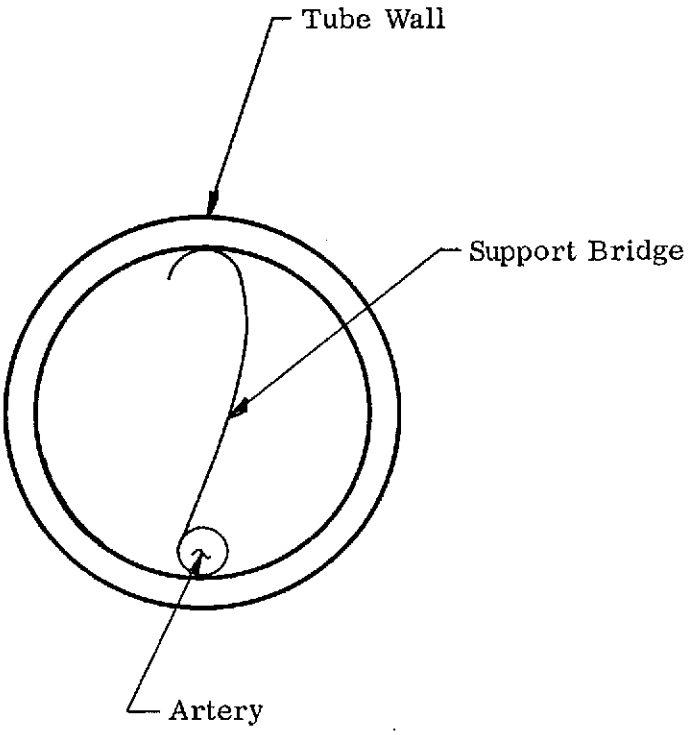

FIGURE 4.3

CROSS-SECTION OF ARTERY-WICK HEAT PIPE

TABLE 4.2

OPTIMUM DESIGN OF AXIAL-GROOVED HEAT PIPE

Groove Design

- 33 grooves
- Groove width: 0.041 cm
- Groove depth: 0.1016 cm
- Fin width: 0.044 cm
- Vapor diameter: 0.889 cm

Working Fluid

- Mass: 12.54 grams of nitrogen
- Pressure at ambient temperature: 1.62×10^7 N/m^2
- Wall thickness to contain fluid: 0.089 cm
- Safety factor for containment of fluid at ambient temperature: 2.4

Evaporator

- Length: 10 cm
- Outside diameter: 2.54 cm
- Heated surface: 2.54 cm diameter flat end

Condenser

- Length: 7 cm
- Outside diameter: 2.54 cm

Transport

- Length: 83 cm
- Outside diameter: 1.27 cm

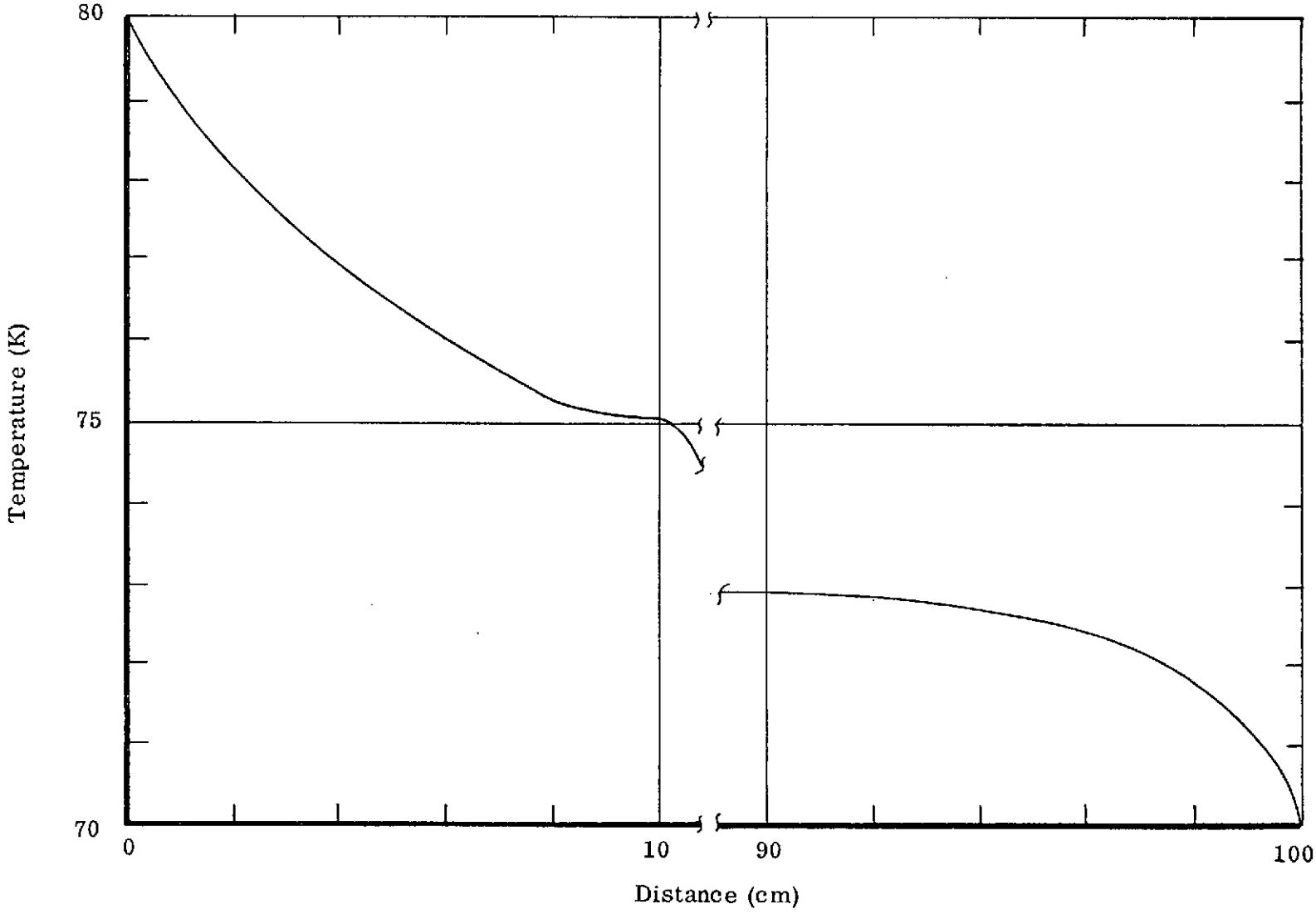

FIGURE 4.4

GROOVED-WICK HEAT PIPE PROFILE

the same outline as shown in Figure 4.1. Figure 4.4 gives a typical temperature profile predicted by CRYOTHERM for this type of heat pipe. An overall temperature drop of $10^{o}C$ occurs for a heat input of 3.0 watts. The maximum heat transport capability is 367 watt-cm at an elevation 0.254 cm.

The internal film coefficients used in the analysis were those measured on the axially-grooved breadboard heat pipe. Actually, the transport region becomes an evaporator because of the parasitic heat leaks; thus the evaporator film coefficient was applied to this region. The external film coefficients were the same as used on the previous two designs.

4.1.4 Condenser Interface

As stated before, the design of the condenser interface was specified in the Airesearch Interface Document. The end of the condenser was configured to this specification so that it could be interfaced to a typical VM engine. Figure 4.5 shows this flange configuration. The interface joint should be filled with either a soft metal such as indium foil or a flight-qualified thermal grease. The interface has an area of 33.6 cm^2 and the pressure is specified as 6.9×10^5 N/m^2.

4.1.5 Heat Shunt

The heat shunt was designed to interface with the condenser end of the heat pipe and to transport the heat load to the liquid nitrogen reservoir which serves as a heat sink. It was fabricated from OFHC copper and designed such that the heat removal rate could be measured during steady-state operation. To accomplish this, a 1.31 cm diameter rod was used as a shunt between the heat pipe and the reservoir. Thermocouples attached to the rod measure the temperature drop associated with the heat flux. A one watt load results in a $1^{o}C$ temperature drop along 7 cm of its length.

4.1.6 Supports

The supports were designed to minimize heat conduction and withstand launch forces. The heat pipe was supported at three axial positions -- one near each end and one in the center. The supports are shown schematically in Figure 4.6. Stainless steel

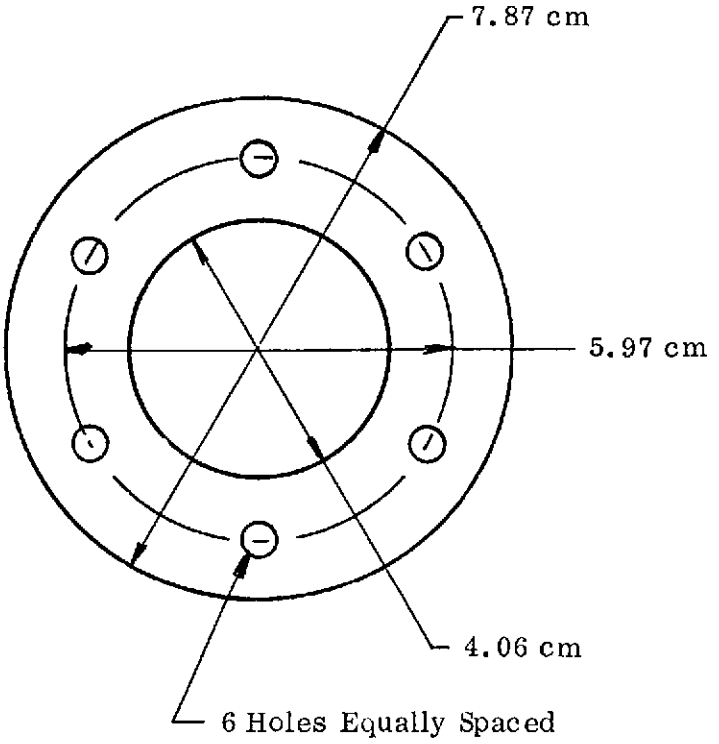

FIGURE 4.5

INTERFACE FLANGE DESIGN

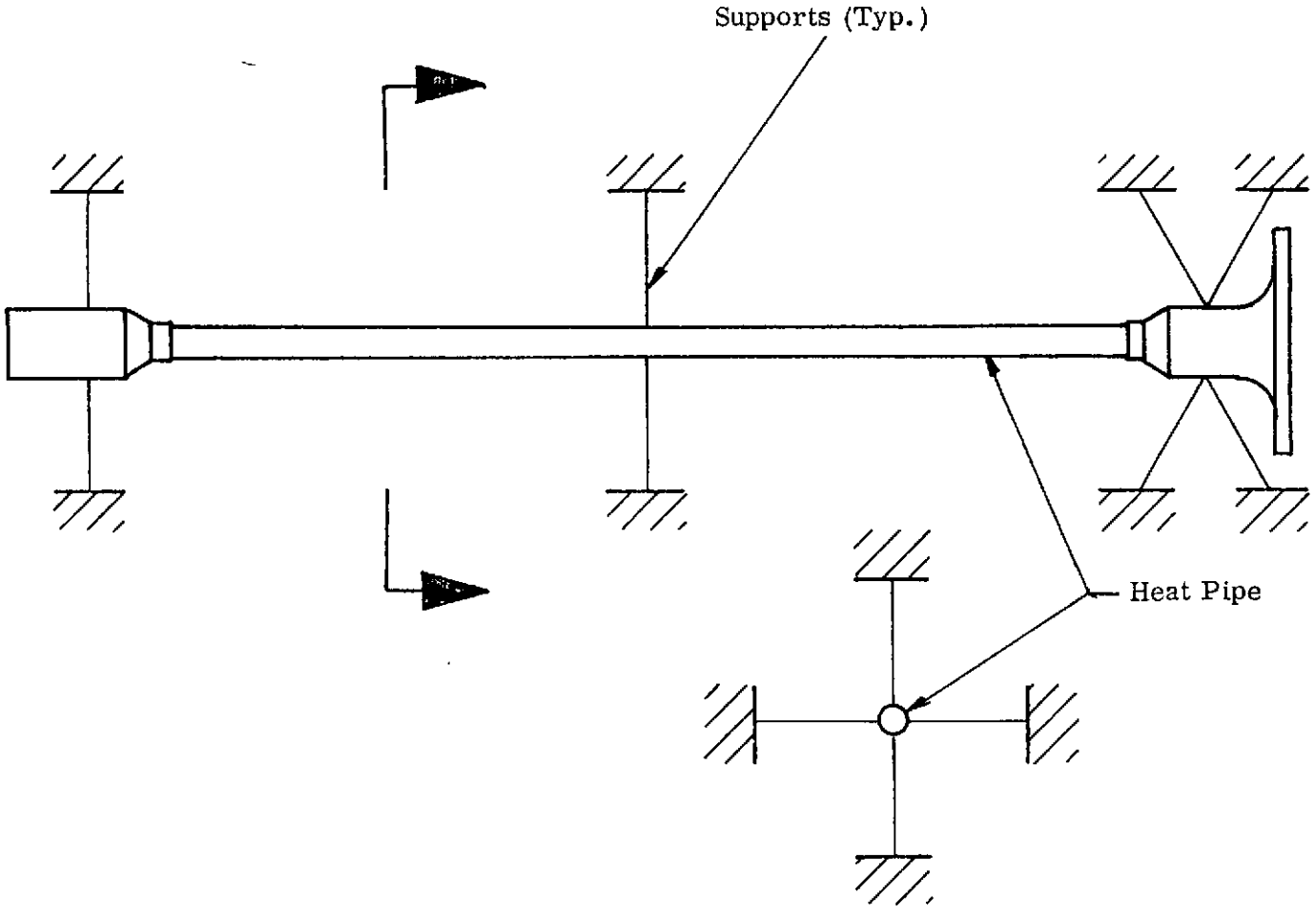

FIGURE 4.6

SCHEMATIC OF SUPPORT DESIGN

stringers were chosen as main supports. Other stringers were investigated, such as Kapton ribbons; but stainless steel wire (0.0635 cm diameter) was found to be superior because of its high Young's Modulus, resistiveness to "notching", and low thermal conductivity. At each location, supports were formed at four orthogonal orientations. At two of these locations (the evaporator end and the center), the four stringers were oriented perpendicular to the heat pipe wall. At the condenser end (Figure 4.6), eight supports were used and opposed each other in pairs at an angle of 60 degrees to the heat pipe wall. This support configuration restrains the heat pipe along all axes of vibration. Static analyses have been performed on the cryogenic heat pipe support structure for the specified vibration environment. The loads in the three orthogonal axes produce stresses considerably below the yield stress of the stainless steel support elements.

Dynamic vibration analyses were performed to identify the resonant frequencies of the heat pipe system which are in the specified frequency spectrum. The model for this analysis is shown in Figure 4.7a. The heat pipe is assumed to be completely rigid and is of a uniform mass per unit length. The spring constant for the individual stringer wire is related to Young's Modulus ($Y = 2 \times 10^{11}$ N/m^2) and the dimensions of the wire by the following expression:

$$k = Y \frac{A}{L} \qquad 4\text{-}1$$

where A is the cross-sectional area (3.16×10^{-3} cm^2) and L the length of the wire (2.54 cm). The stringer wires used in this design have a spring constant of 3.48×10^6 N/m.

For axial vibrations, the restoring forces are applied by the axial components of the stringer wires oriented at 60 degrees to the heat pipe. The system can be reduced to a single mass (M) supported axially between two springs -- each with a spring constant $K = 4\,k \cos 60^{\circ}$. The resonant frequency for this case is given by:

$$f = \frac{1}{2\pi} \sqrt{\frac{2K}{M}} \qquad 4\text{-}2$$

For a heat pipe weighing 454 grams, the resonant frequency is 743 sec^{-1}.

FIGURE 4.7a

MODEL FOR DYNAMIC VIBRATION ANALYSIS

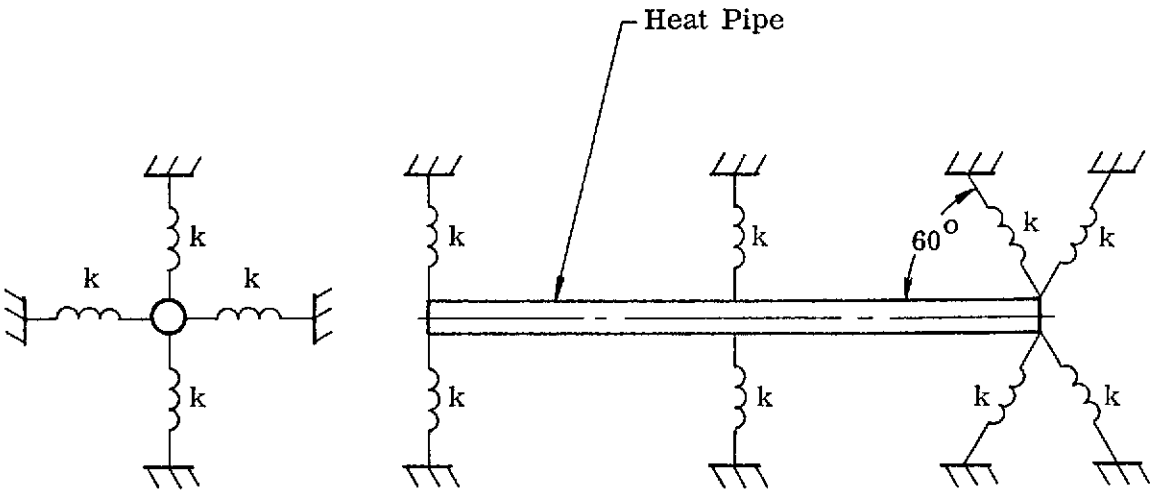

FIGURE 4.7b

MODEL FOR LATERAL VIBRATIONAL MOTION

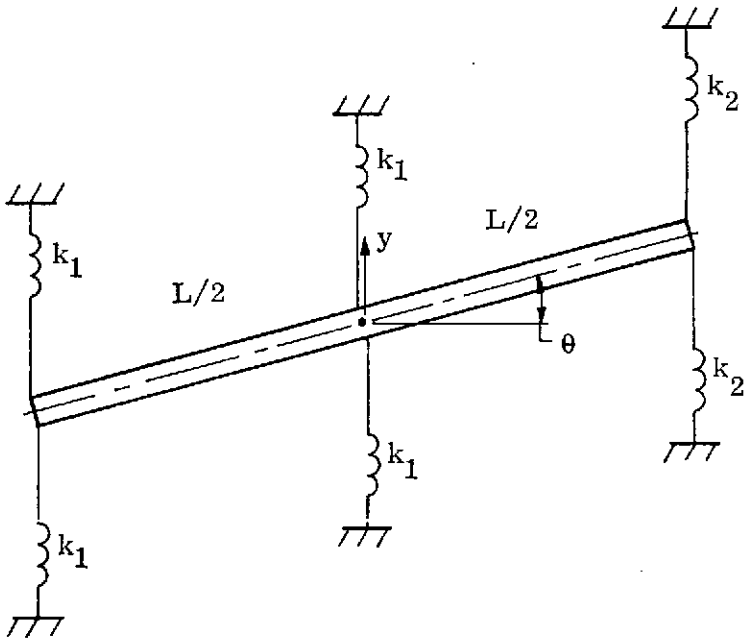

$k_1 = k$

$k_2 = 2k \sin 60^\circ$

The resonant frequency in either of the other two directions is more difficult to determine. The worst case occurs when the vibration is applied along the direction of the support wires because, in this case, only two wires are reacting at each support. Force components applied in any other direction will result in a greater restoring force than experienced with a single wire. Only the worst case was analyzed. The motion of the heat pipe (Figure 4.7b) can be expressed by a pair of differential equations -- one for lateral displacement (y) and the other for rotational motion (θ):

$$\ddot{y} = -\frac{2}{M}(2k_1 + k_2)y - \frac{L}{M}(k_2 - k_1)\theta \qquad 4\text{-}3$$

$$\ddot{\theta} = -\frac{12}{ML}(k_2 - k_1)y - \frac{12}{M}(k_1 + k_2)\theta \qquad 4\text{-}4$$

These equations assume small angular displacements. The solution of these simultaneous equations results in two resonant frequencies -- 2130 sec^{-1} and 956 sec^{-1}.

The longitudinal resonant frequency and one of the transverse frequencies (956 sec^{-1}) are within the frequency range specified for the vibration test (10-2000 sec^{-1}). However, the greatest acceleration load of 18.5 g occurs below 400 sec^{-1}. Above 400 sec^{-1} the applied g-load drops off to approximately 5-7 g. The model used in determining the resonance frequencies assumes no hard mount. However, when this system is used to cool an infrared sensor, it may be necessary to hard mount the evaporator end of the heat pipe. This would increase the resonance frequencies substantially. Based on this analysis and until the heat pipe application and support system is specified more completely, it is recommended that the designed support structure be accepted.

4.1.7 Thermal Insulation

An approach to insulating the heat pipe which is similar to that described in Section 2.3 was used in the prototype heat pipe design. However, since an electric heater was substituted for an infrared sensor, an insulation system was used which enclosed the entire heat pipe and made it unnecessary to use a radiation barrier. In addition to the 1.27×10^{-3} cm thick aluminized mylar multilayer wraps, an outer wrap of heavier gauge aluminized Kapton was employed to support the mylar film and prevent it from being compacted.

Good installation practices require that no exposed edges be permitted since these would absorb energy like a black body. Also, continuous wraps were not permitted on the inner 12 layers. Ideally, each layer of insulation should be an isothermal surface. Successive layers overlap one another where penetrations are made for supports, heater leads, and thermocouple leads. This minimizes heat leaks around the holes; however, a considerable leakage occurs by conduction and radiation associated with these supports and wires. A total of 29 wraps of insulation were specified and results in a heat leak of 8×10^{-4} watt/cm of length along the heat pipe.

4.1.8 Final Design Selection

Of the three designs selected for study, the slab wick is the first choice because it met the thermal requirements with a minimum temperature drop and can be easily fabricated. The thermal performance of the axial-grooved heat pipe is adequate; however, it is extremely sensitive to elevation and the fabrication of the grooved tubing may be very difficult and expensive. The artery heat pipe is relatively easy to fabricate and, once primed, it possesses the required thermal capability. However, priming the artery is elevation sensitive and potentially unreliable. The cost of fabricating the grooved tubing was the main reason for ruling out its use for this program. The slab and artery designs were chosen for the two prototype heat pipes.

Assembly and detail drawings were made for the two designs and the processes were specified. An Acceptance Test Plan, which specified the tests to be conducted on the prototype heat pipes, was prepared.

4.2 Development Tests

Development tests were conducted to qualify the containment design (ability to withstand ambient temperature pressures, creep, and thermal fatigue). Tests were conducted on tubing samples configured to the adiabatic region of the prototype heat pipes. A full-scale prototype heat pipe was hydrostatically tested to burst to check the effects of welding.

Six qualification samples (Figure 4.8) were fabricated. The cleaning was in

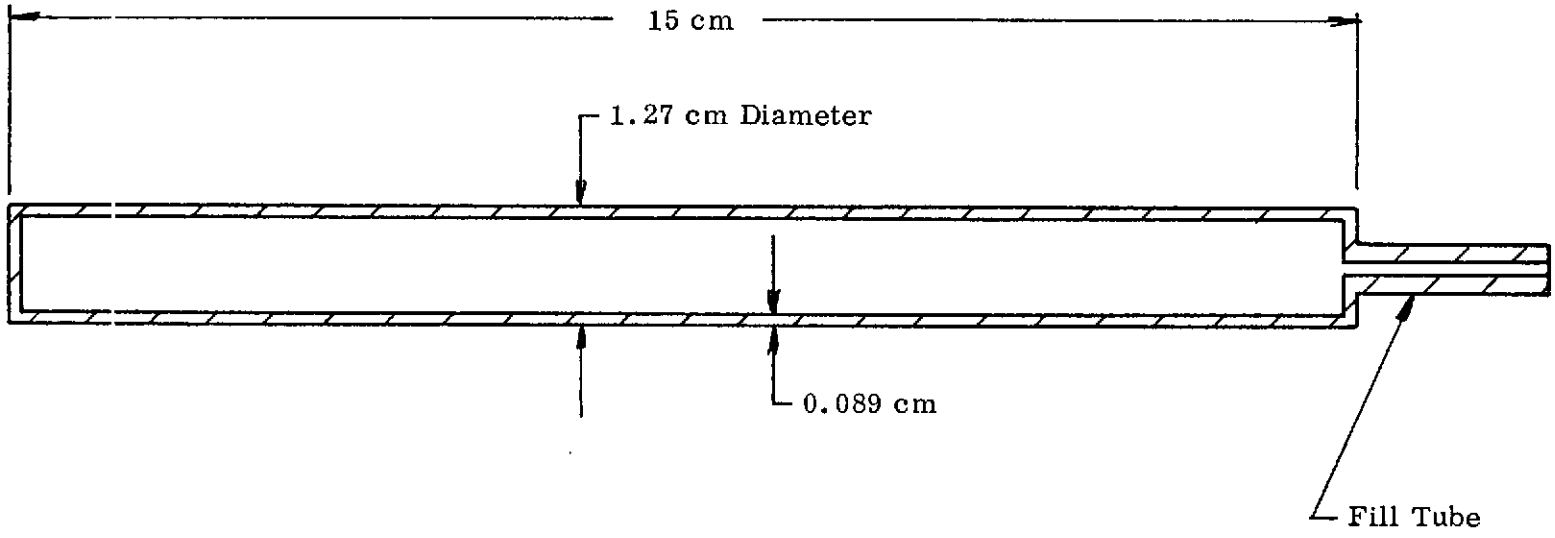

Material: 6061-T6 Aluminum

FIGURE 4.8

QUALIFICATION SAMPLE

accordance with the cleaning procedure 031-1021 (Appendix C). The samples were welded after cleaning and heat treated to restore the T6 condition. Subsequently, the samples were helium leak tested and radiographically inspected.

Each sample was tested in accordance with 4.3 of 031-1023 (Appendix D). The nitrogen charge of the slab-wick design was used because it is the largest and, consequently, represents the most severe condition.

Each sample was initially subjected (for 10 minutes) to an internal hydrostatic pressure of 1.69×10^7 N/m^2 (2450 psia) which corresponds to the pressure at a storage temperature of 65°C (150°F). The samples remained helium leak tight and did not distort during this test.

The samples were then charged with $2.44 \pm .05$ grams of nitrogen which was slightly greater than the intended charge of 2.34 grams. Three of these samples were stored at 25°C, and no noticeable changes in either weight or dimensions have taken place after 15,000 hours of storage. Since a 1 mgm change in weight can easily be detected, the gross leakage rate must be less than 1.5×10^{-8} std cm^3/sec. The measurement sensitivity for detecting a dimensional change is about 0.0005 cm which corresponds to an ambient temperature creep rate of less than 2.7×10^{-8} cm/cm-hr at a stress of 9.65×10^7 N/m^2.

The three remaining samples (SN-4, SN-5, SN6) were cycled between 77 K and 300 K for a total of ten times each to evaluate the fatigue of the material during transient start-up and shutdown portions of a cycle. No weight or dimensional changes were observed as a result of this test, indicating that no permanent deformation or gross leak occurred.

Samples SN-4, SN-5, and SN-6 were then burst pressure tested to verify an adequate safety margin for the design. Each sample was heated slowly until it burst. Table 4.3 summarizes the results of these tests.

Figure 4.9 presents the theoretical burst pressure of a 6061-T6 aluminum tube versus temperature. The curve is for a 1.27 cm diameter tube with a wall thickness of 0.089 cm. Also included are the experimental data from Table 4.3 indicating a burst pressure greater than predicted. This would be expected since the curve is based on minimum material properties.

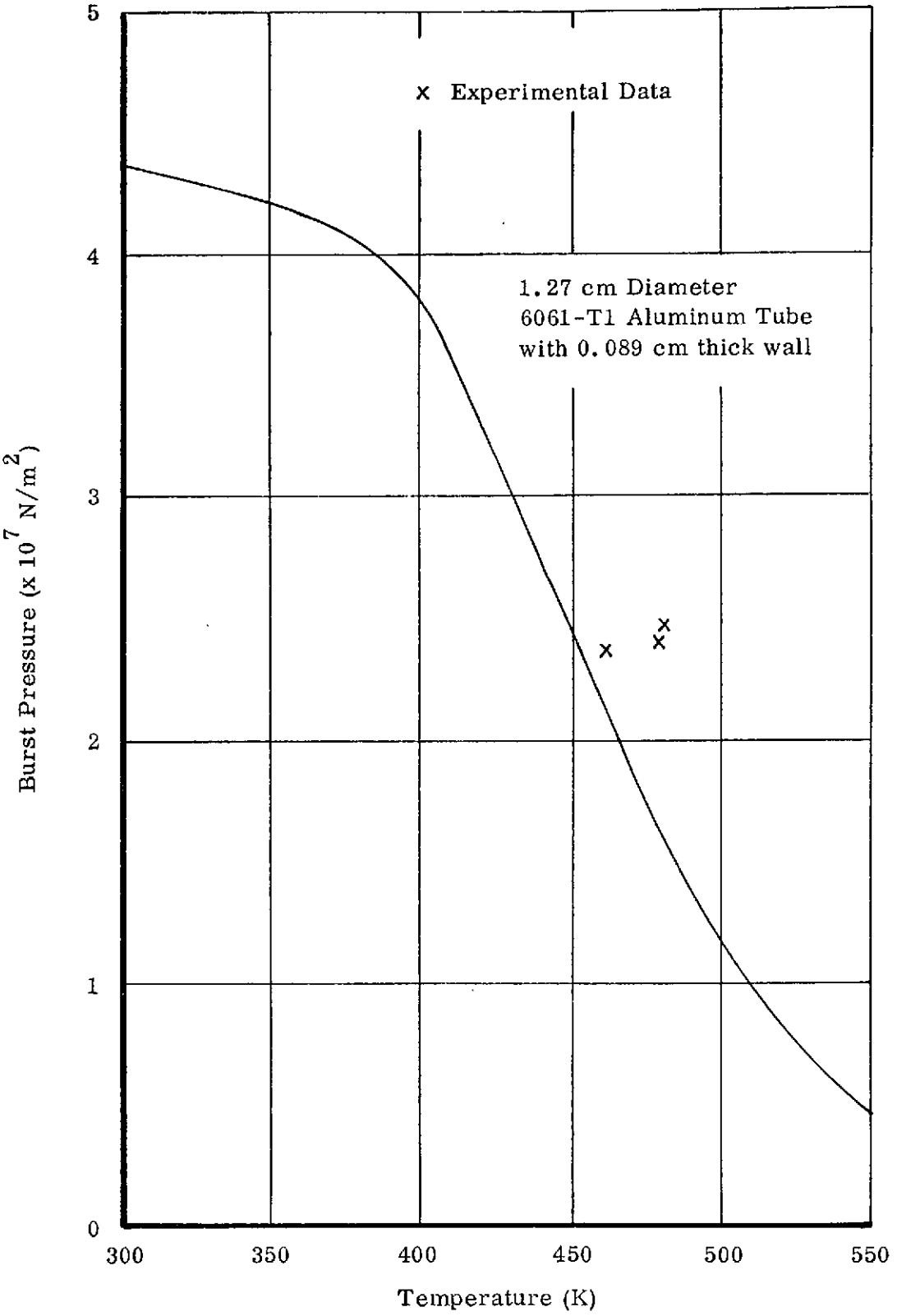

FIGURE 4.9

COMPARISON OF ANALYTICAL AND EXPERIMENTAL BURST TEST RESULTS OF QUALIFICATION SAMPLES

TABLE 4.3

Sample No.	Charge (grams)	Rupture Temperature (°C)	Calculated Burst Pressure N/m^2	Location of Failure
SN-4	2.39	211	2.42×10^7	End Cap Weld
SN-5	2.46	212	2.50×10^7	End Cap Weld
SN-6	2.46	192	2.39×10^7	End Cap Weld

Figure 4.9 indicates that at the maximum nonoperating temperature of 338 K (internal pressure of 1.65×10^7 N/m^2), the heat pipe tube has a burst pressure of about 4.34×10^7 N/m^2 which provides a safety factor of 2.6. The burst pressures given in Table 4.3 were determined for the specified charge and temperature of nitrogen gas, assuming that nitrogen obeys the Ideal Gas Law. The error in making this assumption is approximately 12% within the experimental temperature and pressure range. The values in the table are low by this amount; therefore, the safety factor is greater than the data would indicate.

Failures during the burst tests occurred at the weld in the end cap indicating that the tube itself might sustain a slightly higher pressure. However, dimensional measurements taken on the tubes after failure indicate that the diameter had increased in size by approximately 1% or 0.005 inch. Thus, the tube material was beginning to yield at this temperature and pressure.

A full-size burst sample, which had the same outer configuration as the prototype heat pipes, was fabricated. It contained support collars since the welding associated with their attachment could potentially reduce the strength of the heat pipe. The wick was not installed in this burst sample heat pipe and the external plating was eliminated.

The sample was processed in accordance with the Test Plan 031-1023. The internal hydrostatic pressure was slowly increased until failure occurred at 5.15×10^7 N/m^2. This pressure is about 16% greater than predicted from the burst strength of 6061-T6 and results in a safety factor of 3.8 at room temperature. The failure, as

expected, occurred in the thin walled tube about 5 cm from the condenser collar.

4.3 Fabrication of Prototype Heat Pipes

Two heat pipes were fabricated in accordance to Dynatherm Drawing 031-1007. A summary of the heat pipe design for each wick configuration is given in Section 4.1. One heat pipe contained a slab wick and the other one an artery wick. Except for the type of wicks and the amount of charge, both heat pipes were identical in construction, support structure, insulation protection, and instrumentation.

4.3.1 Wick Fabrication

The slab wick, supplied by Aircraft Porous Media, Inc., consisted of a composite of six layers of 325-mesh and five layers of 60-mesh sintered stainless steel screen. The design and installation of the wick is shown in Figure 4.10. The edges of the wick were machined to proper size. A single layer of 325-mesh screen was then spot welded over the entire wick including the ends. The wick was then fit-checked into the evaporator and condenser sections. The fit was considered acceptable when the wick was difficult to push into the bore of these sections. If the fit was too loose, additional layers of 325-mesh screen were added at the evaporator and condenser ends only. The wick was then inserted into the heat pipe tube, the inner diameter of which was slightly greater than the threaded inner diameter of evaporator and condenser.

The artery wick was fabricated as shown in Figure 4.3. The artery was formed by wrapping 325-mesh screen around a 0.135 cm (0.053 inch) diameter rod and spot welding the overlapping screen to itself. After removing the mandrel, one end of the artery was closed off by spot welding a tab of 325-mesh screen to one end. The artery (about 1 cm longer than needed) was then tested to determine its static pumping height. A small tube was soldered to the open end of the artery and connected to a methanol-filled manometer. The wick was submerged in a trough of methanol, and the air trapped in the artery was pressurized by adding fluid to the manometer. The wicking height was determined by observing the column height which could be supported before bubbles escaped from the artery. The artery had to be patched with solder at several locations before it could support a pressure head of 15 cm of methanol (corresponding to the

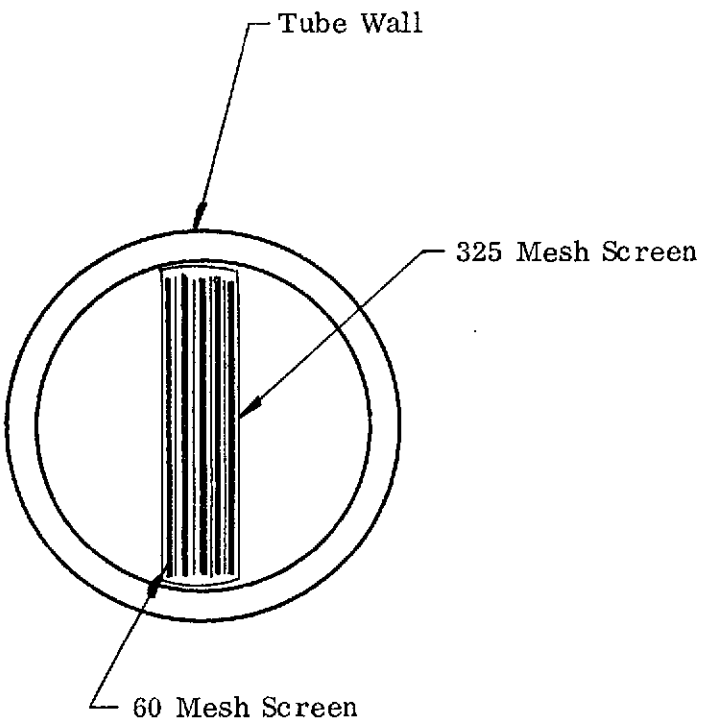

FIGURE 4.10

SLAB WICK CONSTRUCTION

pumping capability of 325-mesh screen). The wick was then trimmed to its final length and the remaining end closed by spot welding a tab over it. Since this final closure of the wick cannot be pressure checked, it was placed at the condenser end so that small leaks would not affect capillary pumping. The bridge of the artery wick (Figure 4.3) was shaped such that when placed in the evaporator and condenser sections, the artery was forced against the threaded surfaces.

4.3.2 Fabrication of Heat Pipes

All aluminum details were cleaned in accordance with 031-1021. The wicks were degreased with acetone and then placed in a solution of nitric acid to remove traces of copper which might be present from spot welding. After cleaning, the parts were stored in the class 100,000 clean room to await final assembly.

Welding of the heat pipes was performed in the clean room using a welding tool. This tool assured proper orientation of the wick, support collars, and condenser end. A line placed on the heat pipe tubes was used to indicate wick orientation. The heat pipes were then evacuated to a pressure less than 1×10^{-6} torr. The slab-wick heat pipe was heat treated. The artery heat pipe could not be heat treated because solder had been used to patch the wick. Burst tests conducted during weld development on the ATS program indicated a 27% reduction in burst pressure strength if 6061 aluminum is not heat treated after welding. Referring to Figure 4.9, the burst pressure at room temperature is reduced to 3.25×10^{7} N/m^2 and at 65°C the burst pressure is 3.17×10^{7} N/m^2. However, the calculated charge for the artery wick is so much smaller than the slab wick charge that these pressures still result in safety factors of 13 at 25°C and 11 at 65°C.

Radiographic examinations were conducted of both heat pipes to verify weld integrity. Also a helium leak check was made to a sensitivity of 1×10^{-9} std cc/sec of air.

The two heat pipes were nickel plated so that thermocouples could be attached by soldering. Before attaching the chromel-alumel thermocouples, they were calibrated at 273 K and 77 K. At the ice point, the thermocouples were within $\pm 1/4$°C; and, at

liquid nitrogen temperature, the agreement was within $\pm 2^{\circ}C$. The heat pipes were instrumented with thermocouples, a heater attached, and the pipes insulated.

A copper heat shunt was installed to interface with the condenser end of the heat pipe. Thermocouples were attached along its length so that the heat conducted by the shunt and delivered by the heat pipe could be measured. The other end of the heat shunt was inserted into a reservoir of liquid nitrogen which served as a heat sink. The heat shunt and the reservoir were also insulated to reduce thermal heat leaks into the system. Stainless steel wires were strung between the support collars and the mounting rings. The heat pipe, supported by the rings, was mounted on a test rack which also contained the heat shunt and reservoir; and the shunt was bolted to the condenser. Figure 4.11 is a photograph of the heat pipe attached to the shunt before the insulation was applied.

4.4 Testing

The two prototype heat pipes were tested in accordance with Paragraph 5.3 of the Acceptance Test Plan. This section also discusses the method of determining the elevation of the heat pipe when it is in the vacuum chamber and the procedure used to charge the heat pipes.

4.4.1 Measurement of Heat Pipe Elevation

The test rack with the heat pipe and the liquid nitrogen reservoir was placed on a bench in the laboratory. The rack was supported by four jack screws which were placed under the rack at the same locations as the supports in the vacuum chamber. Using a transit, the rack was then leveled to within 0.0127 cm (0.005 inch) at four reference points. The heat pipe was then leveled to the same accuracy. Since the heat pipe was already insulated, access holes were provided so that the scale would contact the top surface near each location where the heat pipe was supported. The vacuum chamber was also leveled using two reference points on the extreme ends (the top of the guide pins were used for this purpose). The test rack with heat pipe was then placed inside the vacuum chamber, and the four pads supporting the rack were adjusted until the same four reference points of the rack were again level. With the completion of

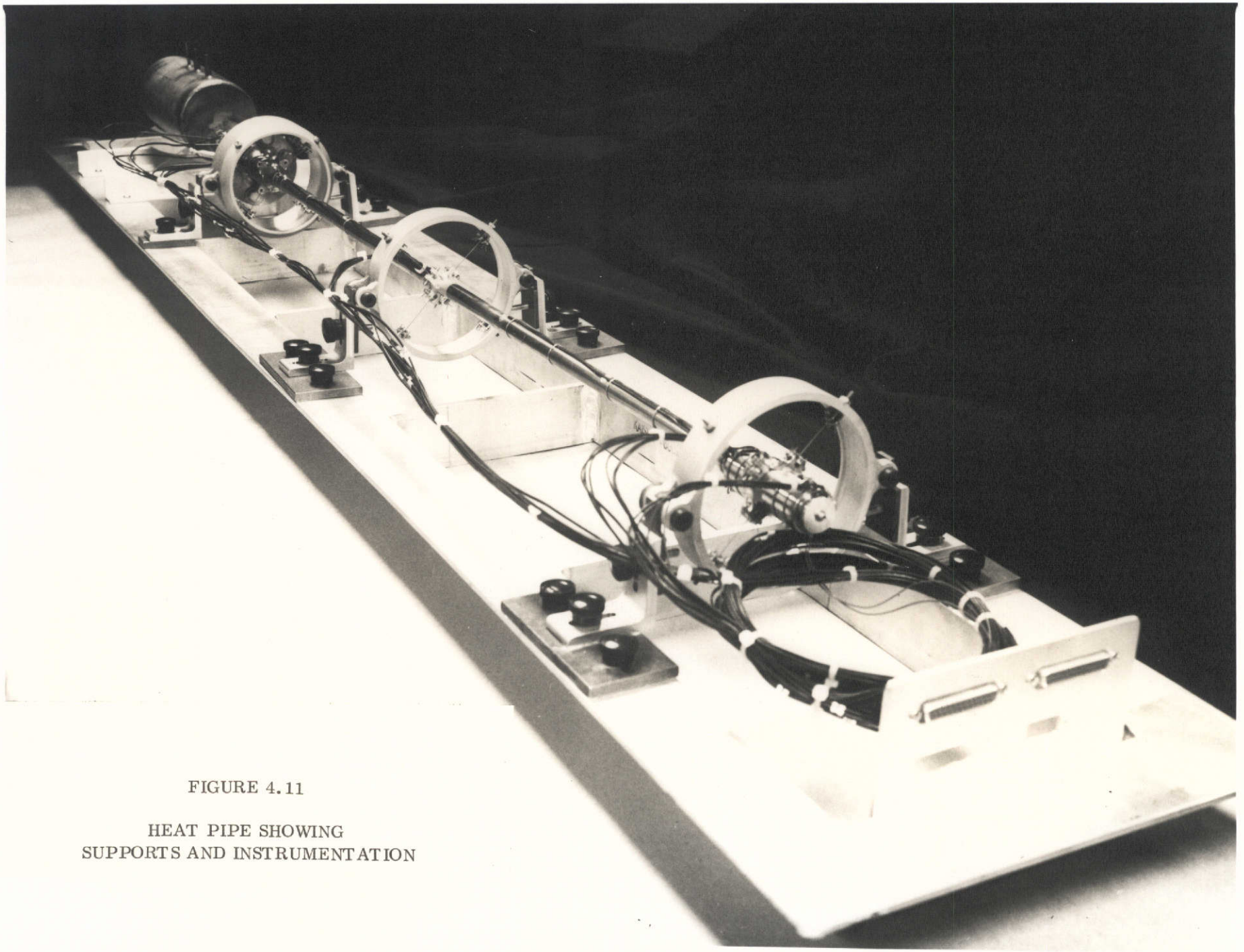

FIGURE 4.11

HEAT PIPE SHOWING
SUPPORTS AND INSTRUMENTATION

this step the heat pipe and the chamber were considered level. In order to change the orientation of the heat pipe, the entire chamber was tilted by means of an adjusting screw at its base. The tilt was measured by observing the difference in elevation of the two guide pins at the ends of the chamber. The actual heat pipe orientation was determined from this measurement and a scale factor (the ratio of the heat pipe length and the distance between the guide pins).

4.4.2 Charging of the Heat Pipes

The heat pipes, with instrumentation and insulation installed, were placed in the vacuum chamber. A schematic of the setup for charging is shown in Figure 4.12. A valve was attached to the fill tube, and a tubular connection was made between this valve and the outside of the chamber through a vacuum tight feed-through.

After the vacuum chamber was evacuated, the heat pipe condenser was cooled to cryogenic temperature by filling the reservoir with liquid nitrogen. The heat pipes were charged by filling the external charging reservoir with a known pressure of nitrogen gas. The volume of the reservoir had been previously measured; thus the mass of nitrogen in the reservoir is determined from the Ideal Gas Law. As the gas is admitted into the heat pipe, it condenses at the cold end, fills the wick, and cools down the entire heat pipe.

Selection of the optimum charge was done empirically. This was accomplished by charging the heat pipes with different amounts of fluid and then conducting a preliminary performance test while the pipes were still installed in the charging fixture.

The slab heat pipe was tested at three nitrogen charges (11.8 grams, 12.4 grams, and 13.1 grams). It was previously determined analytically that 14.16 grams are necessary to fill the wick. However, the sintering process used to form the slab wick results in a somewhat lower porosity than the value used for the analytical determination. The slab heat pipe was tested horizontally and at an evaporator elevation of 0.254 cm above the condenser. At 11.8 grams, the wick was underfilled resulting in a premature burn-out at low power levels. With a charge of 12.4 grams, the heat pipe operated satisfactorily at 2.0 watts and at 0.254 cm evaporator elevation. Larger condenser temperature gradients occurred when the fluid charge was increased to 13.1

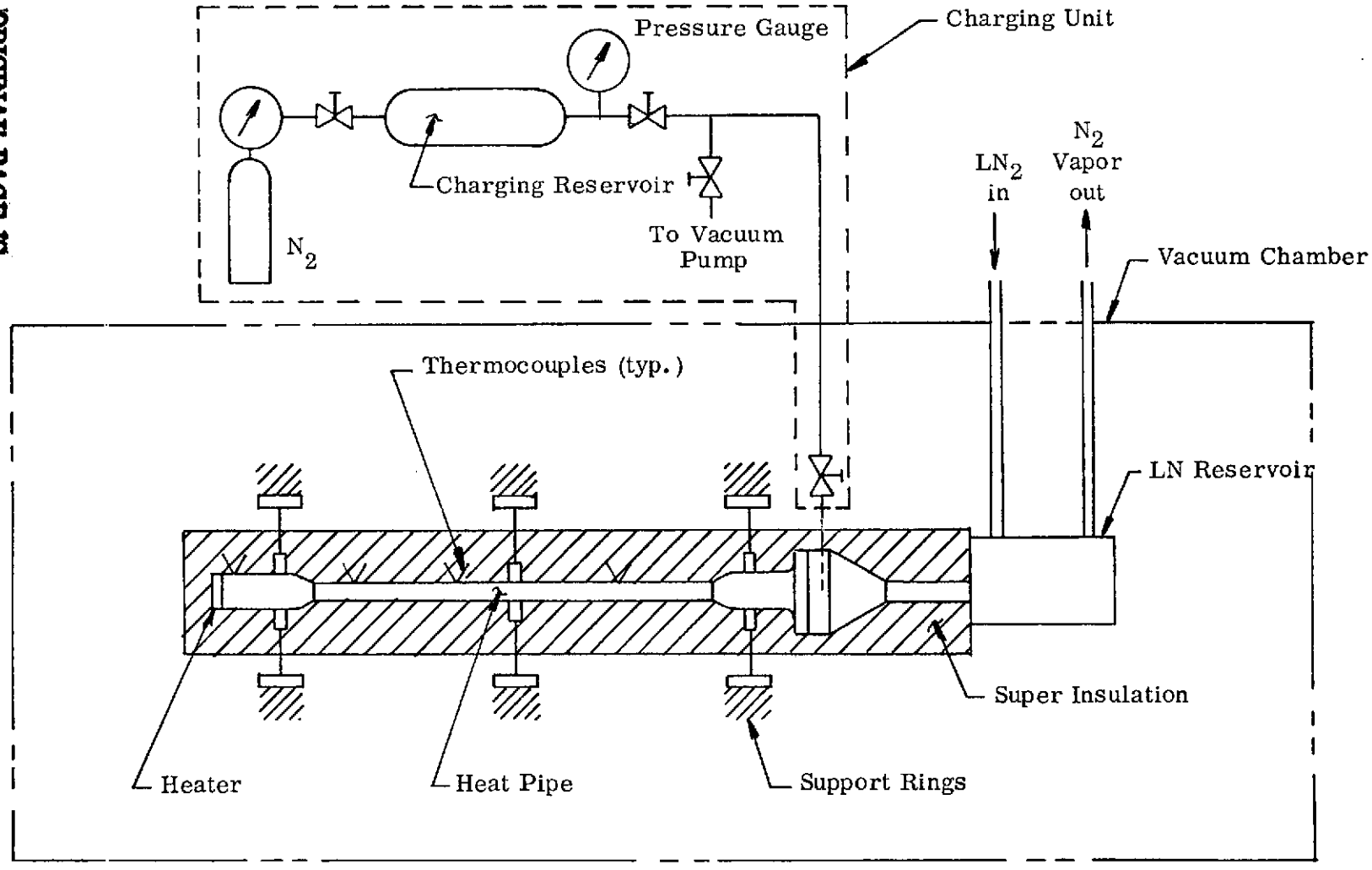

FIGURE 4.12

CHARGING AND TEST SETUP FOR CRYOGENIC PROTOTYPE HEAT PIPE

grams indicating an excess amount of fluid. Thus 12.4 grams was selected as the optimum fill. This charge results in a lower internal pressure (1.45×10^7 N/m^2) and larger safety factor (3.0) at the storage temperature of 65°C than previously discussed in Section 4.2. After evacuating the slab heat pipe, it was removed from the vacuum chamber. With the evaporator oriented down, this end was cooled in a liquid nitrogen bath and the heat pipe refilled with 12.4 grams of nitrogen. The valve on the heat pipe was then closed and, while the heat pipe was kept cold in the liquid nitrogen bath, the fill tube was pinched and welded off to its final dimension. The heat pipe was then allowed to warm up slowly to room temperature before it was prepared for final acceptance testing.

The same charging technique was applied to the arterial-wick heat pipe. However, because of priming difficulties with the artery, this pipe was never pinched off. Instead, it was tested extensively with different charges while the valve was still attached.

4.4.3 Test Results for Prototype Slab-Wick Heat Pipe

The heat pipe was tested in the vacuum chamber in accordance with the Acceptance Test Plan 031-1023. The test setup is the same as the one shown in Figure 4.12 except that the Charging Unit was disconnected during the acceptance tests since the heat pipe was pinched off.

The heat shunt was calibrated by operating the heat pipe with the condenser elevated 0.508 cm above the evaporator. The temperature drop along the shunt was measured for several electrical heat inputs. Figure 4.13 is a plot of this data. The curve has been extrapolated to a zero temperature drop which occurs at a "negative" heat input of 4.0 watts. This value represents the total parasitic heat leak into the heat pipe. This heat leak will not vary appreciably as long as the operating temperature of the heat pipe remains within the range of 80 K to 100 K. Thus, for all subsequent tests, the parasitic heat loss was taken to be 4.0 watts.

4.4.3.1 Heat Pipe Start-Up Test

No electrical power was applied to the evaporator heater during this test, and

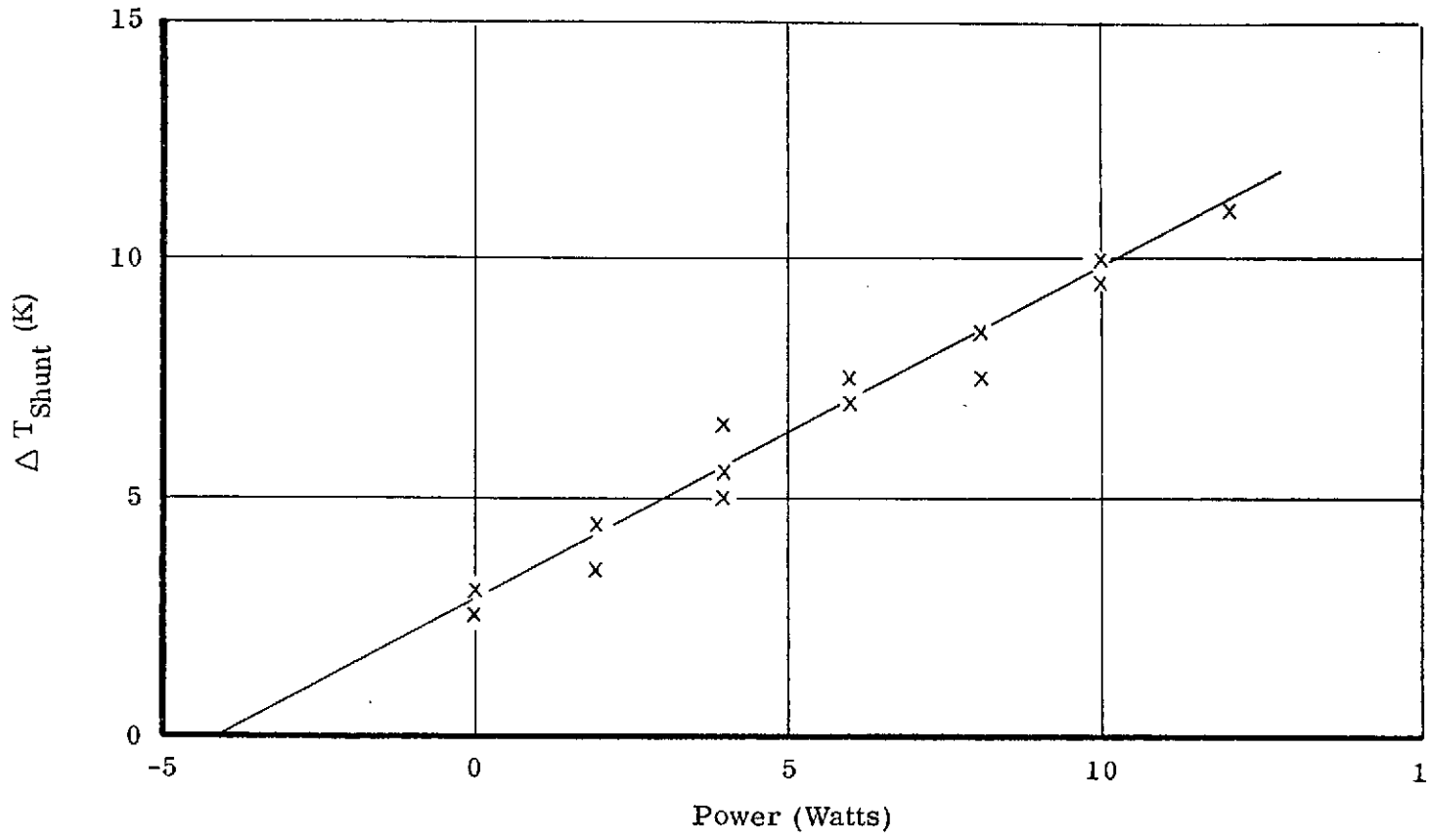

FIGURE 4.13

SHUNT CALIBRATION

the evaporator was elevated 0.254 cm above the condenser. The heat pipe was initially near room ambient temperature. Start-up was simulated by introducing liquid nitrogen into the heat exchanger at a constant rate. The temperature profile was monitored periodically until the entire heat pipe was cooled down to approximately 90 K. Three tests were run, each at a different cool-down rate. An additional fourth test was conducted with the heat pipe oriented horizontally.

Figure 4.14 summarizes the results of the tests. Figure 4.14a shows the cool-down rate of the condenser and Figure 4.14b that of the evaporator. The cool-down rate of the condenser appears to be independent of the cool-down rate of the reservoir. The slope of all curves in Figure 4.14a is approximately the same at temperatures below 220 K. It is believed that this behavior is peculiar to the condenser and shunt design and not indicative for a heat pipe cooled by a VM engine.

The cool-down rates of the evaporator are more representative of the heat pipe behavior. The rates during Runs 1, 2, and 3 follow closely those at the condenser, but the beginning of cooling is delayed by approximately 50 minutes. When the heat pipe is oriented horizontally (Run 4), the cooling occurs at a much faster rate once it is initiated. This can be attributed to the heat transport mechanism in a heat pipe. Heat transport from the evaporator (and its associated cooling) is achieved by capillary forces pumping against viscous flow losses and gravity. In the absence of an adverse gravity vector (Run 4), the capillary forces can sustain larger circulation rates of the working fluid and hence provide a faster cool-down rate of the evaporator.

4.4.3.2 Performance Tests With Design Heat Load

The heat pipe was operated in a steady-state mode with the evaporator elevated 0.254 cm above the condenser and with an electrical heat input load of 0.5 watt. Because of parasitic leaks, the output power is thus 4.5 watts. Figure 4.15 shows the temperature profile along the heat pipe for this input power. The 2^{o}C temperature rise just beyond the evaporator is due to the fact that approximately five thermocouples, including the ones in question, penetrate the super insulation at this point. These thermocouples are being influenced by the warmer environment outside the insulation. Disregarding this rise, the overall temperature drop from evaporator to condenser is 6.5^{o}C with

FIGURE 4.14

START-UP TEST FOR CRYOGENIC HEAT PIPE WITH SLAB WICK

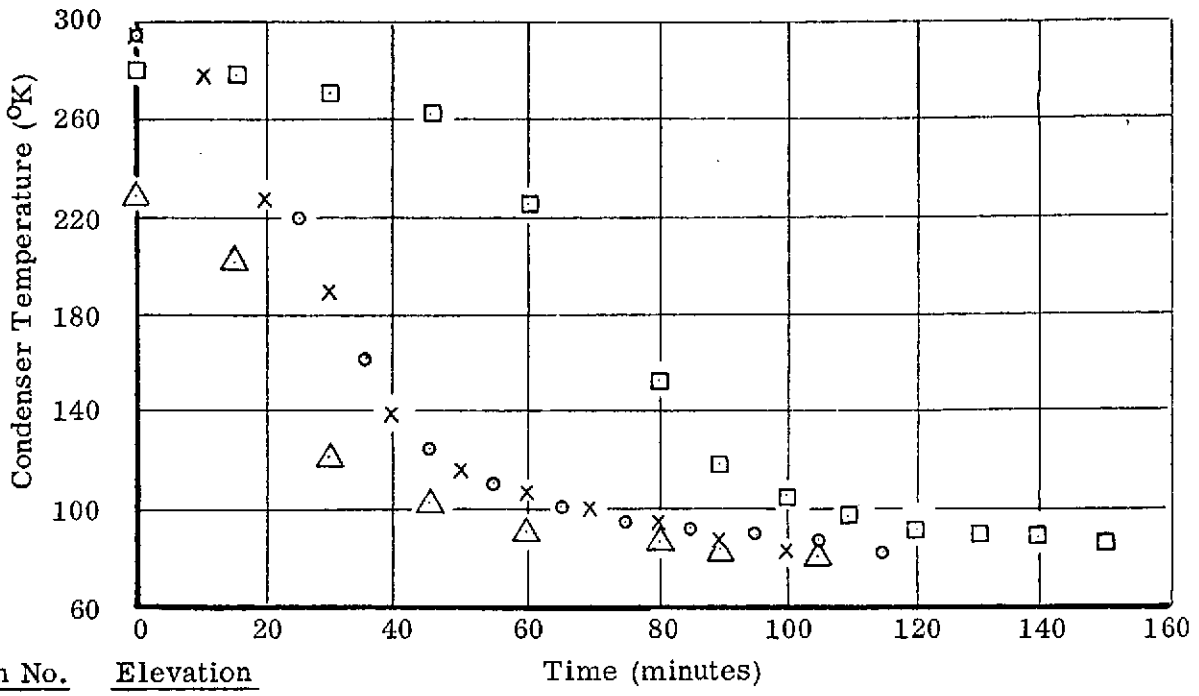

	Run No.	Elevation
○	1	-0.254 cm
□	2	-0.254 cm
△	3	-0.254 cm
×	4	Horizontal

FIGURE 4.14a

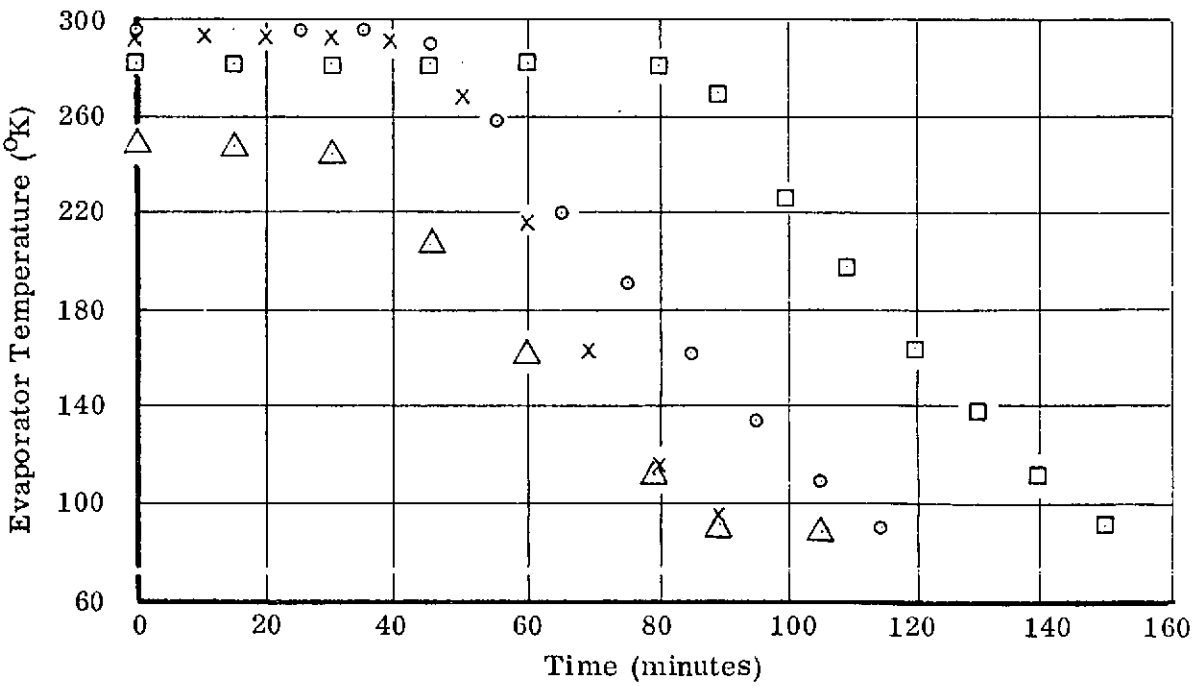

FIGURE 4.14b

FIGURE 4.15

TEMPERATURE PROFILE FOR DESIGN PERFORMANCE TEST

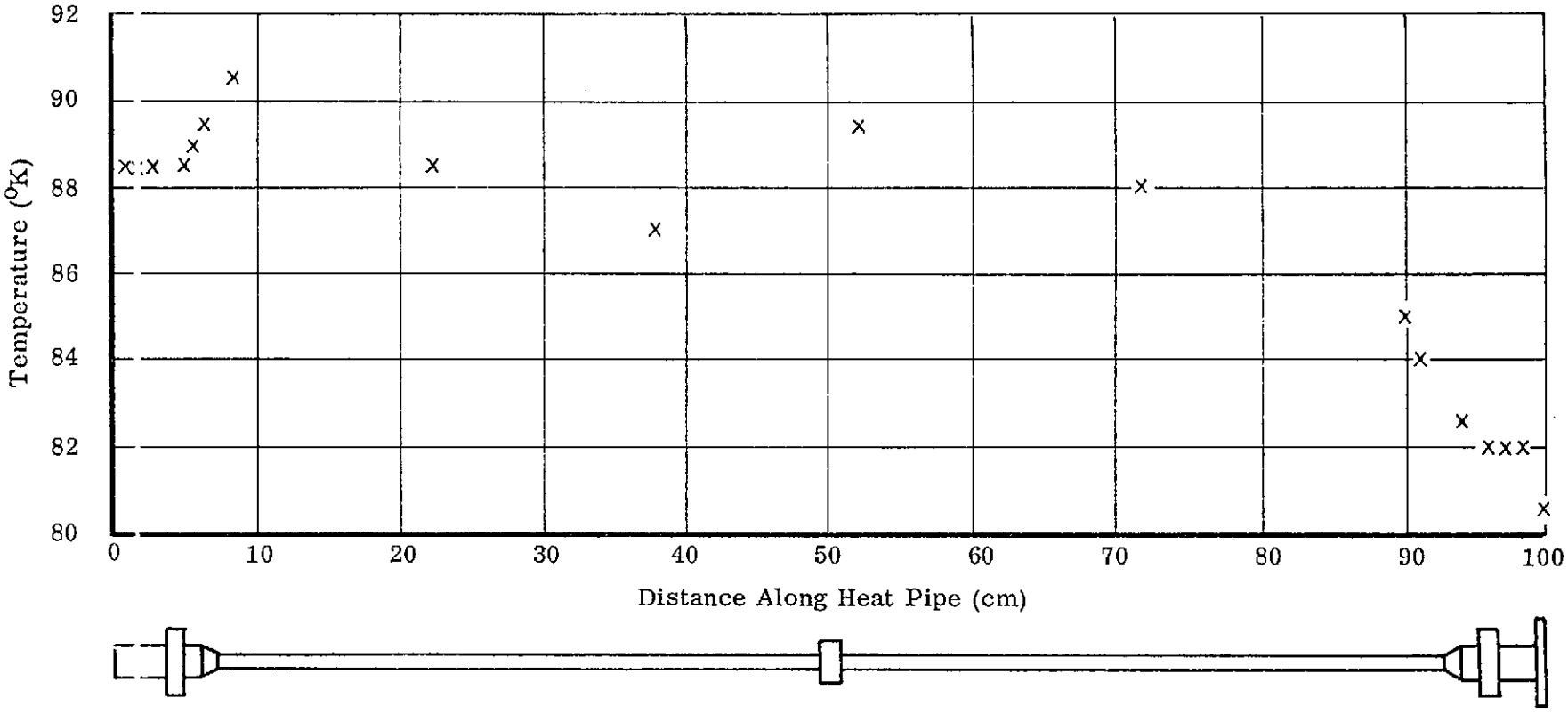

Q_{in} = .5 watts

Elevation = -.254 cm

Q_{out} = 4.5 watts

almost all of this drop occurring at the condenser end. The heat removal rate at the condenser is nine times greater than the heat input rate at the evaporator and is the reason for the large condenser temperature drop. If the temperature drop to the flange is included, the total drop is $8.0^{o}C$ instead of $6.5^{o}C$.

4.4.3.3 Heat Transport Capability Tests

The maximum heat transport capability of the heat pipe was determined at three evaporator elevations (.244 cm, 0.325 cm, and 0.500 cm). Measurements of evaporator temperature drop versus heat input are used to determine the maximum capability at a given elevation. Figure 4.16 summarizes the results for the three elevations tested. Included in the figure are the actual test data and the correction for parasitic heat leaks. It was assumed that the latter occur uniformly along the length of the heat pipe and 2 watts have been added to the effective evaporator load.

The static wicking height is 1.0 cm; and, when the inside diameter of the heat pipe is included, the height becomes 2.1 cm. This is approximately half the wicking height predicted based on the wire size and screen opening for 325-mesh screen. Separate static wicking height measurements made with samples of the slab wick material and methanol yielded the full wicking height calculated for the screen pore size. The discrepancy observed during the cryogenic tests is probably due to either a dry out of the screw threads in the evaporator which resulted in a premature burn-out condition or the outer 325-mesh screen could have been damaged during assembly. The permeability computed from the data of Figure 4.16 is 3.4×10^{-9} meters^{2}. This measured permeability is higher than predicted for a 60-mesh screen.

The extrapolation of the test data to the horizontal orientation yields a heat transport capability of slightly more than 7 watts compared to a prediction of 4.3 watts. The discrepancy is due to a combination of much higher than predicted permeability and somewhat lower effective capillary pumping. The data also yield an evaporator film coefficient of 0.152 watt/cm^{2}-^{o}C which compares favorably with the design value of 0.18 watt/cm^{2}-^{o}C.

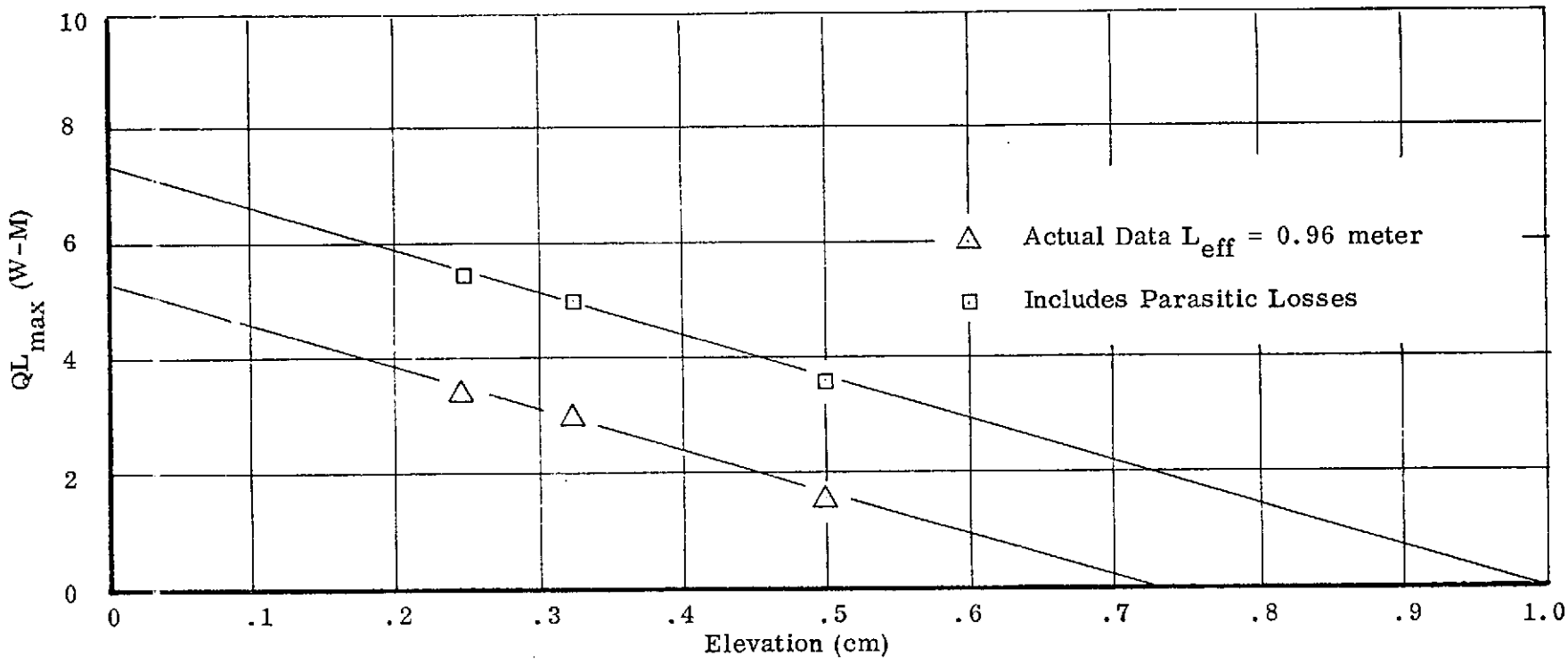

FIGURE 4.16

MAXIMUM TRANSPORT CAPABILITY FOR
CRYOGENIC HEAT PIPE WITH SLAB WICK

4.4.4 Tests With Prototype Artery-Wick Heat Pipe

The prototype heat pipe with an artery wick was placed in the vacuum chamber and prepared for testing in a manner identical to that employed for the slab-wick heat pipe. The fill tube on the heat pipe was connected through a length of tubing to the manifold outside the vacuum chamber so that the nitrogen charge could be introduced and varied. Section 4.4.2 describes this method of charging. A charge of 2.6 grams was determined analytically to be the minimum quantity necessary to fill the artery and screen.

The condenser end was first cooled down with liquid nitrogen in the reservoir. The working fluid was introduced to allow the entire heat pipe to cool down as the wick primed. The elevation was varied from +0.63 cm to -0.63 cm and the charge was varied from 2.6 grams to 12.0 grams during numerous attempts to prime the artery. The pipe cooled down because the screen became saturated with liquid and possibly also because of a puddle for large fluid charges. However, the artery could not be primed.

An X-ray of the heat pipe indicated that the wick in the evaporator end had twisted approximately 90 degrees. This resulted in the artery being elevated about 6 mm, and this would prevent the artery from priming.

The evaporator end of the heat pipe was removed to repair the twist in the wick. A small support was placed in the end of the heat pipe to hold the wick in its proper position so that no further shifting of the wick could take place.

The heat pipe was reinstrumented and installed in the vacuum chamber to test the ability of the artery to prime. The tests were repeated and again the artery failed to prime. More X-rays were taken and indicated a slight twist of the wick in the transport section. The artery appeared to be raised about one millimeter in this area. The static wicking height of the open (unprimed) artery with liquid nitrogen is only approximately 1.5 mm. Thus, it is possible that a combination of the slight elevation of the artery and the heat load during cool-down (which may exceed the steady-state parasitic requirements) resulted in a transport requirement exceeding the capability of the unprimed artery.

Ammonia at room temperature has a larger surface tension and smaller density than liquid nitrogen (at the boiling point of nitrogen). Hence, ammonia would prime the artery easier than liquid nitrogen. Tests with ammonia would, therefore, indicate if the artery was damaged and unable to prime.

The artery heat pipe was tested in ambient air with a charge of 3.42 grams of ammonia which correspond to about a 60% volume overcharge of liquid (compared to the 2.6 grams of nitrogen charge). The heat sink reservoir was filled with water to maintain the heat pipe condenser near room temperature during the tests.

The heat pipe was easily primed with no power applied by letting it come to thermal equilibrium for about 15-30 minutes. It primed at a horizontal elevation and at evaporator elevations up to 1 mm above the condenser. Tests were conducted to measure the transport capability at several elevations from 3 to 12.5 cm. At each elevation, the maximum power transported before evaporator burn-out was about 10-11 watts. The insensitivity of Q_{max} to elevation indicates a dry-out of the secondary screw thread wick because the maximum radial heat flux was exceeded before the axial heat transport capability of the artery was exceeded. The results also verify that the artery is capable of being primed and that the static wicking height is at least 3/4 of the theoretical value.

APPENDIX A

CRYOGENIC HEAT PIPE THERMAL ANALYSIS PROGRAM

This appendix describes the utilization of the digital computer code "Cryogenic Heat Pipe Thermal Analysis (CRYOTHERM)." The mathematical model upon which the program is based and a description of typical results are given in Section 2.1 of this report. A flow chart is shown in Figure A-1. Table A-1 describes the entries to be made on the various input cards. The FORTRAN names, format, and units to be used are also indicated for each entry. A listing of sample input data, for a special case with eight regions, is presented in Table A-2. Finally, a listing of the entire program is presented in Figure A-2.

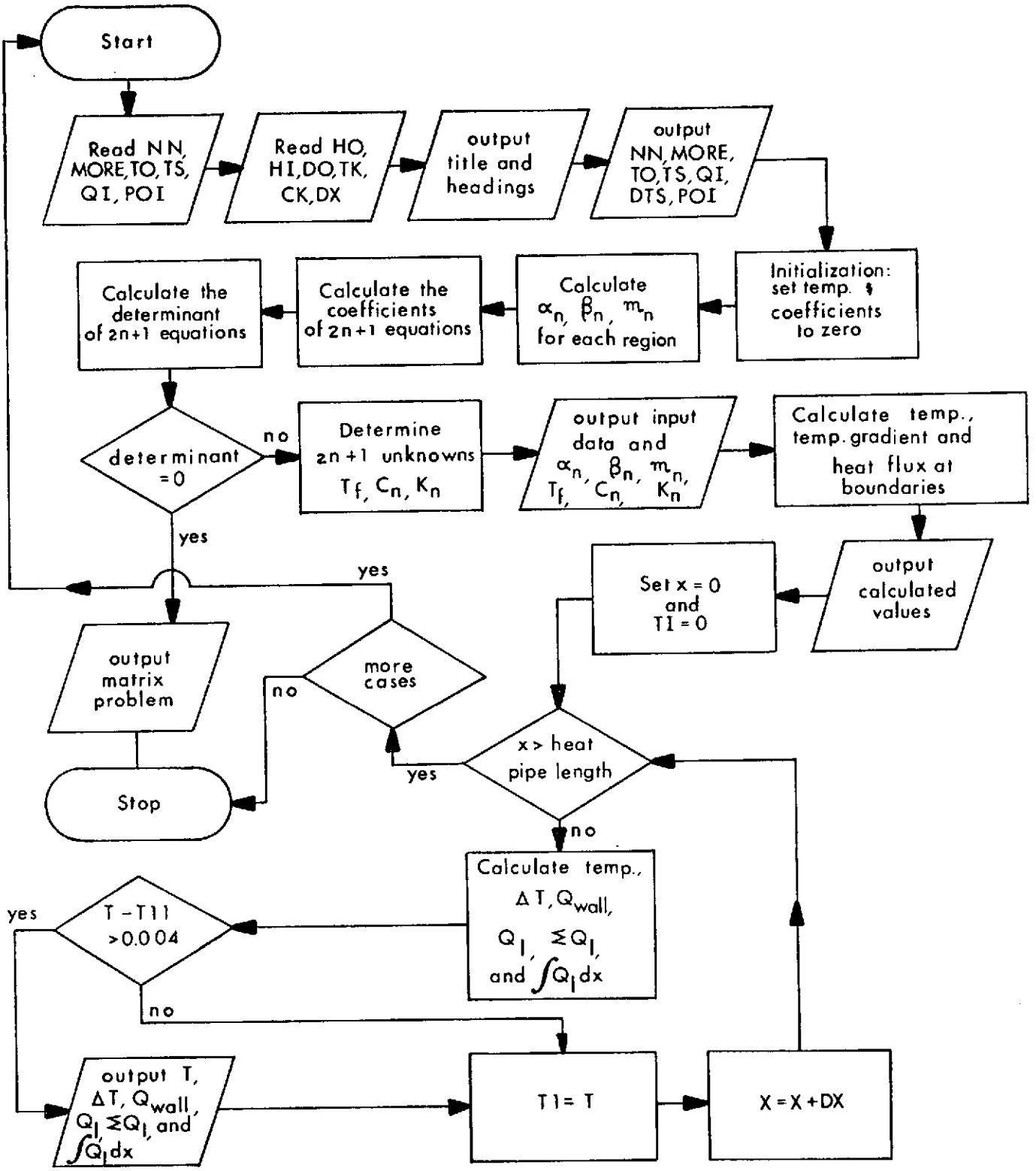

FIGURE A-1
FLOW CHART FOR CRYOTHERM

TABLE A-1

INPUT DATA DESCRIPTION

Input Card No.	Format	Fortran Name	Description	Units
1	2I3	NN	Number of regions (25 maximum)	-
		MORE	Control point (> 0, more cases; ≤ 0 end after this case)	-
	4E6.4	TO	Surrounding environmental temperature	K
		TS	Sensor Temperature at X = 0	K
		QI	Heat Input at X = 0	watt
		POI	Printout interval	M
2 to NN	12E6.4	HO(N)	External film coefficient	watt/cm^2-K
		HI(N)	Internal film coefficient	watt/cm^2-K
		DO(N)	Outside diameter	cm
		TK(N)	Wall thickness	cm
		CK(N)	Thermal conductivity	watt/cm-K
		DX(N)	Length of region	cm

```
   8  2300.0  80.0   3.4    1.0
9100-50.18   2.54   0.72400.692   3.0
1227-30.18   2.54   0.72400.692   1.0
9100-50.18   2.54   0.72400.692   2.0
9100-50.05   1.27   0.08900.692  44.0
2363-30.05   1.27   0.08900.692   1.0
9100-50.05   1.27   0.08900.692  43.0
2363-30.12   2.54   0.72400.692   1.0
9100-50.12   2.54   0.72400.692   5.0
```

TABLE A-2

SAMPLE INPUT DATA

```
C   PROGRAM   CRYOGENIC **** MAXIMUM REGIONS = 25                    (12/21/71)
C
      DIMENSION HO(25),HI(25),DO(25),TK(25),CK(25),DX(25),A(25),B(25),CM
     1(25),PI(25),XL(25),PHI(25),DELT(25),W(25),GAM(25),D(51),C(51,51),
     2DUM(51),TN(51)
    1 FORMAT (2I3,4E6.4)
    2 FORMAT (6E6.4)
    3 FORMAT (//6X,*MATRIX  PROBLEM*)
    6 FORMAT (2I5,5F10.4///)
    7 FORMAT (3X,*NN*,2X,*MORE*,4X,*TO*,8X,*TS*,8X,*QI*,7X,*DTS*,8X,*POI
     1*)
    8 FORMAT (85H1  C R Y O G E N I C  H E A T  P I P E  T H E R M A L
     1A N A L Y S I S  P R O G R A M///)
    9 FORMAT (1X,*REGION*,4X,*HO*,9X,*HI*,8X,*DO*,8X,*TK*,8X,*CK*,7X,*LG
     1TH*,8X,*M*,6X,*ALPHA*,5X,*BETA*,8X,*CONST-C*,8X,*CONST-K*/)
   11 FORMAT (I5,E11.2,6F10.4,2F10.6,2E15.4/)
   12 FORMAT(/10X,34HWORKING FLUID SAT. TEMP.(DEG K)---,F12.4)
  200 FORMAT (///58H AXIAL DISTANCE   HEAT PIPE WALL TEMP.        HEAT TR
     1ANSFER)
  201 FORMAT (7X,4H(CM),13X,7H(DEG K),17X,7H(WATTS)/)
  202 FORMAT (9X,1HX,11X,1HT,9X,4HTS-T,8X,18HIN WALL   TO FLUID,10X,7HQF
     1 X DX, 6X,8HABS(QFL))
  203 FORMAT (3F12.2,4E14.3)
      POI=1.0
      MATPR=0
   99 READ(5,1)NN,MORE,TO,TS,QI,POI
      READ(5,2)(HO(N),HI(N),DO(N),TK(N),CK(N),DX(N),N=1,NN)
      XM=0.0
      S1=3.141593*TK(1)*(DO(1)-TK(1))
      DTS=-QI/(CK(1)*S1)
      WRITE (6,8)
      WRITE (6,7)
      WRITE (6,6) NN,MORE,TO,TS,QI,DTS,POI
      WRITE (6,9)
      MM=2*NN
      LL=MM+1
      DO 15 J=1,LL
      TN(J)=0.0
      D(J)=0.0
      DO 15 K=1,LL
```

FIGURE A-2
PROGRAM LISTING

C-2

```
15   C(J,K)=0.0
     DO 5 N=1,NN
     HP=HO(N)*DO(N)+HI(N)*(DO(N)-2.*TK(N))
     A(N)=HO(N)*DO(N)*TO/HP
     B(N)=HI(N)*(DO(N)-2.*TK(N))/HP
     CM(N)=(HP/(1.*CK(N)*TK(N)*(DO(N)-TK(N))))**.5
     W(N)=3.141593*TK(N)*(DO(N)-TK(N))*CK(N)
     PI(N)=3.14159*(DO(N)-2.*TK(N))
     XL(N)=XM+DX(N)
 5   XM=XL(N)
     KK=NN+1
     KK1=NN+2
     C(1,1)=B(1)
     C(1,2)=1.0
     C(1,KK1)=1.0
     D(1)=TS-A(1)
     C(KK,2)=-1.0
     C(KK,KK1)=1.0
     D(KK)=DTS/CM(1)
     BB=HI(1)*PI(1)
     AA=CM(1)*XL(1)
     C(LL,KK1)=BB*(EXP(AA)-1.0)/CM(1)
     C(LL,  2 )=-BB*(EXP(-AA)-1.)/CM(1)
     CC1=BB*DX(1)*(B(1)-1.)
     DD1=BB*A(1)*DX(1)
     IF (N-1) 25,25,20
20   DO 10 N=2,NN
     M=N-1
     I=KK+N
     IK=N+1
     MK=KK+M
     LK=N
     BB=HI(N)*PI(N)
     AA=CM(N)*XL(N)
     EE=CM(N)*XL(M)
     CC1=CC1+BB*DX(N)*(B(N)-1.)
     DD1=DD1+BB*A(N)*DX(N)
     C(LL,I)=BB*(EXP(AA)-EXP(EE))/CM(N)
     C(LL,IK  )=-BB*(EXP(-AA)-EXP(-EE))/CM(N)
     C(N,N)=EXP(-CM(M)*XL(M))
     C(N,IK)=-EXP(-CM(N)*XL(M))
     C(N,KK+M)=EXP(CM(M)*XL(M))
     C(N,KK+N)=-EXP(CM(N)*XL(M))
     C(N,1)=B(M)-B(N)
```

FIGURE A-2 (Continued)

```
      D(N)=A(N)-A(M)
      C(NN+N,N)=EXP(-CM(M)*XL(M))*CM(M)*W(M)/(CM(N)*W(N))
      C(NN+N,KK+M)=-EXP(CM(M)*XL(M))*CM(M)*W(M)/(CM(N)*W(N))
      C(NN+N,IK)=-EXP(-CM(N)*XL(M))
   10 C(NN+N,KK+N)=EXP(CM(N)*XL(M))
   25 C(MM+1,I)=CCI
      D(MM+1)=-DDI
      JJ=NN
      NN=LL
      N1=NN-1
      DO 51 I=1,N1
      DD=C(I,I)
      IF(DD)47,41,47
   41 JS=I+1
      DO 42 J=JS,NN
      IF(C(J,I))43,42,43
   42 CONTINUE
      WRITE (6,3)
      GO TO 999
   43 DO 44 J1=I,NN
   44 DUM(J1)=C(I,J1)
      DM=D(I)
      DO 45 J1=I,NN
   45 C(I,J1)=C(J,J1)
      D(I)=D(J)
      DO 46 J1=I,NN
   46 C(J,J1)=DUM(J1)
      D(J)=DM
      DD=C(I,I)
   47 DO 48 J=I,NN
   48 C(I,J)=C(I,J)/DD
      D(I)=D(I)/DD
      K=I+1
      DO 51 L=K,NN
      R=C(L,I)
      IF(R)49,51,49
   49 DO 50 J=I,NN
   50 C(L,J)=C(L,J)-R*C(I,J)
      D(L)=D(L)-R*D(I)
   51 CONTINUE
      TN(NN)=D(NN)/C(NN,NN)
      K=NN
```

FIGURE A-2 (Continued)

```
   52 NN=NN-1
      N=NN
      IF(N)53,53,54
   53 NN=K
      GO TO 60
   54 TN(N)=D(N)
      NP=N+1
      DO 55 I=NP,K
   55 TN(N)=TN(N)-C(N,I)*TN(I)
      GO TO 52
   60 DO 59 N=1,JJ
   59 WRITE (6,11)N,HO(N),HI(N),DO(N),TK(N),CK(N),DX(N),CM(N),A(N),B(N),
     1TN(KK+N),TN(N+1)
      WRITE (6,12) TN(1)
      T11=A(1)+B(1)*TN(1)+TN(5)*EXP(CM(1)*XL(1))+TN(2)*EXP(-CM(1)*XL(1))
      T12=A(2)+B(2)*TN(1)+TN(6)*EXP(CM(2)*XL(1))+TN(3)*EXP(-CM(2)*XL(1))
      T22=A(2)+B(2)*TN(1)+TN(6)*EXP(CM(2)*XL(2))+TN(3)*EXP(-CM(2)*XL(2))
      T23=A(3)+B(3)*TN(1)+TN(7)*EXP(CM(3)*XL(2))+TN(4)*EXP(-CM(3)*XL(2))
      Q11=W(1)*CM(1)*(TN(5)*EXP(CM(1)*XL(1))-TN(2)*EXP(-CM(1)*XL(1)))
      Q12=W(2)*CM(2)*(TN(6)*EXP(CM(2)*XL(1))-TN(3)*EXP(-CM(2)*XL(1)))
      Q22=W(2)*CM(2)*(TN(6)*EXP(CM(2)*XL(2))-TN(3)*EXP(-CM(2)*XL(2)))
      Q23=W(3)*CM(3)*(TN(7)*EXP(CM(3)*XL(2))-TN(4)*EXP(-CM(3)*XL(2)))
      SL11=Q11/W(1)
      SL12=Q12/W(2)
      SL22=Q22/W(2)
      SL23=Q23/W(3)
  855 FORMAT (/*  CHECK AT BDY PTS...*,4F15.8/)
      WRITE(6,855) T11,T12,T22,T23
      WRITE(6,855) Q11,Q12,Q22,Q23
      WRITE(6,855) SL11,SL12,SL22,SL23
      NN=JJ
      X=0.0
      N=1
      TI=0.0
      XL(NN)=XL(NN)+ .0001
      XE=XL(NN)
   70 T=A(N)+B(N)*TN(1)+TN(KK+N  )*EXP(CM(N)*X)+TN(   N+1)*EXP(-CM(N)*X)
      DTX=CM(N)*(TN(  KK+N)*EXP(CM(N)*X)-TN(   N+1)*EXP(-CM(N)*X))
      QW=-3.14159*TK(N)*(DO(N)-TK(N))*CK(N)*DTX
      IF (X) 210,210,220
  210 WRITE (6,200)
      WRITE (6,201)
      WRITE (6,202)
```

FIGURE A-2 (Continued)

```
      QDX=0.0
      QF=0.0
      QFL=0.0
      GO TO 225
  220 QF=QF+HI(N)*PI(N)*POI*((T+TI)/2.-TN(1))
      QFL = HI(N)*PI(N)*POI*((T+TI)/2.-TN(1))
      QDX=QDX+QF*POI
  225 DT=TS-T
      ADB=ABS(T-TI)
      IF (ADB-.004   ) 72,71,71
   71 WRITE (6,203)X,T,DT,QW,QF,QDX,QFL
   72 TI=T
      X=X+POI
      IF(X-XE) 73,73,998
   73 IF(X-XL(N)) 70,70,74
   74 N=N+1
      GO TO 70
  998 IF (MORE) 999,999,99
  999 STOP
      END
      FUNCTION SINH(X)
      SINH=(EXP(X)-EXP(-X))/2.
      RETURN
      END
      FUNCTION COSH(X)
      COSH=(EXP(X)+EXP(-X))/2.
      RETURN
      END
```

FIGURE A-2 (Continued)

APPENDIX B

CRYOGENIC HEAT PIPE TRANSPORT ANALYSIS PROGRAM

This appendix describes the utilization of the digital computer code "Cryogenic Heat Pipe Transport Analysis Program (CRYOTA)." A flow chart of this program is shown in Figure B-1. Table B-1 describes the entries to be made on the various input cards. The FORTRAN names, format, and units to be used are also indicated for each entry. A listing of sample input data is presented in Table B-2. Finally, a listing of the entire program is presented in Figure B-2.

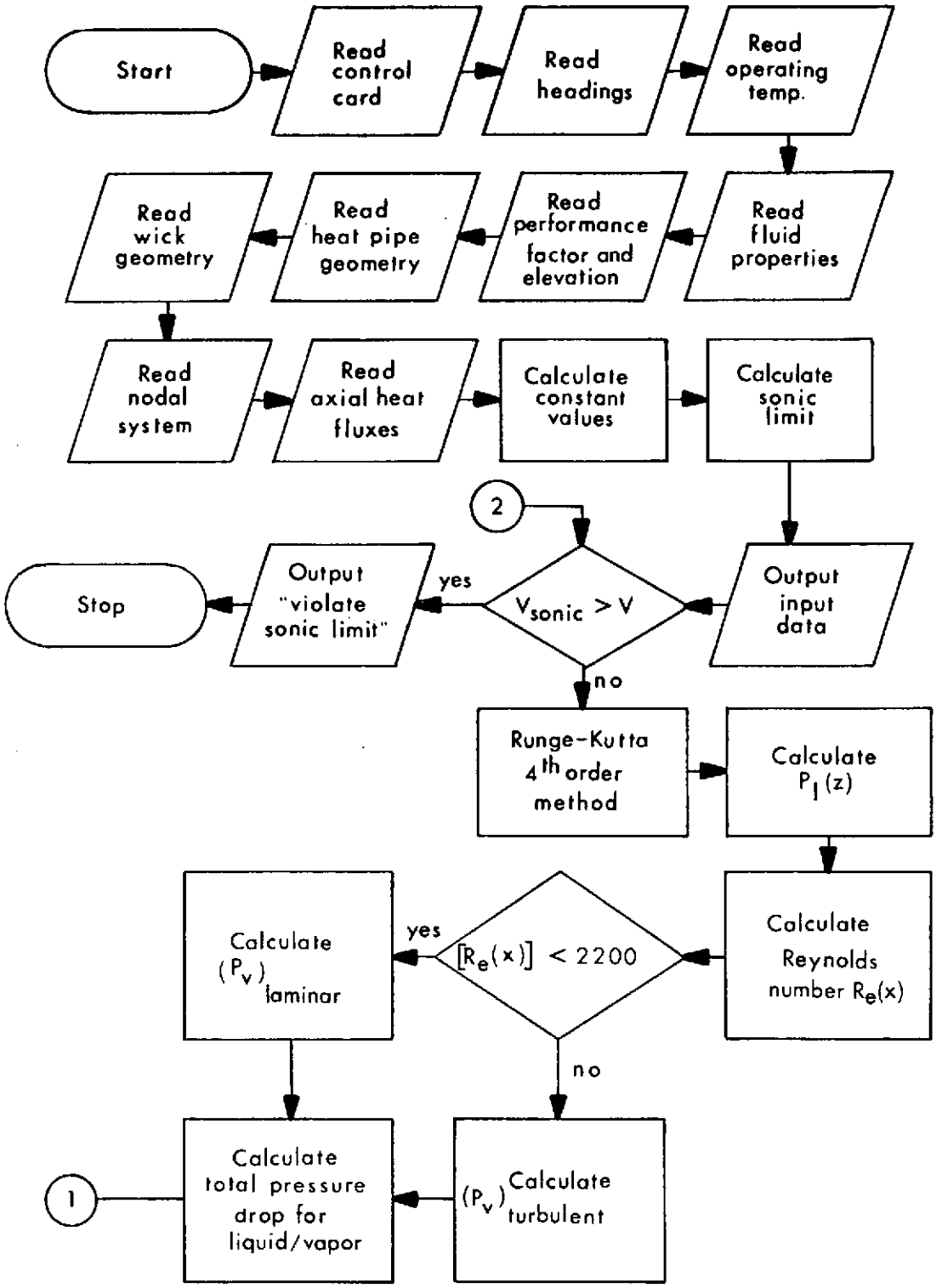

FIGURE B-1
FLOW CHART FOR CRYOTA

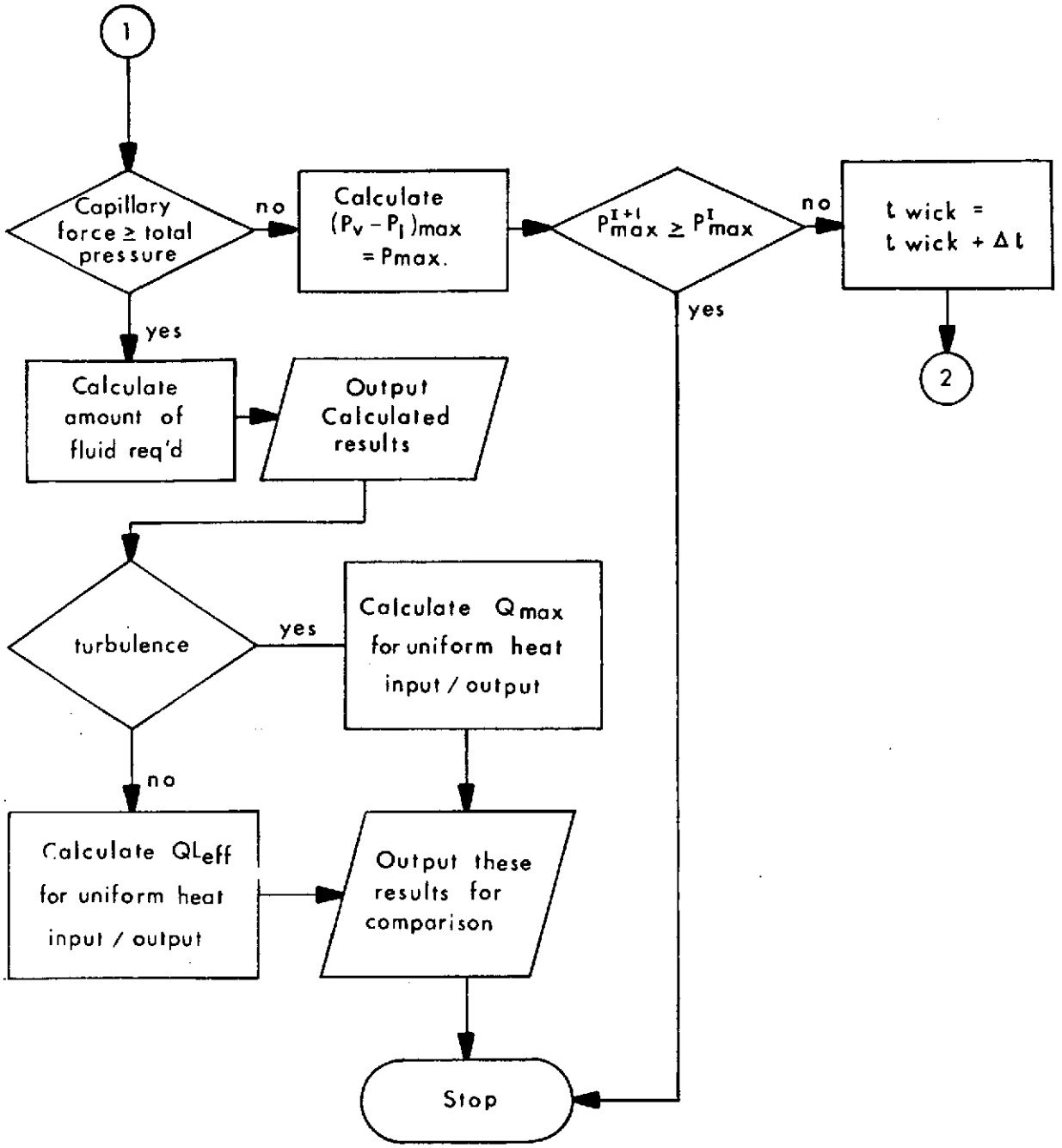

ORIGINAL PAGE IS OF POOR QUALITY

FIGURE B1 (cont.)

TABLE B-1

INPUT DATA DESCRIPTION

Input Card No.	Format	Fortran Name	Description	Units
1	I3	MORE	Control point, integer < 1 for last set of data, otherwise integer > 1	-
2	A10, A5	HD1 HD2	Headings (working fluid)	-
3	F10.5	TEMP	Operating temperature	K
4	8E10.4	RHOL	Liquid density	kg/m^3
		RHOV	Vapor density	kg/m^3
		XLAMD	Latent heat of vaporization	W-sec/kg
		SIGMA	Surface tension	N/m
		XMUL	Dynamic liquid viscosity	kg/m-sec
		XMUV	Dynamic vapor viscosity	kg/kg-sec
5	2F10.5	XMW	Molecular weight	kg/kg-mole
		GAMMA	Ratio of specific heats	-
6	F10.5	G	G = 0 Zero "g" environment G = 1 One "g" environment	-
7	2F10.5	PERF	Performance factor	-
		HIGH	Elevation between condenser end and evaporator end	m

Input Card No.	Format	Fortran Name	Description	Units
8	3F10.5	XLEV	Length of evaporator section	m
		XLAD	Length of adiabatic section	m
		XLCO	Length of condenser section	m
9	2I3	I1	Mesh size of coarse wick material	-
		I2	Mesh size of fine wick material	-
10	E10.4	XMI	Minimum Wick Width	m
11	3E10.4	XKP	Permeability	m^2
		RPE	Effective pumping radius for heat transport	m
		CCORE	Effective pore radius for self-priming	m
12	4E10.4	XOD	Outside diameter of heat pipe	m
		TWALL	Wall thickness of heat pipe	m
		D1	Diameter of coarse wick material	m
		D2	Diameter of fine wick material	m
13	3I3	NNE	No. of divisions of evaporator section	-
		NNA	No. of divisions of adiabatic section	-
		NNC	No. of divisions of condenser section	-
14	8E10.1	XAXIS(I)*	Distance from condenser end	m
15	8E10.1	QR(I)*	The corresponding heat flux at XAXIS(I)	w/m^2

*NOTE: Where I is from 1 to (NNE + NNA + NNC)

```
  0
NITROGEN
  80.
8.0000E+025.9000E+001.9500E+058.2000E-031.4480E-045.8400E-06
  28.0        1.4
   1.0
   1.0        0.00254
   0.09       0.82       0.09
 60325
2.2660E-03
4.5000E-103.9400E-052.3600E-04
1.2700E-028.9000E-041.9100E-043.5600E-05
  9  0 92
   1.0E-02   2.0E-02   3.0E-02   4.0E-02   5.0E-02   6.0E-02   7.0E-02   8.0E-02
   9.0E-02   1.0E-01   1.1E-01   1.2E-01   1.3E-01   1.4E-01   1.5E-01   1.6E-01
   1.7E-01   1.8E-01   1.9E-01   2.0E-01   2.1E-01   2.2E-01   2.3E-01   2.4E-01
   2.5E-01   2.6E-01   2.7E-01   2.8E-01   2.9E-01   3.0E-01   3.1E-01   3.2E-01
   3.3E-01   3.4E-01   3.5E-01   3.6E-01   3.7E-01   3.8E-01   3.9E-01   4.0E-01
   4.1E-01   4.2E-01   4.3E-01   4.4E-01   4.5E-01   4.6E-01   4.7E-01   4.8E-01
   4.9E-01   5.0E-01   5.1E-01   5.2E-01   5.3E-01   5.4E-01   5.5E-01   5.6E-01
   5.7E-01   5.8E-01   5.9E-01   6.0E-01   6.1E-01   6.2E-01   6.3E-01   6.4E-01
   6.5E-01   6.6E-01   6.7E-01   6.8E-01   6.9E-01   7.0E-01   7.1E-01   7.2E-01
   7.3E-01   7.4E-01   7.5E-01   7.6E-01   7.7E-01   7.8E-01   7.9E-01   8.0E-01
   8.1E-01   8.2E-01   8.3E-01   8.4E-01   8.5E-01   8.6E-01   8.7E-01   8.8E-01
   8.9E-01   9.0E-01   9.1E-01   9.2E-01   9.3E-01   9.4E-01   9.5E-01   9.6E-01
   9.7E-01   9.8E-01   9.9E-01   1.0E+00
-1.254E+02-8.631E+01-6.005E+01-4.278E+01-3.199E+01-2.609E+01-6.934E+00-2.448E+00
-5.614E-01 2.317E-01 5.651E-01 7.053E-01 7.642E-01 7.890E-01 7.994E-01 8.038E-01
 8.056E-01 8.064E-01 8.067E-01 8.068E-01 8.069E-01 8.069E-01 8.069E-01 8.069E-01
 8.069E-01 8.069E-01 8.069E-01 8.069E-01 8.069E-01 8.069E-01 8.069E-01 8.069E-01
 8.069E-01 8.069E-01 8.069E-01 8.069E-01 8.069E-01 8.069E-01 8.069E-01 8.069E-01
 8.069E-01 8.069E-01 8.069E-01 8.069E-01 8.069E-01 8.069E-01 8.069E-01 8.069E-01
 8.069E-01 8.069E-01 8.069E-01 8.069E-01 8.069E-01 8.069E-01 8.069E-01 8.069E-01
 8.069E-01 8.069E-01 8.069E-01 8.069E-01 8.069E-01 8.069E-01 8.069E-01 8.069E-01
 8.070E-01 8.070E-01 8.071E-01 8.074E-01 8.081E-01 8.096E-01 8.133E-01 8.220E-01
 8.428E-01 8.922E-01 1.010E+00 1.290E+00 1.955E+00 3.538E+00 1.808E+01 2.269E+01
 3.194E+01 4.787E+01 7.396E+01 1.160E+02
```

TABLE B-2

SAMPLE LISTING OF INPUT DATA

```
C       NOEL LEE, DYNATHERM CORP., COCKEYSVILLE, MD., JUNE 1973
        DIMENSION XQ(110),XA(110),XB(110),XL(110),XC(110),XQL(110),QT(3)
        DIMENSION A(3),DA(3),QTEMP(5),QR(110),X(110),P(110),XMLZ(110)
        DIMENSION APENO(110),PVML(110),PVFL(110),PV(110),PL(110),V2(110)
        DIMENSION FL(110),XMVZ(110),V1(110),BODYF(110),XAXIS(110),S1(110)
        DIMENSION S2(110)
   32 FORMAT (/E20.7)
   93 FORMAT (//*  MASS OF THE WORKING FLUID REQUIRED(KG)*)
   94 FORMAT (/E20.7)
  126 FORMAT (//*  THE PERFORMANCE FACTOR IS*)
  132 FORMAT (/7X,F4.2)
  500 READ(5,498) MORE
        READ (5,5005) HD1,HD2
 5005 FORMAT (A10,A5)
  498 FORMAT (4I3)
        READ (5,5010) TEMP
 5010 FORMAT (8E10.5)
        READ (5,5009) RHOL,RHOV,XLAMD,SIGMA,XMUL,XMUV
 5009 FORMAT (8E10.4)
        READ (5,5010) XMW,GAMMA
        READ (5,5010) G
        READ (5,5010) PERF,HIGH
        READ (5,5010) XLEV,XLAD,XLCO
        READ (5,498) I1,I2
        READ (5,5009) XWI
        READ (5,5009) XKP,PPE,CCORE
        READ (5,5009) XOD,TWALL,D1,D2
        PHI=0.0
        SIGN=1.0
        XMWI=2.0*D1+4.0*D2
        READ (5,498)    NNE,NNA,NNC
        NN=NNE+NNA+NNC
        NM=NN-1
        XAXIS(1)=0.0
        READ (5,702) (XAXIS(I),I=2,NN)
  702 FORMAT (8F10.1)
        READ (5,764) (QR(I),I=1,NM)
```

FIGURE B-2

PROGRAM LISTING FOR CRYOTA

```
764 FORMAT (8F10.3)
    LEE=NN
    LEEC2=NNC
    LEEA1=NNC+1
    LEEA2=NNC+NNA
    NAD=1
    IF (LEEA2.GE.LEEA1) GO TO 703
    NAD=0
703 LEEE1=NNC+NNA+1
    DO 706 I=1,LEE
    QR(I)=QR(I)*PERF
706 CONTINUE
    II=1
    IND=0
    XLHP=XLEV+XLAD+XLCO
    XLEFF=XLAD*XLEV/2.0+XLCO/2.0
    XID=XOD-2.0*TWALL
    RHEAD=XID+SIGN*HIGH
    CAREA=(XID*XID/4.0)*3.14159*(1.0/10.0)
    T2R=XWI
    XNL=SIGMA*XLAMD*RHOL/XMUL
    CPGHD=2.0*SIGMA*COS(PHI)/RPE
    BODY=RHOL*9.8*(XID+SIGN*HIGH)
    CHEAD=CPGHD-BODY
    R=XID/2.0
    CCORE=2.0*SIGMA* COS(PHI)/CCORE
    CCORE=CCORE/(RHOL*9.8)
    SONIC=((GAMMA*TEMP*1.8*1544.33*32.2/XMW)**0.5)*0.3048
    WRITE (6,10)
 10 FORMAT (*1*)
    WRITE (6,60)
 60 FORMAT (/////*  H E A T    T R A N S P O R T    A N A L Y S I S
   1 F O R    C R Y O G E N I C    H E A T    P I P E*)
    WRITE (6,61)
 61 FORMAT (////*  I N P U T    D A T A*)
    WRITE (6,62)
 62 FORMAT (////*  H E A T    P I P E    P R O P E R T I E S*)
    WRITE (6,66)
 66 FORMAT (//*  OUTSIDE DIAMETER(M)      MIN. WALL THICKNESS(M)*)
    WRITE (6,67) XOD,TWALL
 67 FORMAT (/2E20.7)
```

FIGURE B-2 (Continued)

```
 68 FORMAT (//* LENGTH OF THE HEAT PIPE SECTIONS*)
    WRITE (6,69)
 69 FORMAT (//*          EVAP(M)          AD(M)          COND
   1(M)          TOTAL(M)*)
    WRITE (6,70) XLEV,XLAD,XLCO,XLHP
 70 FORMAT (/4E20.7)
    WRITE (6,73)
 73 FORMAT (////*  W I C K    G E O M E T R Y*)
    WRITE (6,74)
 74 FORMAT (//*  SLAB WICK GEOMETRY*)
    WRITE (6,174) I1,I2
174 FORMAT(//18H  COMPOSITE WICK (,I3,22H MESH SCREEN CORE AND ,I3,13H
   1 MESH SCREEN))
    WRITE (6,75)
 75 FORMAT (//*  PERMEABILITY(M-M)     MIN. EFF. PUMPING RAD.(M)    MIN.
   1 WICK THICKNESS(M)*)
    WRITE (6,76) XKP,RPE,XMWI
 76 FORMAT (/2E20.7,5X,E20.7)
    WRITE (6,10)
    WRITE (6,77)
 77 FORMAT (//*  F L U I D     P R O P E R T I E S*)
    WRITE (6,78) HD1,HD2,TEMP
 78 FORMAT (//18H  WORKING FLUID = ,A10,A5,4H AT ,F6.2,3H(K))
    WRITE (6,79)
 79 FORMAT (//*  SURFACE TENSION(N/M)     LATENT HEAT(W-S/KG)*)
    WRITE (6,80)  SIGMA,XLAMD
 80 FORMAT (/2E20.7)
    WRITE (6,81)
 81 FORMAT (//*  LIQ. DENSITY(KG/M-M-M)     VAPOR DENSITY(KG/M-M-M)*)
    WRITE (6,82) RHOL,RHOV
 82 FORMAT (/2E20.7)
    WRITE (6,83)
 83 FORMAT (//*  LIQ. VISCOSITY(KG/M-S)     VAPOR VISCOSITY(KG/M-S)*)
    WRITE (6,84) XMUL,XMUV
 84 FORMAT (/2E20.7)
    WRITE (6,2000)
2000 FORMAT (//*  MOLECULAR WT          RATIO OF SPECIFIC HEATS*)
    WRITE (6,84) XMW,GAMMA
    WRITE (6,184)
184 FORMAT (//*  LIQUID TRANSPORT FACTOR(W/M-M) *)
    WRITE (6,185) XNL
185 FORMAT (/E20.7)
    WRITE (6,888)
```

FIGURE B-2 (Continued)

```
888 FORMAT (////* H E A T   T R A N S P O R T   R E Q U I R E M E N
    1 T*)
      WRITE (6,126)
      WRITE (6,132) PERF
      WRITE (6,889)
889 FORMAT (//* ELEVATION(M)*)
      WRITE (6,32) HIGH
      CHECK2=0.0
      CONP=0.0
      WRITE (6,805)
805 FORMAT (/////)
      WRITE (6,790)
790 FORMAT (//* H E A T   F L U X (W/M)   V E R S U S   D I S T A
    1N C E (M)   F R O M   T H E   C O N D E N S E R   E N D*)
      WRITE (6,791)
791 FORMAT (//*          X(M)          HEAT FLUX(W/M)
    1          X(M)          HEAT FLUX(W/M)*)
      WRITE (6,792) (XAXIS(I),QR(I),I=1,NM)
792 FORMAT (2E20.7,20X,2E20.7)
      IN=1
      QRMAX=QR(1)
      DO 771 J=2,LEE
      IF (QRMAX-QR(J)) 772,771,771
772   IN=J
      QRMAX=QR(IN)
771   CONTINUE
      ASONIC=QRMAX*(2.0*(GAMMA+1.0))**0.5/(XLAMD*RHOV*SONIC)
      WRITE (6,10)
      WRITE (6,85)
 85 FORMAT (////* O U T P U T   D A T A*)
      WRITE (6,86)
 86 FORMAT (////* S E L F - P R I M I N G   R E Q U I R E M E N T*)
      WRITE (6,87)
 87 FORMAT (//* CAPILLARY HEAD FOR CORE(M)   REQUIRED HEAD(M)*)
      WRITE (6,88) CCORE,RHEAD
 88 FORMAT (/E20.7,10X,E20.7)
      WRITE (6,769)
769 FORMAT (//* S O N I C   L I M I T A T I O N   (B A S E D   O N
    1   M A X I M U M   H E A T   F L U X (W/M))*)
      WRITE (6,201)
201 FORMAT (//* SONIC VELOCITY(M/S)          MINIMUM VAPOR AREA(M-M
    1) FOR SONIC LIMITATION*)
      WRITE (6,202) SONIC,ASONIC
```

FIGURE B-2 (Continued)

```
202 FORMAT (/E20.7,10X,E20.7)
    B=T2B/2.0
    THETA=ACOS(B/R)
    C=R*SIN(THETA)
    AFV=2.0*R*R*THETA-2.0*B*C
    AV=AFV
    IF (ASONIC.GT.AFV) GO TO 3
    WRITE (6,10)
    WRITE (6,50)
 50 FORMAT (////*  H E A T    T R A N S P O R T    A N A L Y S I S*)
    R=XID/2.0
761 B=T2B/2.0
    CHECK1=CHECK2
    THETA=ACOS(B/R)
    C=R*SIN(THETA)
    AFV=2.0*R*R*THETA-2.0*B*C
    AV=AFV
    AW=3.14159*R*R-AFV
    WP=4.0*(C+R*THETA)
    DHV=4.0*AFV/WP
    RV=DHV/2.0
    DO 708 I=1,LEE
    BODYF(I)=RHOL*9.8*(XID+SIGN*HIGH*XAXIS(I)/XLHP)*G
    V1(I)=CPGHD-BODYF(I)
708 CONTINUE
    N=1
    IND=1
    ISCAN=1
    T=0.0
    X(1)=0.0
    XMLZ(1)=X(1)
709 CALL RK(QR,XLAMD,Q,XAXIS,RV,XI,CO,RHOV,XMUV,XMVZ,XMUL,XMLZ,RHOL,AW,
   1XKP,ISCAN,X,P,T,N,IND,AFV)
    IND=IND+1
    XMLZ(IND)=X(1)
    IF (IND-LEEC2) 709,710,710
710 T=XAXIS(LEEC2)
    X(1)=XMLZ(LEEC2)
    IF (NAD.LT.1) GO TO 719
717 CALL RK(QR,XLAMD,Q,XAXIS,RV,XI,CO,RHOV,XMUV,XMVZ,XMUL,XMLZ,RHOL,AW,
   1XKP,ISCAN,X,P,T,N,IND,AFV)
    IND=IND+1
    XMLZ(IND)=X(1)
    IF (IND-LEEF1) 717,718,718
```

FIGURE B-2 (Continued)

```
      T=XAXIS(LEEE1)
      X(1)=XMLZ(LEEE1)
  719 CALL RK(QR,XLAMD,0,XAXIS,RV,XLCO,RHOV,XMUV,XMVZ,XMUL,XMLZ,RHOL,AW,
     1XKP,ISCAN,X,P,T,N,IND,AFV)
      IND=IND+1
      XMLZ(IND)=X(1)
      IF (IND.LT.LEE) GO TO 719
      DO 720 I=1,LEE
      XMVZ(I)=XMLZ(I)
  720 CONTINUE
      IMAX=1
      AMAX=XMLZ(1)
      DO 721 J=2,LEE
      IF (AMAX-XMLZ(J)) 723,721,721
  723 IMAX=J
      AMAX=XMLZ(J)
  721 CONTINUE
      DO 724 I=1,LEE
      ARENO(I)=2.0*XMVZ(I)/(3.14159*XMUV*RV)
  724 CONTINUE
      ARENO(IMAX)=2.0*XMLZ(IMAX)/(3.14159*XMUV*RV)
      IF (ARENO(IMAX).GT.2200.0) GO TO 751
      IND=1
      ISCAN=3
      T=0.0
      X(1)=CONP
      PV(1)=X(1)
  725 CALL RK(QR,XLAMD,0,XAXIS,RV,XLCO,RHOV,XMUV,XMVZ,XMUL,XMLZ,RHOL,AW,
     1XKP,ISCAN,X,P,T,N,IND,AFV)
      IND=IND+1
      PV(IND)=X(1)
      IF (IND-LEEC2) 725,726,726
  726 T=XAXIS(LEEC2)
      X(1)=PV(LEEC2)
      IF (NAD.LT.1) GO TO 729
  727 CALL RK(QR,XLAMD,0,XAXIS,RV,XLCO,RHOV,XMUV,XMVZ,XMUL,XMLZ,RHOL,AW,
     1XKP,ISCAN,X,P,T,N,IND,AFV)
      IND=IND+1
      PV(IND)=X(1)
      IF (IND-LEEE1) 727,728,728
  728 T=XAXIS(LEEE1)
      X(1)=PV(LEEE1)
```

FIGURE B-2 (Continued)

```
729 CALL RK(QR,XLAMD,0,XAXIS,RV,XLCO,RHOV,XMUV,XMVZ,XMUL,XMLZ,RHOL,AW,
    1XKP,ISCAN,X,P,T,N,IND,AFV)
      IND=IND+1
      PV(IND)=X(1)
      IF (IND.LT.LEE) GO TO 729
      GO TO 730
751   IND=1
      T=0.0
      ISCAN=2
      X(1)=CONP
      PV(1)=X(1)
731   CALL RK(QR,XLAMD,0,XAXIS,RV,XLCO,RHOV,XMUV,XMVZ,XMUL,XMLZ,RHOL,AW,
     1XKP,ISCAN,X,P,T,N,IND,AFV)
      IND=IND+1
      PV(IND)=X(1)
      IF (IND-LEEC2) 731,732,732
732   T=XAXIS(LEEC2)
      X(1)=PV(LEEC2)
      IF (NAD.LT.1) GO TO 7350
      ISCAN=5
733   CALL RK(QR,XLAMD,0,XAXIS,RV,XLCO,RHOV,XMUV,XMVZ,XMUL,XMLZ,RHOL,AW,
     1XKP,ISCAN,X,P,T,N,IND,AFV)
      IND=IND+1
      PV(IND)=X(1)
      PV(1)=X(1)
      IF (IND-LEEE1) 733,734,734
734   T=XAXIS(LEEE1)
      X(1)=PV(LEEE1)
7350  ISCAN=6
735   CALL RK(QR,XLAMD,0,XAXIS,RV,XLCO,RHOV,XMUV,XMVZ,XMUL,XMLZ,RHOL,AW,
     1XKP,ISCAN,X,P,T,N,IND,AFV)
      IND=IND+1
      PV(IND)=X(1)
      IF (IND.LT.LEE) GO TO 735
730   IND=1
      ISCAN=4
      T=0.0
      X(1)=CONP
      PL(1)=X(1)
736   CALL RK(QR,XLAMD,0,XAXIS,RV,XLCO,RHOV,XMUV,XMVZ,XMUL,XMLZ,RHOL,AW,
     1XKP,ISCAN,X,P,T,N,IND,AFV)
      IND=IND+1
      PL(IND)=X(1)
      IF (IND-LEEC2) 736,737,737
```

FIGURE B-2 (Continued)

```
737 T=XAXIS(LEEC2)
    X(1)=PL(LEEC2)
    IF (NAD.LT.1) GO TO 740
738 CALL RK(QR,XLAMD,Q,XAXIS,RV,XLCO,RHOV,XMUV,XMVZ,XMUL,XMLZ,RHOL,AW,
   1XKP,ISCAN,X,P,T,N,IND,AFV)
    IND=IND+1
    PL(IND)=X(1)
    IF (IND-LEEE1) 738,739,739
739 T=XAXIS(LEEE1)
    X(1)=PL(LEEE1)
740 CALL RK(QR,XLAMD,Q,XAXIS,RV,XLCO,RHOV,XMUV,XMVZ,XMUL,XMLZ,RHOL,AW,
   1XKP,ISCAN,X,P,T,N,IND,AFV)
    IND=IND+1
    PL(IND)=X(1)
    IF (IND.LT.LEE) GO TO 740
    DO 763 I=1,LEE
    S2(I)=PV(I)-PL(I)
    S1(I)=V1(I)-S2(I)
763 CONTINUE
    IIMIN=1
    S1MIN=S1(1)
    DO 765 J=2,LEE
    IF (S1(J)-S1MIN) 766,765,765
766 IIMIN=J
    S1MIN=S1(IIMIN)
765 CONTINUE
    CHECK0=S1MIN
    IF (CHECK0.GT.0.0) GO TO 770
    IIMAX=1
    S2MAX=S2(1)
    DO 767 J=2,LEE
    IF (S2MAX-S2(J)) 768,767,767
768 IIMAX=J
    S2MAX=S2(IIMAX)
767 CONTINUE
    CHECK2=S2MAX
    IF (AFV.LT.CAREA) GO TO 762
    IF (AFV.LT.ASONIC) GO TO 762
    IF (T2B.GT.XID) GO TO 762
    T2B=T2B+2.*(D1+D2)
    IF (CHECK1.EQ.0.0) GO TO 761
    IF (CHECK2.LT.CHECK1) GO TO 761
    GO TO 762
```

FIGURE B-2 (Continued)

```
770 WIDTH=T2B
    XMFLD=RHOL*(1.0-VOID)*AW*XLHP+XLHP*AV*RHOV
    WRITE (6,26)
 26 FORMAT (//*  THE VAPOR AREA(M-M) SATISFIES THE HEAT TRANSPORT REQU
   1IREMENT IS*)
    WRITE (6,27) AV
 27 FORMAT (/E20.7)
    WRITE (6,89)
 89 FORMAT (//*  THE WICK WIDTH(M) SATISFIES THE HEAT TRANSPORT REQUIR
   1EMENT IS*)
    WRITE (6,27) T2B
    WRITE (6,91)
 91 FORMAT (//*  THE WICK AREA(M-M) SATISFIES HEAT TRANSPORT REQUIREME
   1NT IS*)
    WRITE (6,27) AW
    WRITE (6,93)
    WRITE (6,94) XMFLD
    WRITE (6,773)
773 FORMAT (//*  NOTE   THE FOLLOWING DATA OF (QLEFF)MAX(W-M),QMAX(W)
   1AND DQ/DH(W/M) ARE BASED ON UNIFORM HEAT INPUT AND OUTPUT*)
    WRITE (6,776)
776 FORMAT (  *          (PRESENTED HERE AS A COMPARISON)*)
    WRITE (6,111)
111 FORMAT (//*      WICK THICKNESS          WICK AREA                ( G=
   11  )          (  G=1  )          (  G=0  )          ( G=0 )       ( G
   2=1 )*)
    WRITE (6,11)
 11 FORMAT (/*            (M)                    (M-M)                (QLEFF)MA
   1X(W-M)        QMAX(W)          (QLEFF)MAX(W-M)     QMAX(W)       DQ/D
   2H(W/M)*)
    IF (ARFNO(IMAX).GT.2200.0) GO TO 40
    DQDH=-0.5*(9.8*RHOL*SIGN/XLEFF)/(XMUL/(2.0*RHOL*AW*XKP*XLAMD)+4.0*
   1XMUV/(AFV*RHOV*XLAMD*RV**2.0))
    QLMAX=0.5*CHEAD/(XMUL/(2.0*RHOL*AW*XKP*XLAMD)+4.0*XMUV/(AFV*RHOV*X
   1LAMD*RV**2.0))
    QLM0G=0.5*CPGHD/(XMUL/(2.0*RHOL*AW*XKP*XLAMD)+4.0*XMUV/(AFV*RHOV*X
   1LAMD*RV**2.0))
    QMAXC=QLMAX/XLEFF
    QMA0G=QLM0G/XLEFF
    WRITE (6,801) T2B,AW,QLMAX,QMAXC,QLM0G,QMA0G,DQDH
801 FORMAT (/5E20.7,2F15.7)
    GO TO 1
 40 WRITE (6,151)
```

FIGURE B-2 (Continued)

```
151 FORMAT(//*        FLOW IS NOW TURBULENT (REYNOLD NO. GREATER THAN 2
   1200).*)
 48 C1=CHEAD
    C2=XMUL*(XLHP+XLAD)/(2.0*RHOL*AW*XKP*XLAMD)
    C3=0.0655*XMUV**0.25*XLAD/(RHOV*RV**4.75*(XLAMD*3.14159)**1.75)
    C4=(1.0-4.0/3.14159**2.0)/(8.0*RHOV*RV**4.0*XLAMD**2.0)
    CHECK=0.0
    QT(1)=2.0*C1/(C2+C3+C4)
 41 CHECK=CHECK+1.0
    IF (CHECK.GT.15.0) GO TO 45
    N=1
    A(N)=C4*QT(N)**2.0+C3*QT(N)**1.75+C2*QT(N)-C1
    DA(N)=2.0*C4*QT(N)+1.75*C3*QT(N)**0.75+C2
    IF (DA(N)) 43,44,43
 44 QT(N)=QT(N)+0.02
    GO TO 41
 43 QT(N+1)=QT(N)-A(N)/DA(N)
    QTEMP(II)=QT(N)
    IF (ABS((QT(2)-QT(1))/QT(1)).LT.0.01) GO TO 45
    QT(N)=QT(N+1)
    GO TO 41
 45 IF (II.GT.1) GO TO 818
    II=II+1
    CHEAD=CPGHD
    GO TO 48
818 WRITE (6,804) T2B,AW,QTEMP(1),QTEMP(2)
804 FORMAT (/2E20.7,11X,4HN.A.,5X,E20.7,11X,4HN.A.,5X,E15.7,5X,4HN.A.)
    GO TO 1
762 WRITE (6,23)
 23 FORMAT (//*  NO SUCH AREA EXISTS TO SATISFY THE HEAT TRANSFER REQU
   1IREMENT*)
    GO TO 1
  3 WRITE (6,203)
203 FORMAT (//*   MINIMUM WICK THICKNESS VIOLATES THE SONIC LIMITATION
   1. NO HEAT TRANSPORT IS PRESENTED*)
  1 IF (MORE.GT.1) GO TO 500
    STOP
    END
```

FIGURE B-2 (Continued)

```
      SUBROUTINE    RK(QR,XLAMD,Q,XAXIS,RV,XLCO,RHOV,XMUV,XMVZ,XMUL,XMLZ
     1,RHOL,AW,XKP,ISCAN,X,P,T,N,IND,AFV)
      DIMENSION QR(110),XAXIS(110),XMLZ(110),XMVZ(110),X(50),P(50)
      DIMENSION XZ(50),XK(5,5)
      IND1=IND+1
      H=XAXIS(IND1)-XAXIS(IND)
      CALL        AUXRK(QR,XLAMD,Q,XAXIS,RV,XLCO,RHOV,XMUV,XMVZ,XMUL,XMLZ
     1,RHOL,AW,XKP,ISCAN,X,P,T,N,IND,AFV)
      DO 10 I=1,N
   10 XZ(I)=X(I)
      T=T+0.5*H
      DO 20 I=1,N
      XK(I,1)=H*P(I)
   20 X(I)=XZ(I)+0.5*XK(I,1)
      CALL        AUXRK(QR,XLAMD,Q,XAXIS,RV,XLCO,RHOV,XMUV,XMVZ,XMUL,XMLZ
     1,RHOL,AW,XKP,ISCAN,X,P,T,N,IND,AFV)
      DO 30 I=1,N
      XK(I,2)=H*P(I)
   30 X(I)=XZ(I)+0.5*XK(I,2)
      CALL        AUXRK(QR,XLAMD,Q,XAXIS,RV,XLCO,RHOV,XMUV,XMVZ,XMUL,XMLZ
     1,RHOL,AW,XKP,ISCAN,X,P,T,N,IND,AFV)
      T=T+0.5*H
      DO 40 I=1,N
      XK(I,3)=H*P(I)
   40 X(I)=XZ(I)+XK(I,3)
      DO 50 I=1,N
      XK(I,4)=H*P(I)
   50 X(I)=XZ(I)+(XK(I,1)+2.0*XK(I,2)+2.0*XK(I,3)+XK(I,4))/6.0
      RETURN
      END
C
C
C
C
      SUBROUTINE AUXRK(QR,XLAMD,Q,XAXIS,RV,XLCO,RHOV,XMUV,XMVZ,XMUL,XMLZ
     1,RHOL,AW,XKP,ISCAN,X,P,T,N,IND,AFV)
      DIMENSION QR(110),XAXIS(110),XMLZ(110),XMVZ(110),X(50),P(50)
      DIMENSION XZ(50)
      GO TO (1,2,3,4,5,6) ISCAN
    1 P(1)=-QR(IND)/XLAMD
      GO TO 10
```

FIGURE B-2 (Continued)

```
 2 P(1)=Q*Q*XAXIS(IND)/(3.14159**2.*RHOV*RV**4.*XLAMD**2.*XLCO**2)
   GO TO 10
 3 P(1)=8.0*XMUV*(XMVZ(IND)+3.0*XMVZ(IND)*(QR(IND)/XLAMD)/(8.0*3.1415
  19*XMUV))/(AFV*RHOV*RV**2.0)
   GO TO 10
 4 P(1)=-XMUL*XMLZ(IND)/(RHOL*AW*XKP)
   GO TO 10
 5 P(1)=0.0655*XMUV**2.0*(Q/(XLAMD*3.14159*RV*XMUV))**(7.0/4.0)/(RHOV
  1*RV**3.0)
   GO TO 10
 6 P(1)=XMVZ(IND)*(QR(IND)/XLAMD)/(3.14159*RHOV*RV**4.0)
10 RETURN
   END
```

FIGURE B-2 (Continued)

APPENDIX C

CLEANING PROCEDURE FOR NITROGEN/ALUMINUM CRYOGENIC HEAT PIPE

REVISIONS

LTR	PAGE	DESCRIPTION	DATE	APPROVED

CONTRACT NO.

dynaTherm CORPORATION | COCKEYSVILLE, MARYLAND 21030

D. S Trimmer — PREPARED BY — 3/9/72 DATE

D. S Trimmer — REVIEWED/APPROVED — 3/11/72 DATE

C. A Skrabek — APPROVED — 6/1/72 DATE

APPROVED — DATE

TITLE

CLEANING PROCEDURE FOR
NITROGEN/ALUMINUM CRYOGENIC HEAT PIPE

SIZE	CODE IDENT NO.	DRAWING NO.
A	34881	031-1021

SCALE: | SHEET 1 OF 3

FORM D-0103 REV A

1.0 SCOPE

This procedure defines the final cleaning of aluminum tubing for use with nitrogen in cryogenic heat pipe applications just prior to welding end caps. It applies to the tubing itself and any form of stainless steel wick structure which may be inside at the time of this final cleaning.

2.0 APPLICABLE DOCUMENTS

Federal:	O-M-232	Methyl Alcohol, Methanol
Military:	Mil-T-81533	1, 1, 1 - Trichloroethane (Methyl Chloroform)Inhibited Vapor Degreasing

3.0 WARNINGS & CAUTIONS

3.1 Use in a ventilated area. Avoid prolonged or repeated breathing of trichloroethane and methanol vapors.

3.2 Avoid prolonged contact with skin. Wear rubber gloves while handling trichloroethane.

3.3 Trichloroethane and methanol should be kept away from flames and other ignition sources when used where vapors may be concentrated.

4.0 PROCEDURE

4.1 Rinse tube thoroughly in clean hot (100-120^{o}F) trichloroethane for five (5) minutes.

4.2 Repeat step 4.1 using room temperature clean methanol.

4.3 Drain in air for fifteen (15) minutes.

4.4 Submerge in room temperature solution of 20% nitric acid for five (5) minutes.

4.5 Rinse thoroughly in clean tap water. Flush at least twenty (20) tube volumes of water through pipe.

4.6 Rinse with distilled water and drain for twenty (20) minutes in a class 100,000 controlled environment area. This step must be initiated immediately after completion of prior step (before tap water dries in tube).

4.7 Cover open ends of tube with lint-free pure cellulose cloth and tie in place.

4.8 Dry in oven at 250°F for 1 hour.

4.9 Store in class 100,000 controlled environment area.

5.0 NOTES

This section is not applicable to this procedure.

APPENDIX D

ACCEPTANCE TEST PLAN FOR CRYOGENIC PROTOTYPE HEAT PIPE

REVISIONS

LTR	PAGE	DESCRIPTION	DATE	APPROVED

CONTRACT NO.
NAS5-21563

dynatherm
CORPORATION

COCKEYSVILLE, MARYLAND
21030

D. S. Trimmer 4/17/72
PREPARED BY DATE

W. S. Trimmer 6/1/72
REVIEWED/APPROVED DATE

Walter Brenner 6/1/72
APPROVED DATE

APPROVED DATE

TITLE

ACCEPTANCE TEST PLAN
FOR CRYOGENIC PROTOTYPE HEAT PIPE

SIZE	CODE IDENT NO.	DRAWING NO.
A	34881	031-1023

SCALE: | SHEET 1 OF 16

FORM D-0103 REV A

TABLE OF CONTENTS

5.3.3 Heat Pipe Performance

5.3.3.1 Design Performance

5.3.3.2 Heat Transport Capability Tests

6.0 REPORTING

1.0 INTRODUCTION

1.1 Scope

The testing program for the Cryogenic Prototype Heat Pipes consists of a series of mechanical, environmental, and thermal performance tests. This Test Plan details the types of tests to be performed to verify the heat pipes' operating parameters.

1.2 Item Description

1.2.1 Qualification Samples

Six (6) small samples and one (1) full size sample will be fabricated according to Dynatherm Drawing 031-1026-009 and to 031-1007-029 respectively and subjected to radiographic and pressure tests to verify the integrity of the chosen design. All samples will undergo the same machining, handling, and welding processes as the final prototype heat pipes.

1.2.2 Prototype Heat Pipes

Two (2) prototype heat pipes will be fabricated according to Dynatherm Drawing 031-1003-009 and 031-1003-019. They shall be capable of interfacing with the VM engine and be suitable for space application with the ICICLE System.

1.3 Design Requirements

1.3.1 Mechanical Requirements

The cryogenic heat pipe system as defined in Dynatherm Drawing 031-1003 must be capable of meeting the VM interface requirements specified in Airesearch Manufacturing Company document

#69-5869 (21) Appendix A.

The prototype heat pipes shall have a mechanical integrity capable of withstanding a nonoperating storage at temperatures up to 340 K (150°F) and thermal cycles down to 75 to 80 K.

1.3.2 Thermal Performance Requirements

The heat pipes will be designed for a maximum heat rejection at the condenser of 4 watts with an elevation head of 0.254 cm. The heat pipe will be designed for an optimum heat transport at 80 K measured on the condenser wall but shall be operable over the range from 75 K to 90 K.

2.0 APPLICABLE DOCUMENTS

Unless otherwise indicated, the latest issue of the documents listed below are a part of this test plan to the extent described and in the manner interpreted herein.

MIL-C-45662	Calibration System Requirements
MIL-STD-453	X-Ray Laboratory Procedures for the Certification of Inspection of Aircraft Components
MIL-R-45774 (MI)	Radiographic Inspection, Soundness Requirements for Fusion Welds in Aluminum
DTM-031-1026-009	Qualification Samples (6 Small Samples)
DTM-031-1007-029	Qualification Samples (Full Size Samples)
DTM-031-1003	Prototype Heat Pipes
Airesearch #69-5869 (21) Appendix A	VM Engine Interface Requirements

3.0 GENERAL REQUIREMENTS

3.1 Standard Conditions for Test Area

Laboratory conditions for conducting tests shall be as listed below

unless otherwise specified herein:

a. Temperature : $25^{o} \pm 4^{o}C$

b. Relative Humidity : 55% or less

c. Barametric Pressure : Room ambient

3.2 Test Equipment Calibration

Instrument calibration shall be in accordance with MIL-C-45662, specifying instrument accuracy, calibration periods, calibration facilities, and the procedure used to control instrument certification. All calibration shall be made with instruments whose calibration is traceable to the National Bureau of Standards.

4.0 QUALIFICATION TESTS

4.1 Test Objectives

To demonstrate the reliability and safeness of the heat pipes during storage at ambient temperature.

4.2 Test Equipment

(a) Veeco Leak Detector

Model : MS 90 AB

Sensitivity : 2×10^{-10} std.cc/sec.

(b) Hydrostatic Test Stand

Range : 0-8650 PSI

(c) Harvard Trip Balance

Model : Double Beam

Range : 0-2000 gm

Sensitivity : 0.1 gm

(d) Digital Voltmeter

Model : Cubic Model V-70 and Amplifier A-45

Range : 10 millivolts to 1000 volts

Sensitivity : 0.01 millivolt maximum

(e) Liquid Nitrogen Bath

4.3 Qualification Tests

Six (6) small samples will be fabricated according to Dynatherm Drawing 031-1026-009. Each sample will be helium leak checked to a sensitivity of 1×10^{-9} std.cc/sec. and the welds will be radiographically inspected per MIL-STD-453 and interpreted per MIL-R-45774 (MI).

4.3.1 Hydrostatic Proof Pressure Tests

Each sample will be hydrostatically tested at room temperature for 10 minutes to a pressure corresponding to that expected within the prototype heat pipes during storage at the maximum temperature of 150°F. Figure 4.3-1 is a schematic of the setup for the hydrostatic tests.

4.3.2 Cryogen Leakage Tests

After passing the Hydrostatic Proof Pressure Test, each sample will be tested for possible cryogen leakage. The six (6) samples will be helium leak checked, filled with representative quantities of cryogen and then seal welded. The actual charge will be determined by weighing the samples to an accuracy of ± 0.1 gm before and after filling. Figure 4.3-2 illustrates the test setup for filling the samples.

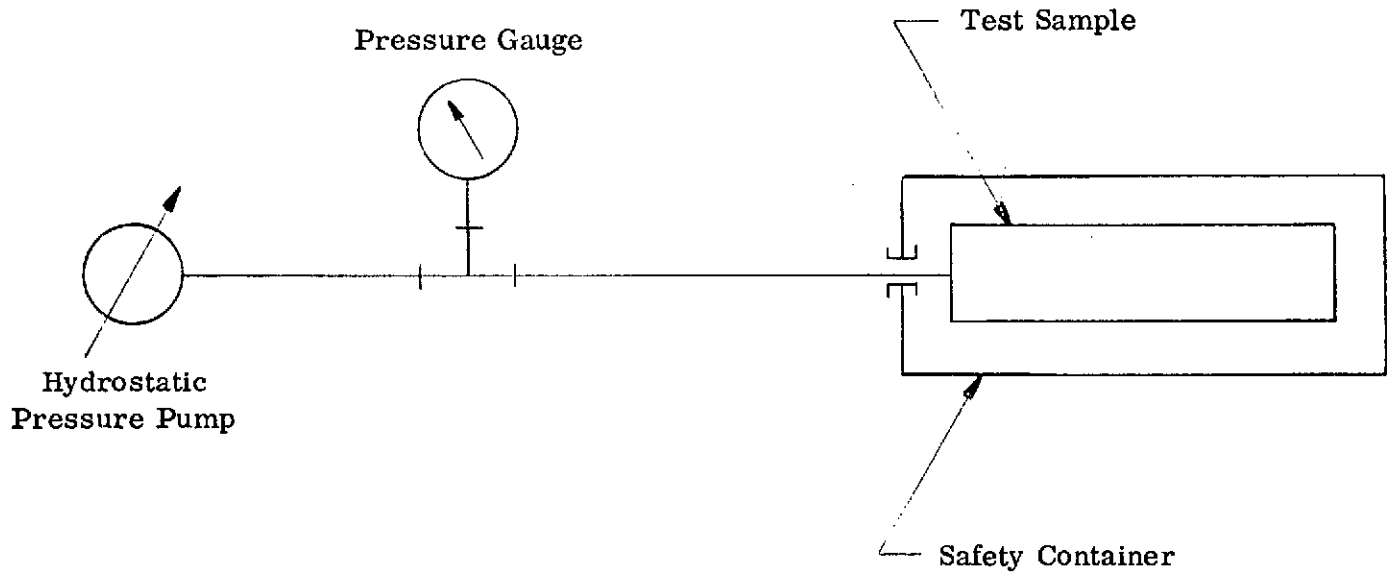

FIGURE 4.3-1

MECHANICAL SCHEMATIC OF HYDROSTATIC PRESSURE TEST

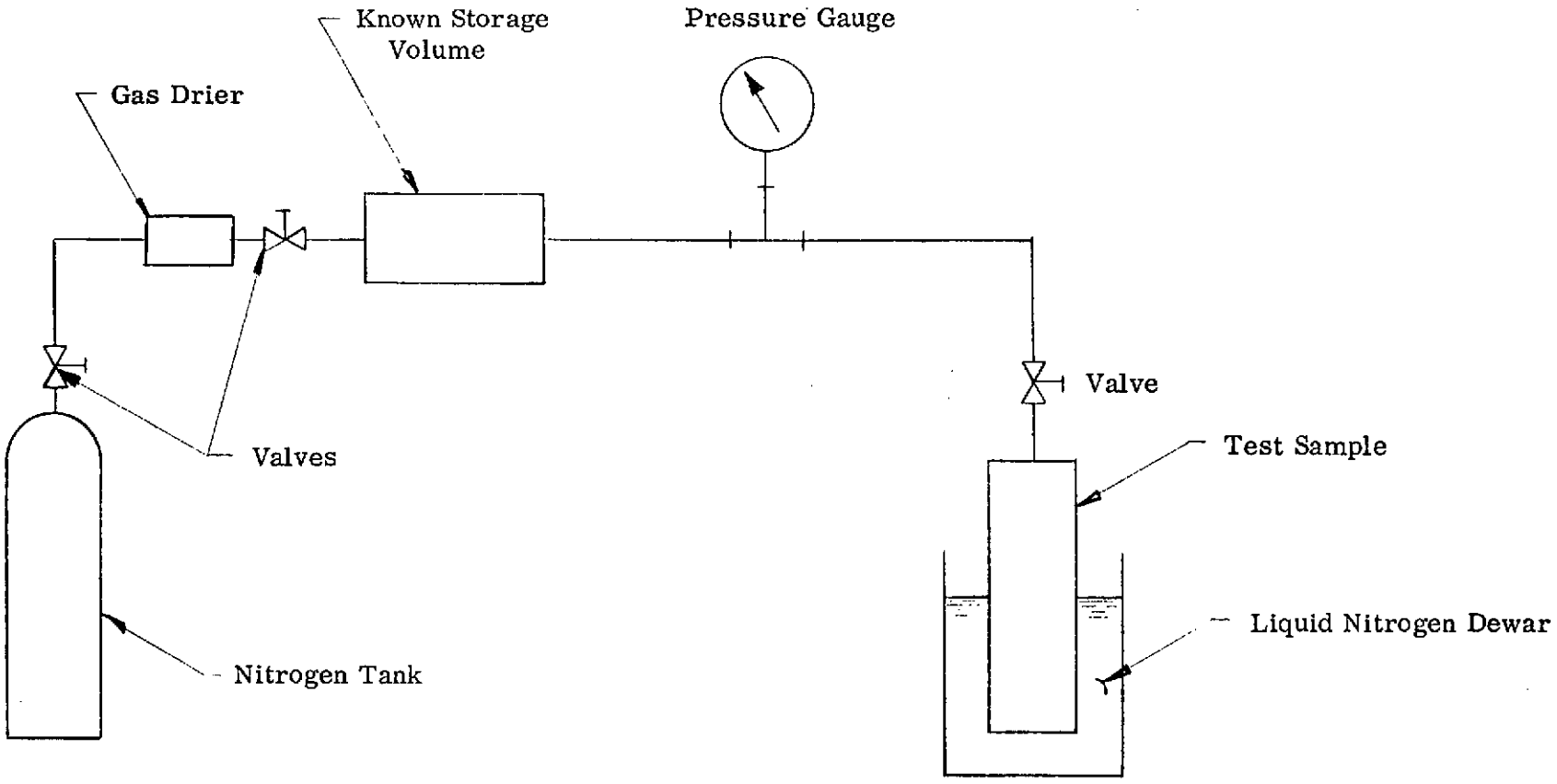

FIGURE 4.3-2

SCHEMATIC OF TEST SETUP FOR FILLING TEST SAMPLES

Throughout the subsequent non-destructive tests, the charged samples will be periodically observed for any loss of weight indicating a loss of cryogen.

4.3.3 Long-Term Storage Test

Three of the filled samples will be stored at $75^{o}F \pm 5^{o}F$ for the remainder of the program to confirm the long-term creep strength of the containment material. Dimensional measurements on the samples at the beginning and end of this test will be used to determine the importance of creep.

4.3.4 Material Fatigue Test

The remaining three filled samples will undergo a series of 10 thermal cycles between 77 K and 300 K to provide a material fatigue safety margin. Dimensional measurements made on the samples before and after the thermal cycle test will be used as the criteria for determining if any distortion occurred and a weight measurement will determine the integrity of the walls and welds.

4.3.5 Burst Pressure Tests

The three (3) samples used in the material fatigue test will then be subjected to a burst test by heating the samples slowly and monitoring the temperature until failure occurs. Figure 4.3-3 is a schematic of the setup for this test. The pressure corresponding to the burst temperature will be determined analytically.

4.3.6 Full Scale Hydrostatic Pressure Tests

A final pressure test will be made on a full scale heat pipe

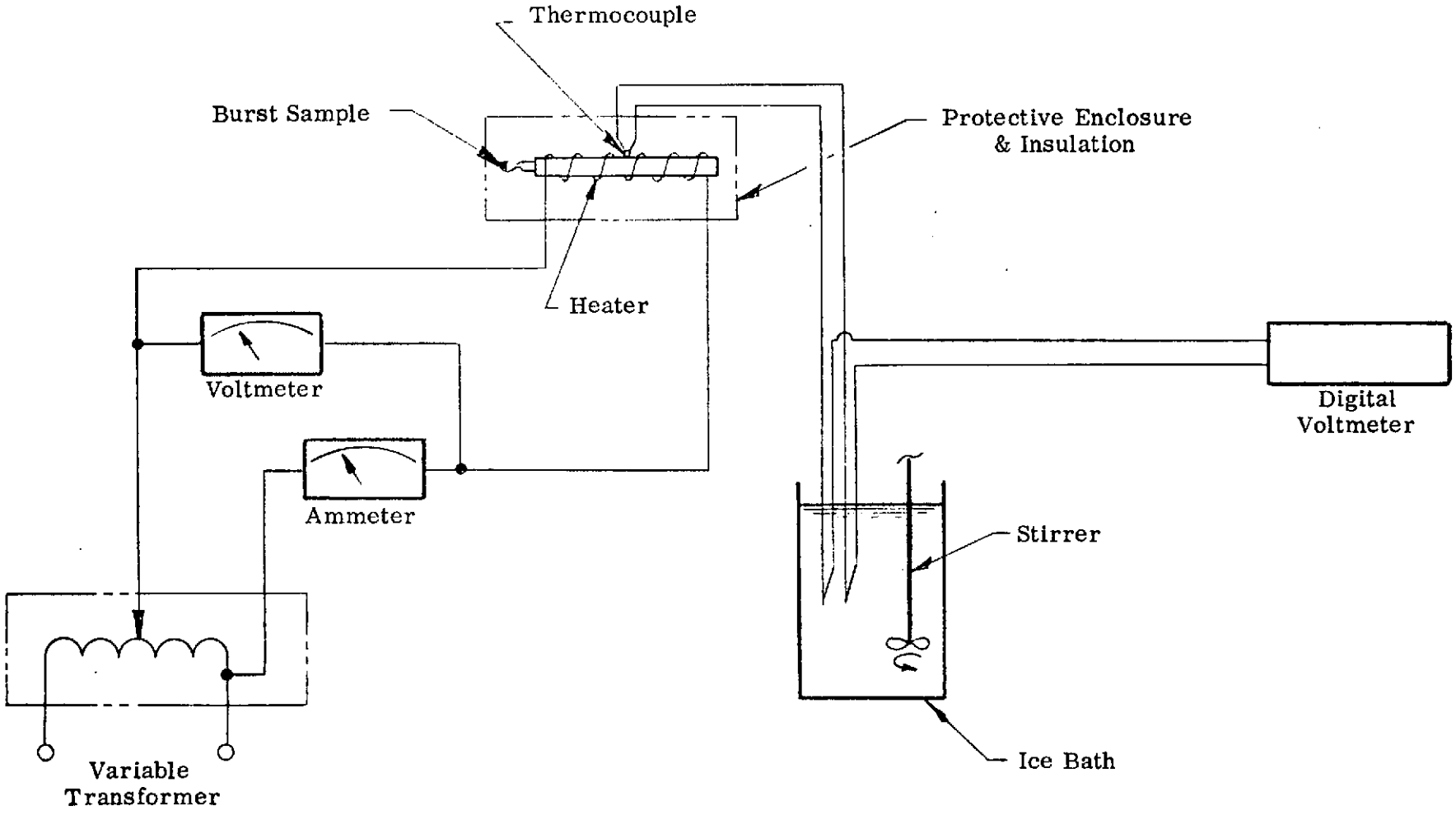

FIGURE 4.3-3

SCHEMATIC OF BURST PRESSURE TEST SETUP

of the same configuration as the prototype heat pipes, including the storage volume if required. This sample will be hydrostatically proof pressure tested in the same manner as the small samples previously tested (see Figure 4.3-1). The sample will also be hydrostatically pressure tested at room temperature on the same test fixture until failure occurs in order to determine the actual safety margin in the design.

5.0 PERFORMANCE TESTS

5.1 Test Objectives

It is the objective of these tests to verify the predicted thermal performance and the operating limitations of the heat pipes. Engineering data will be generated to design cryogenic temperature heat pipes for space-craft environments as well as ground testing. It is also an objective of these tests to uncover design weaknesses so that improvements can be evaluated.

5.2 Test Equipment

(a) Digital Voltmeter

Model : Cubic Model V-70 and Amplifier A-45
Range : 10 millivolts to 1000 volts
Sensitivity : 0.01 millivolt maximum

(b) Weston Wattmeter

Model : 310
Accuracy : $\pm$ 1/4%

(c) Surveyor's Transit

Model : K & E
Accuracy : $\pm$ .005 inch at 10 feet

(d) Ice Bath

(e) Vacuum Chamber

5.3 Performance Tests

5.3.1 Calibration of Thermocouples and Test Fixture

Chromel-alumel thermocouples to be used in the performance tests will be calibrated against two reference baths; i.e., boiling N_2 at one atmosphere and an ice bath. Only those thermocouples which meet a maximum tolerance of ± 5 K at the two temperatures will be accepted for use in the test program.

With a prototype heat pipe installed in the vacuum chamber, a series of tests will be conducted to determine the parasitic heat leak into the walls of the heat pipe. This test will also be used to calibrate the heat shunt for measuring the heat removal at the condenser end of the heat pipe. Figure 5.3-1 is a schematic of this test. The temperature drop across the thermal shunt will be measured for various electrical heat inputs. A linear relationship should exist between temperature drop and electrical heat input. The heat shunt calibration is determined from the slope of this line and the heat input intercept when ΔT is zero (this value is the parasitic heat leak and should occur at a negative heat input). An analysis of the insulation effectiveness will be performed from these results.

5.3.2 Start-Up Procedure

The prototype heat pipe will be mounted in the vacuum chamber and instrumented. Tests will be conducted only in the

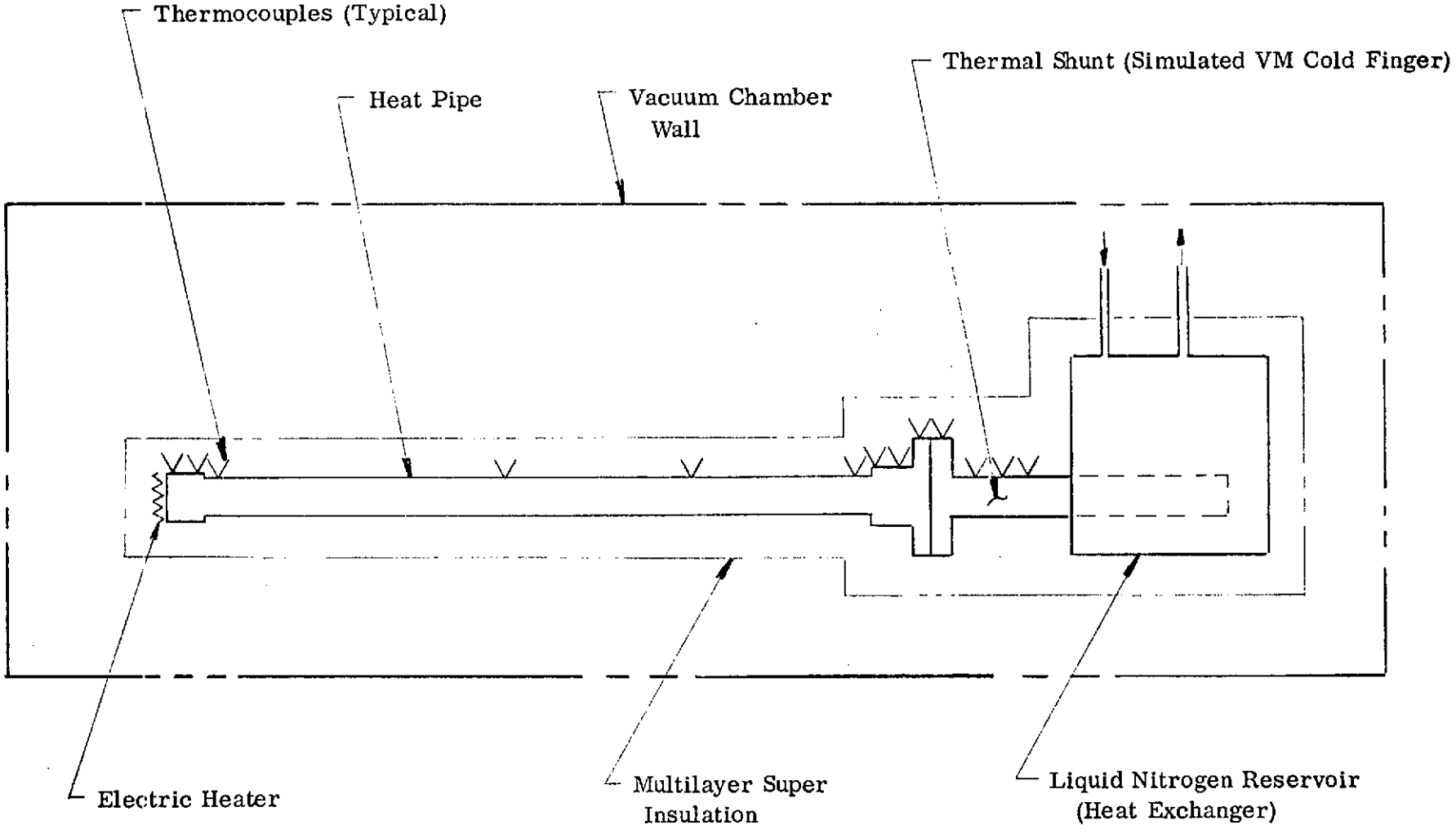

FIGURE 5.3-1

SCHEMATIC FOR TESTS IN VACUUM CHAMBER

sensor-off (zero electrical power) condition and with the evaporator elevated 0.254 cm above the condenser. Cool-down of the system will be initiated by introducing liquid nitrogen into the heat exchanger (see Figure 5.3-1). The temperature along the heat pipe will be monitored to observe changes with time as the heat pipe cools down to cryogenic temperatures. This procedure will be repeated for several different cool-down times by varying the rate at which liquid nitrogen is introduced into the heat exchanger. A cool down time is defined as the time it takes to cool the condenser as measured at the interface joint, from room temperature to 80 K $\pm$ 5 K. Three tests will be conducted for different cool-down times from a maximum of 120 minutes to a minimum of 60 minutes.

5.3.3 Heat Pipe Performance

5.3.3.1 Design Performance

The heat pipes will be operated with the evaporator elevated 0.254 cm above the condenser at an electrical heat load of 0.5 watts. The condenser temperature shall be 80 K $\pm$ 5 K. Temperature profiles along the heat pipes will be measured in order to determine the evaporator and condenser Δ T's.

5.3.3.2 Heat Transport Capability Tests

The performance design margin and the heat pipe's sensitivity to elevation will be determined by measuring the maximum heat transport capability at several